

THE ROTATION PERIOD DISTRIBUTION OF PRE-MAIN-SEQUENCE STARS IN AND AROUND THE ORION NEBULA

KEIVAN G. STASSUN,¹ ROBERT D. MATHIEU,¹ TSEVI MAZEH,² AND FREDERICK J. VRBA³

Received 1998 November 30; accepted 1999 March 9

ABSTRACT

We report rotation periods for 254 stars in an area $40' \times 80'$ centered on the Orion Nebula. We show that these stars are likely members of the young ($\sim 10^6$ yr) Orion OB1c/d association. The rotation period distribution we determine, which is sensitive to periods $0.1 < P < 8$ days, shows a sharp cutoff for periods $P < 0.5$ days, corresponding to breakup velocity for these stars. Above 0.5 days the distribution is consistent with a uniform distribution; we do not find evidence for a “gap” of periods at 4–5 days. We find signatures of active accretion among stars at all periods; active accretion does not occur preferentially among slow rotators in our sample. We find no correlation between rotation period and near-IR signatures of circumstellar disks. In addition, we show that the distribution of $v \sin i$ among stars in our sample bears striking resemblance to that of low-mass Pleiades stars. We discuss the implications of our findings for the evolution of stellar angular momentum during the pre-main-sequence phase. We argue that all stars in our sample must still deplete angular momentum by factors of roughly 5–10, if they are to preserve their $v \sin i$ distribution over approximately the next 100 Myr. We consider in detail whether our findings are consistent with disk-regulated stellar rotation. We do not find observational evidence that magnetic disk-locking is the dominant mechanism in angular momentum evolution during the pre-main-sequence phase.

Key words: stars: evolution — stars: pre-main-sequence — stars: rotation — stars: spots

1. INTRODUCTION

A long-standing question in the study of star formation is the evolution of angular momentum in the pre-main-sequence (PMS) phase. T Tauri stars (TTS), the precursors of low-mass main-sequence stars, typically rotate at $\lesssim 10\%$ of breakup velocity (Vogel & Kuhl 1981; Hartmann et al. 1986; Bouvier et al. 1986). This is contrary to the expectation that these stars should spin close to breakup speed, having recently contracted from their natal clouds. In addition, PMS stars should subsequently spin up considerably as they accrete circumstellar material of high specific angular momentum and as they contract to the main sequence. However, the rotation rates of TTS projected to the main sequence under the assumption that angular momentum is conserved (e.g., Stauffer & Hartmann 1987) do not even closely reproduce the observed rotation rates of zero-age main-sequence (ZAMS) stars, which are predominantly slow rotators (e.g., Stauffer & Hartmann 1987; Queloz et al. 1998). Apparently, stellar angular momentum is not conserved in the PMS phase.

This angular momentum “conundrum” has served as a subtext for much of the observational and theoretical work relating to the rotational evolution of PMS stars. On the observational front, photometric monitoring campaigns of various star forming regions (e.g., Bouvier et al. 1993; Herbst et al. 1994; Choi & Herbst 1996; Makidon et al. 1997; Wichmann et al. 1998) have provided rotation periods for hundreds of TTS on the basis of periodic photometric variability, presumably arising from stellar spots. For many of these stars, spot temperatures have been mea-

sured (e.g., Bouvier et al. 1993; Vrba, Herbst, & Booth 1988; Vrba et al. 1986), and near-IR photometry has been used to identify systems with circumstellar disks (e.g., Strom et al. 1989; Beckwith et al. 1990; Hillenbrand et al. 1998).

Meanwhile, theoretical mechanisms for depleting stellar angular momentum have been developed. Early work centered largely on magnetically driven outflows (e.g., Hartmann & MacGregor 1982; Shu et al. 1988 and references therein). More recently, a model involving a magnetic star-disk interaction (Ghosh & Lamb 1979a, 1979b; Königl 1991; Shu et al. 1994; Ostriker & Shu 1995) has become favored. According to this model, the stellar magnetic field threads the star’s circumstellar disk, truncating it at a characteristic radius, which is set by the balance between accretion rate and magnetic field strength. Accretion of disk material onto the stellar surface occurs along magnetic field lines, producing hot spots near the magnetic poles. At the same time, magnetic torques transfer angular momentum away from the star to the disk (e.g., Najita 1995 and references therein). This model, in addition to providing a mechanism for the depletion of stellar angular momentum, provides a unifying framework for many observed properties of TTS: spectroscopic outflow signatures (Edwards et al. 1993a and references therein), ultraviolet excess emission and “veiling” (e.g., Basri & Bertout 1989; Basri & Batalha 1990), hot surface spots (Herbst et al. 1994 and references therein), and truncated circumstellar disks (e.g., Meyer, Calvet, & Hillenbrand 1997; Kenyon, Yi, & Hartmann 1996; Lada & Adams 1992).

This idea of disk-regulated stellar angular momentum has been supported observationally by several key studies of stellar rotation and circumstellar disks. Herbst and collaborators (Attridge & Herbst 1992; Eaton, Herbst, & Hillenbrand 1995; Choi & Herbst 1996) have reported the distribution of rotation periods among 75 stars in the Orion Nebula Cluster (ONC) to be bimodal, dividing at a period of 4–5 days. The bimodal distribution suggests two distinct,

¹ Department of Astronomy, University of Wisconsin, 475 North Charter Street, Madison, WI 53706; keivan@astro.wisc.edu.

² Wise Observatory, Tel Aviv University, Ramat Aviv, Tel Aviv 69978 Israel.

³ US Naval Observatory, Flagstaff Station, P.O. Box 1149, Flagstaff, AZ 86002-1149.

well-separated populations of slow ($P > 4$ days) and fast ($P < 4$ days) rotators. Bouvier et al. (1993) reported that among 26 stars in Taurus-Auriga, classical TTS (CTTS; those showing evidence of active accretion and circumstellar disks) rotate more slowly on average than their weak-lined TTS (WTTS) counterparts, implying that disked stars rotate more slowly than nondisked stars. Edwards et al. (1993b) observed a direct correlation between TTS rotation period and a near-IR disk-emission signature among 34 late K and M stars drawn from the samples of Bouvier (1990) and Attridge & Herbst (1992). Only stars with $P > 4$ days showed significant near-IR emission indicative of circumstellar disks. Together, these studies suggest a connection between TTS rotation and circumstellar disks.

Indeed, disk-regulated stellar rotation has become central to our paradigm of the rotational evolution of PMS stars. The recent extensive modeling of the angular momentum evolution of stars from the ages of TTS to the present-day Sun (e.g., Bouvier, Forestini, & Allain 1997; Krishnamurthi et al. 1997; Collier Cameron, Campbell, & Quaintrell 1995; Keppens, MacGregor, & Charbonneau 1995) relies largely on disk-regulated stellar rotation among low-mass stars in the PMS phase to reproduce the predominance of slow rotators at the age of the Pleiades. Similarly, studies of rotation periods among stars slightly older than the ONC (e.g., Kearns et al. 1997; Adams, Walter, & Wolk 1998) have used the presumed disk-regulated rotation in the ONC to infer disk lifetimes among their samples. In addition, magnetospheric accretion theory has been invoked to successfully explain the observed correlation between accretion and outflow signatures in TTS (e.g., Hartigan, Edwards, & Ghandour 1995) and to model various observed properties of accretion kinematics and morphology in PMS systems, including modeling of emission-line profiles (e.g., Hartmann, Hewett, & Calvet 1994; Edwards et al. 1994; Kenyon et al. 1996; Muzerolle, Calvet, & Hartmann 1998a; Muzerolle, Hartmann, & Calvet 1998b), modeling of photopolarimetric variability (Wood et al. 1996; Stassun & Wood 1999), modeling of hot spots on stellar surfaces (e.g., Kenyon et al. 1994), and modeling of time variability in scattered-light reflection nebulae around embedded sources (e.g., Wood & Whitney 1998; Wood et al. 1998).

In this paper we present the results of an extensive photometric study of rotation among PMS stars in and around the Orion Nebula. We report rotation periods for 254 members of the Orion OB1c/d association, including numerous stars rotating at or near breakup velocity. The distribution of rotation periods is indistinguishable from a uniform distribution; a bimodal distribution with a deep gap at 4–5 days is not supported by the present data. Furthermore, from spectra we have obtained with the WIYN multiobject spectrograph, we find accretion signatures among stars at all rotation periods. Combining our data with data from the literature, we find no correlation between stellar rotation period and near-IR signatures of circumstellar disks among stars in the ONC. In addition, we show that the $v \sin i$ distribution of stars in the ONC bears a remarkable resemblance to that of low-mass Pleiades stars, and we suggest this implies that significant angular momentum losses must continue well beyond typical lifetimes of disks. Finally, by considering the evidence for disk material at the corotation distance from the stars in our sample, we argue that the case for a causal connection between disks and stellar rotation is not well supported.

Taken together, these findings challenge the ability of the disk-regulation paradigm to explain the depletion of stellar angular momentum in the PMS phase.

In § 2, we discuss our photometric and spectroscopic observations, their reduction, our method for determining periodic photometric variability and biases therein, and the data from the literature, which we combine with our own in our analysis. We summarize our results in § 3. In § 4 we discuss the implications of our results for various questions relating to the evolution of angular momentum in the PMS phase: the bimodal distribution of rotation periods, the case for disk-regulated rotation, and the dissipation of stellar angular momentum leading up to the ZAMS. We summarize our conclusions in § 5.

2. OBSERVATIONS, METHODS, AND DATA FROM THE LITERATURE

We have photometrically and spectroscopically surveyed stars in a region approximately 40' east-west and 80' north-south centered on the Trapezium in the Orion Nebula. The result is a database of differential photometric I -band light curves for more than 4600 stars with approximately $12 < I < 18$. Our light curves are sampled approximately 1 hr^{-1} , and in this study we restrict our analysis to the subset of 2279 stars with $12 < I < 16.5$ (for which our photometric precision is flat-field limited, $\sigma_{\text{mag}} \lesssim 0.02 \text{ mag}$) and possessing light curves that span at least 10 days. From this database we derive rotation periods for 254 stars, of which more than half are observed spectroscopically.

The region we surveyed is roughly coincident with that designated Orion Ic by Blaauw (1964, 1991; see latter reference for a schematic) and represents one of the four principal subgroups (a–d) of the large Orion I OB association. The Ic subgroup—the central part of which is designated Id or the “Trapezium cluster”—has been further subdivided by Warren & Hesser (1977) into the sub-subgroups c1–c4, d1 (ONC), and d (Trapezium). Our survey region roughly encompasses their c2, c3, c4, d1, and d designations (note that their region Ic is much larger than the region surveyed by us). This region contains numerous associated objects in addition to the Orion Nebula, including NGC 1773, 1775, 1780, and 1781 (Maddalena et al. 1986), as well as several classified subclusters in addition to the Trapezium and ONC, including NGC 1777, OMC-2, and the “Lower Sword” (e.g., Gomez & Lada 1998). Historically, these various designations and subgroupings have been assigned arbitrarily on the basis of visual impression, and recently Hillenbrand & Hartmann (1998) and Gomez & Lada (1998) have attempted to characterize the morphology of the stellar distribution more quantitatively. Numerous investigators have looked for age differences among the various subgroups of Orion I (e.g., Blaauw 1964, 1991; Warren & Hesser 1977; Brown, de Geus, & de Zeeuw 1994) and among the “clustered” and “distributed” stellar populations (e.g., Allen 1996) in the region. We defer discussion of this issue, as it pertains to this study, to § 4.1. For now, we note simply that the size and shape of our survey region corresponds to the morphology of the underlying cloud- and star-forming complex as indicated by the roughly north-south rectangular distribution (Gomez & Lada 1998) of $H\alpha$ emission-line stars from the Kiso survey (Nakano, Wiramihardja, & Kogure 1995; Kogure et al. 1989; Wiramihardja et al. 1989, 1991, 1993), and by the prominent north-south molecular “ridge” seen in ^{13}CO emission

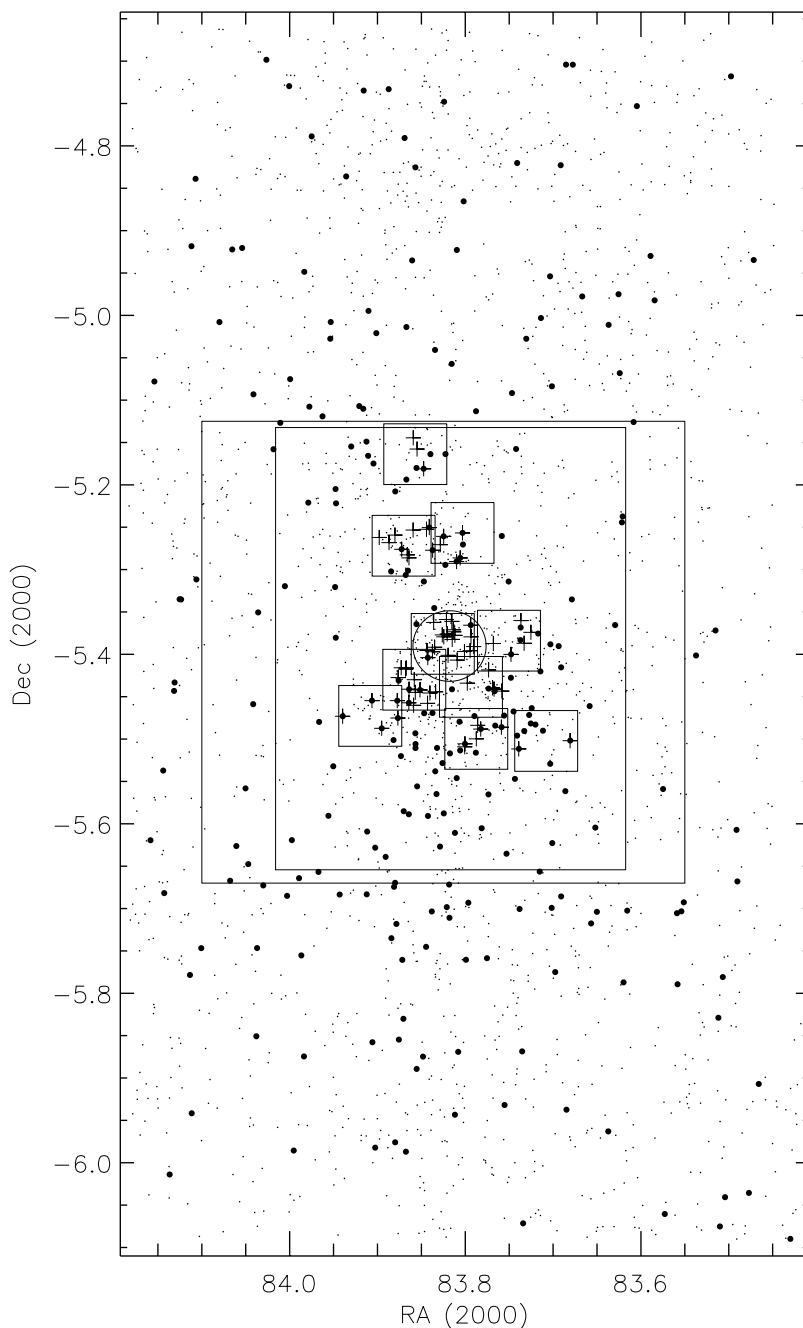


FIG. 1.—Survey region for this study. Small dots indicate positions of all 2279 sources in our synoptic photometric database, with $12 < I < 16.5$ and with light curves spanning at least 10 days. Large dots indicate the 254 stars for which we report rotation periods. Crosses mark the 75 stars with rotation periods reported in the literature. Boxes indicate the regions surveyed by CH (10 small boxes), Jones & Walker 1988 (inner large box), and Hillenbrand 1997 (outer large box). The small circle in the center of the field has a radius of 2.5 and indicates the region within which severe nebulosity imposes incompleteness on our photometry (see text).

(Bally et al. 1987) extending from approximately $-4^{\circ}8$ to $-6^{\circ}2$ decl. (See Allen & Hillenbrand 1999 for a nice diagram combining these observations.)

In this section we present our photometric and spectroscopic observations, and we describe their reduction. We begin by summarizing some existing data from the literature, which we combine with our own data in our analysis of the connection between stellar rotation, accretion, and circumstellar disks. Next, we describe the synoptic photometric database that forms the foundation for this study. Finally, we describe our methods for detecting periodic

photometric variability as a measure of stellar rotation period, measuring stellar $H\alpha$ emission strength as a proxy for accretion activity, and measuring stellar lithium and radial velocities as indicators of membership in the Orion OB1c/d association. The reader wishing only a brief summary will find a synopsis of this section in § 2.5.

2.1. Data From the Literature

The region in the immediate vicinity of the Orion Nebula has been studied by numerous researchers with varying degrees of depth and spatial coverage. In our analysis of the

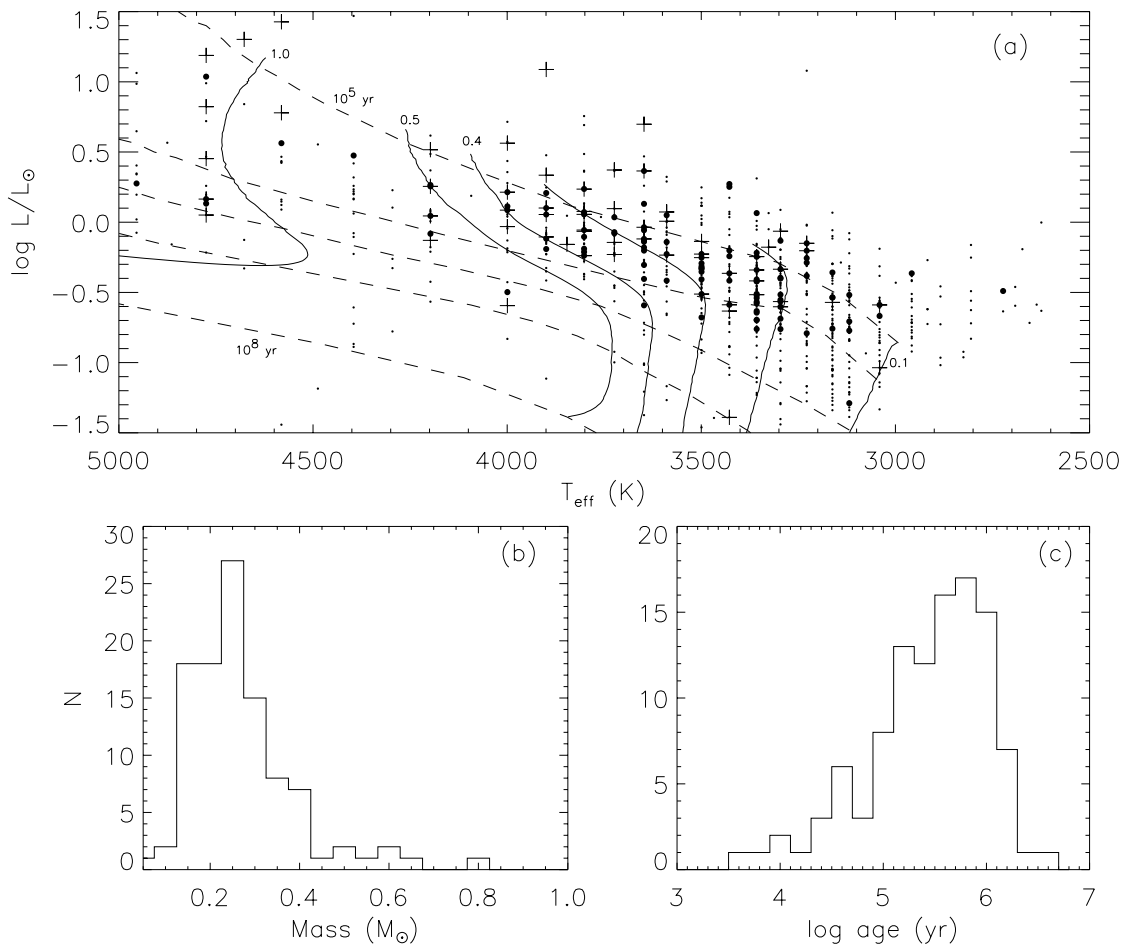


FIG. 2.—Basic parameters for ONC stars in our sample. (a) H-R diagram shown for the 744 stars in our database with data available from Hillenbrand 1997 (small dots); 108 stars (large dots) have rotation periods measured by us. Also shown are stars with rotation periods reported by CH (crosses). Evolutionary tracks from D’Antona & Mazzitelli 1994 (model 1) are also shown: mass tracks are for stellar masses 0.1, 0.2, 0.3, 0.4, 0.5, 1.0 M_{\odot} and isochrones are for ages 10^5 , 10^6 , 3×10^6 , 10^7 , 10^8 yr. (b) Most stars in our ONC sample fall in the narrow range of stellar mass $0.15 < M/M_{\odot} < 0.4$. (c) Stars in our sample of rotators are characterized by ages $4 \lesssim \log \tau \lesssim 6.5$.

relationships between stellar rotation, accretion, and circumstellar disks, we combine our own photometric and spectroscopic observations with data taken from the literature to form a more complete picture of the objects under consideration. We will draw primarily from the proper-motion membership study of Jones & Walker (1988), the photometric monitoring study of Choi & Herbst (1996), the stellar population study of Hillenbrand (1997),⁴ and the near-IR photometric study of Hillenbrand et al. (1998). Figure 1 shows the spatial relationship among the regions surveyed by these previous studies and the region surveyed by us.

The proper-motion study of stars with $I \lesssim 16$ in the central $15'$ (radius) of the ONC by Jones & Walker (1988; hereafter JW) provides a robust measure of association membership probability for 863 stars in our database (114 with measured rotation periods). For stars not in the JW database or outside their survey region, we rely on our own spectroscopic diagnostics of membership (§ 2.4.2).

The ongoing Wesleyan photometric monitoring program (most recently published in Choi & Herbst 1996, hereafter CH) has so far produced rotation periods for 75 JW stars in a set of 10 small fields within the JW proper-motion survey region in the ONC. The rotation periods produced by the Wesleyan program (which is sensitive to periods $P \gtrsim 2$ days for $I \lesssim 16$) are extremely secure, many of them confirmed over multiple observing seasons. Fifty-three of the CH rotators have appropriate magnitude limits to appear in our database, and we derive independent rotation periods for 25 of them (see § 2.3.1).

Hillenbrand (1997) has conducted a stellar census of the ONC, in a region slightly larger than the JW proper-motion survey region, sensitive to $I \sim 17$. Placing these stars on a theoretical H-R diagram and comparing them with the theoretical PMS evolutionary tracks⁵ of D’Antona & Mazzitelli (1994), Hillenbrand (1997) derives stellar masses, radii, and ages for 744 stars in our database (108 with rotation periods). These 108 stars show a narrow range in spectral

⁴ The data from Hillenbrand (1997) used in this paper were obtained via private communication in 1997 November. Updated tables are now available from L. Hillenbrand.

⁵ Hillenbrand (1997) uses D’Antona & Mazzitelli (1994) model 1 i.e., Alexander, Augason, & Johnson (1989) opacities and Canuto & Mazzitelli (1990, 1992) convection.

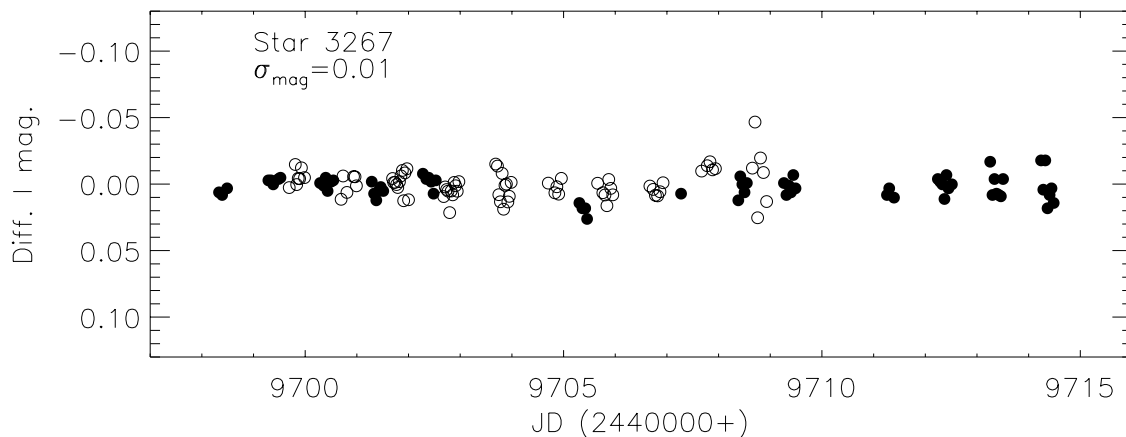


FIG. 3.—Sample light curve from our photometric database. Open symbols are KPNO/USNO data and filled symbols are Wise data. A typical star in our database has KPNO/USNO data spanning 10 days. Approximately 25% of stars have Wise data spanning 17 days. Note that Wise data largely fill in diurnal gaps in the KPNO/USNO data. This light curve is not periodic.

types (Fig. 2) K5–M5, with a most common spectral type of M3. This range in spectral type corresponds to a range in stellar mass of $0.1 M_{\odot} < M < 0.7 M_{\odot}$, although the majority of these stars (90%) have $0.15 M_{\odot} < M < 0.4 M_{\odot}$ and the most common mass is $0.25 M_{\odot}$ (Fig. 2, panel b); such stars are believed to be fully convective throughout their PMS evolution. These stars are thus homogeneous in mass and in internal structure. The observed range in L represents a 5–6 σ spread, given the quoted uncertainties in $\log L$ of 0.2 dex (see Fig. 2; also see Fig. 13 in Hillenbrand 1997). Thus Hillenbrand (1997) derives an age spread among stars in the ONC of $4 \lesssim \log \tau \lesssim 6.5$. Our photometric limits allow us to sample stars with $0.06 M_{\odot} \lesssim M \lesssim 0.8 M_{\odot}$ and $\log \tau \lesssim 7$ (see Fig. 2), indicating that our sample is not significantly biased in the basic stellar parameters that typify the low-mass population of the ONC. Using *JHK* photometry, Hillenbrand et al. (1998) also measure near-IR excess emission, $\Delta(I-K)$, and report Ca II triplet emission strengths for stars in the ONC.

Although these studies of the stellar population in and around the Orion Nebula have photometric limits comparable to our database, they focus on the ONC, which covers a central area only about 25% of our survey region. In § 4.1 we discuss the possible age difference of stars in this central region and stars in the larger region we surveyed. We are presently assembling the necessary photometric and spectroscopic data to construct an H-R diagram for our entire survey region, and we are collecting *JHK* photometry for our entire sample of rotators. In lieu of these data, we couple the above-mentioned sources to our sample of rotators to explore the connection between stellar rotation, accretion, and circumstellar disks.

2.2. Differential Photometry

We observed a rectangular region, centered on the Trapezium in the Orion Nebula, approximately 40' east-west and 80' north-south, over the 17 nights from 1994 December 11 to 1994 December 27. We used the KPNO 0.9 m telescope for the five consecutive nights 1994 December 13 to 1994 December 17, and the USNO 1 m telescope for the subsequent five consecutive nights. We used the Wise Observatory 1 m telescope to monitor the central portion of the survey region on 13 nights over the full 17 night run.

The KPNO and USNO telescopes have nearly identical fields of view, 23' square, so to cover our survey region we observed a 2×4 mosaic with adjacent fields overlapping by a few arcminutes. With the Wise 512×512 CCD (12' square) we observed a 4×4 mosaic, covering the central $40' \times 40'$ region. We varied our exposure times depending upon seeing conditions, with the aim of saturating at $I = 12$. At each telescope, we monitored with a frequency of approximately 1 hr^{-1} . Here we describe the basic reductions we performed on our CCD data and the construction of our synoptic photometric database.

2.2.1. Basic Reductions

We reduced our CCD frames using the standard IRAF CCDRED package. We used the IRAF STSDAS GASP package to compute a simple linear transformation of pixel coordinates to equatorial coordinates for each frame, using as reference approximately 20 DSS stars per frame. Our derived stellar positions show a frame-to-frame scatter of about 0".2 in each direction, comparable to the positional precision of the DSS. As an independent, external accuracy check, we compare our derived stellar positions to the USNO-A1.0 astrometric database⁶ (Monet et al. 1996), accurate typically to about 0".25 for stars brighter than $E \sim 20$. We find global positional agreement with formal uncertainties of $1/3''$ in each direction among 991 matches using a 3" search radius. A systematic offset of about 0".7 in each direction relative to the USNO database has been removed. In addition, we find small local systematic offsets between stellar positions derived by us and those derived by JW. These systematic offsets vary across the field, but they can be as large as 0".4–0".5 and most likely reflect plate solution discontinuities at frame boundaries. Thus, while our global positional uncertainties are formally about 0".33 in each direction, nonsmoothness of the plate solution probably degrades positional accuracy to 0".4–0".5 at frame boundaries.

2.2.2. Aperture Photometry and Light Curves

We performed simple aperture photometry using the IRAF APPHOT package. We first identified stellar sources

⁶ See <http://www.nofs.navy.mil/projects/pmm/>.

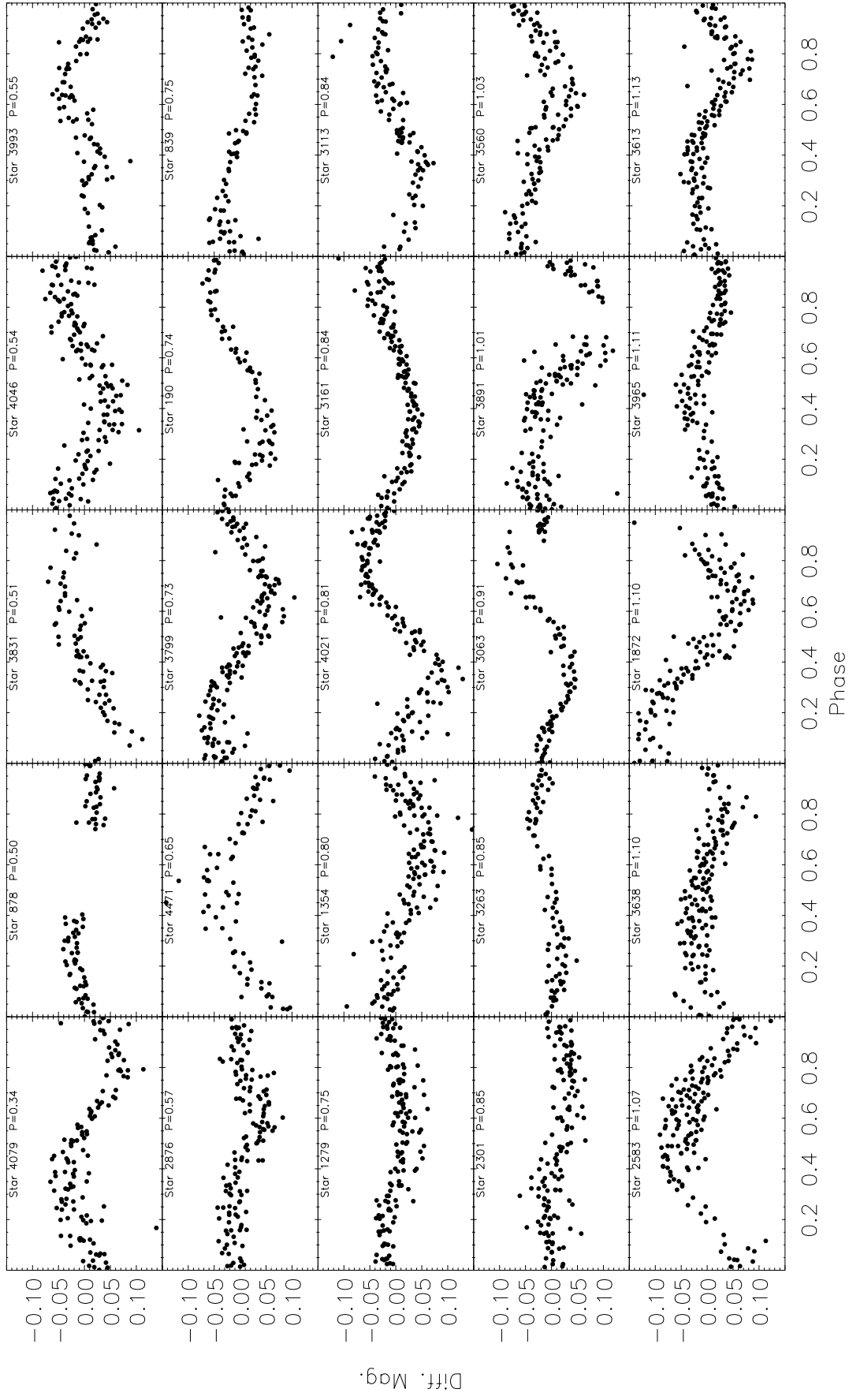
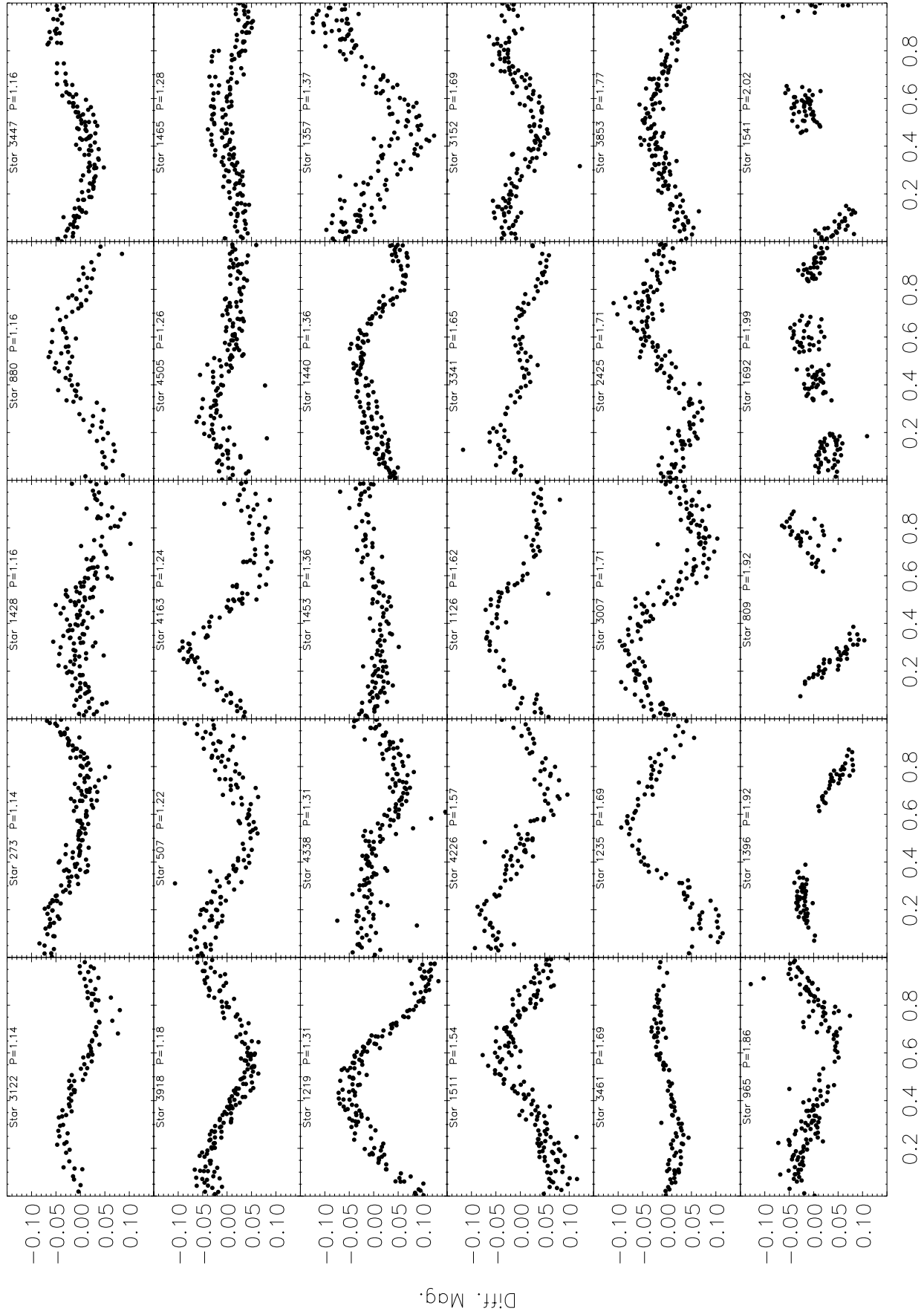


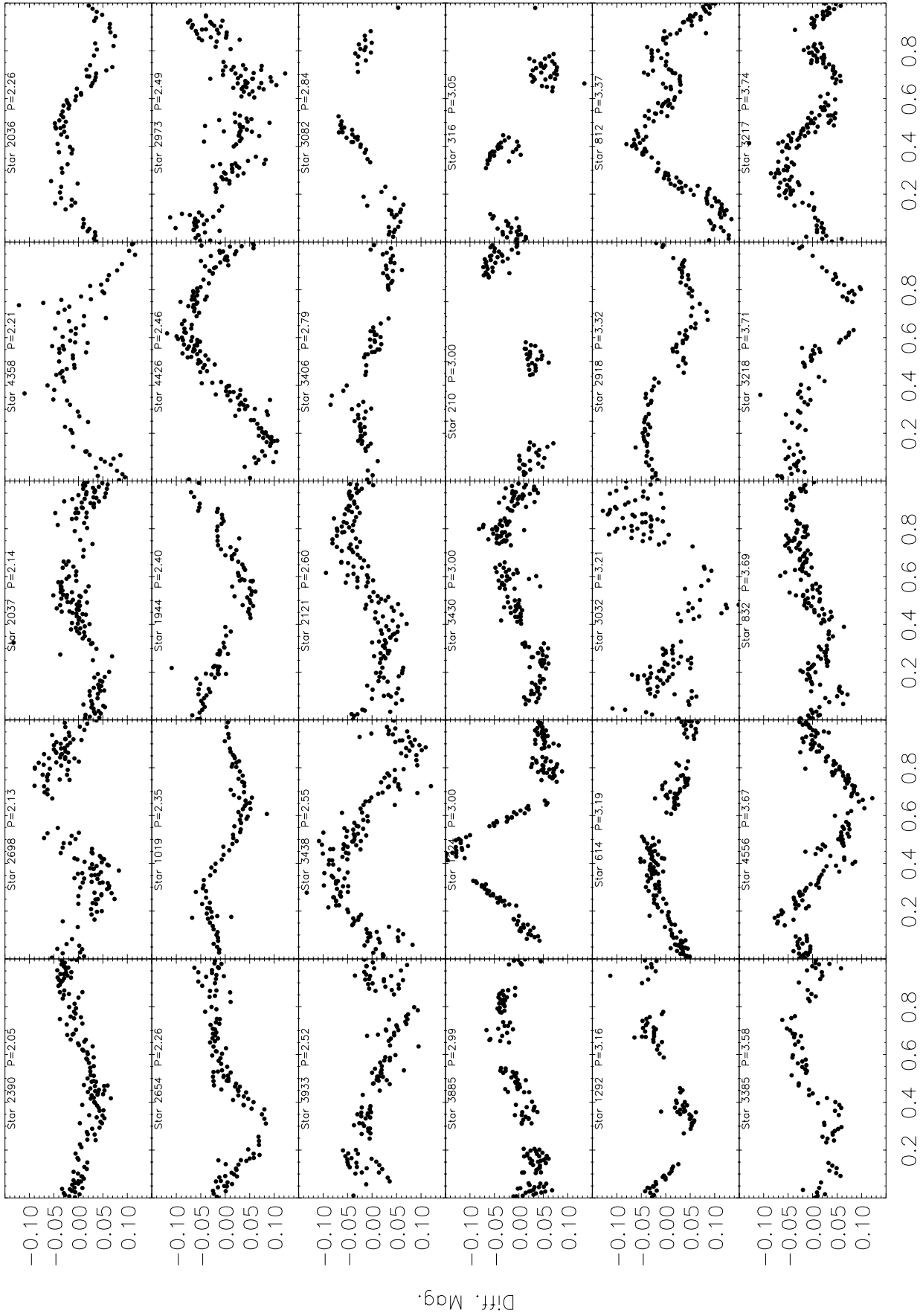
FIG. 4a

FIG. 4.—Light curves of our sample of rotators, phased on the period shown. Stars are sorted by period (days) in three groups based on amplitude of variability. ($a-g$): $\Delta I < 0.2$ mag; ($h-i$): $0.2 < \Delta I < 0.5$ mag; (j): $\Delta I > 0.5$ mag. A single cycle is shown. Data for these stars are provided in Table 1.



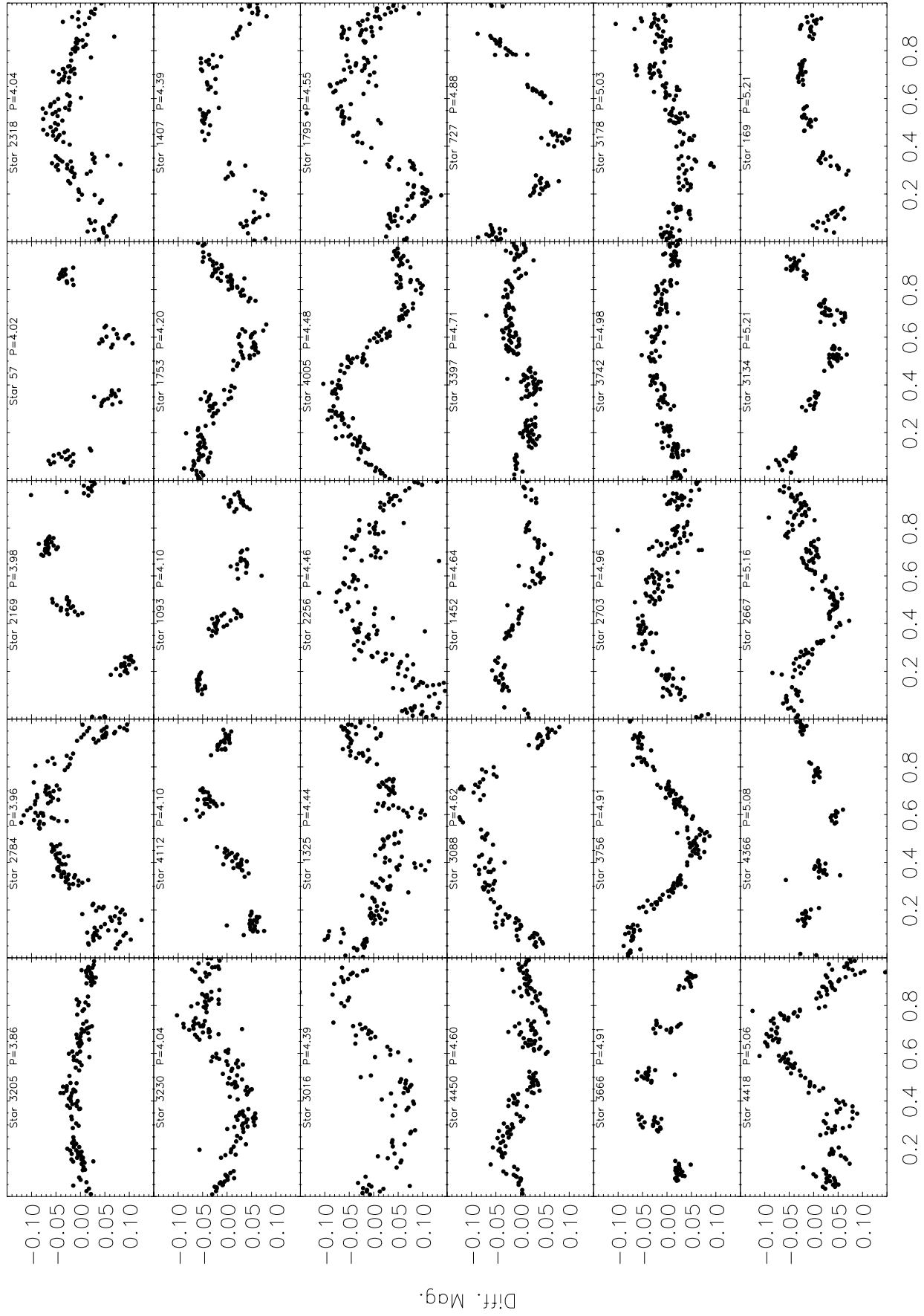
Phase

FIG. 4b

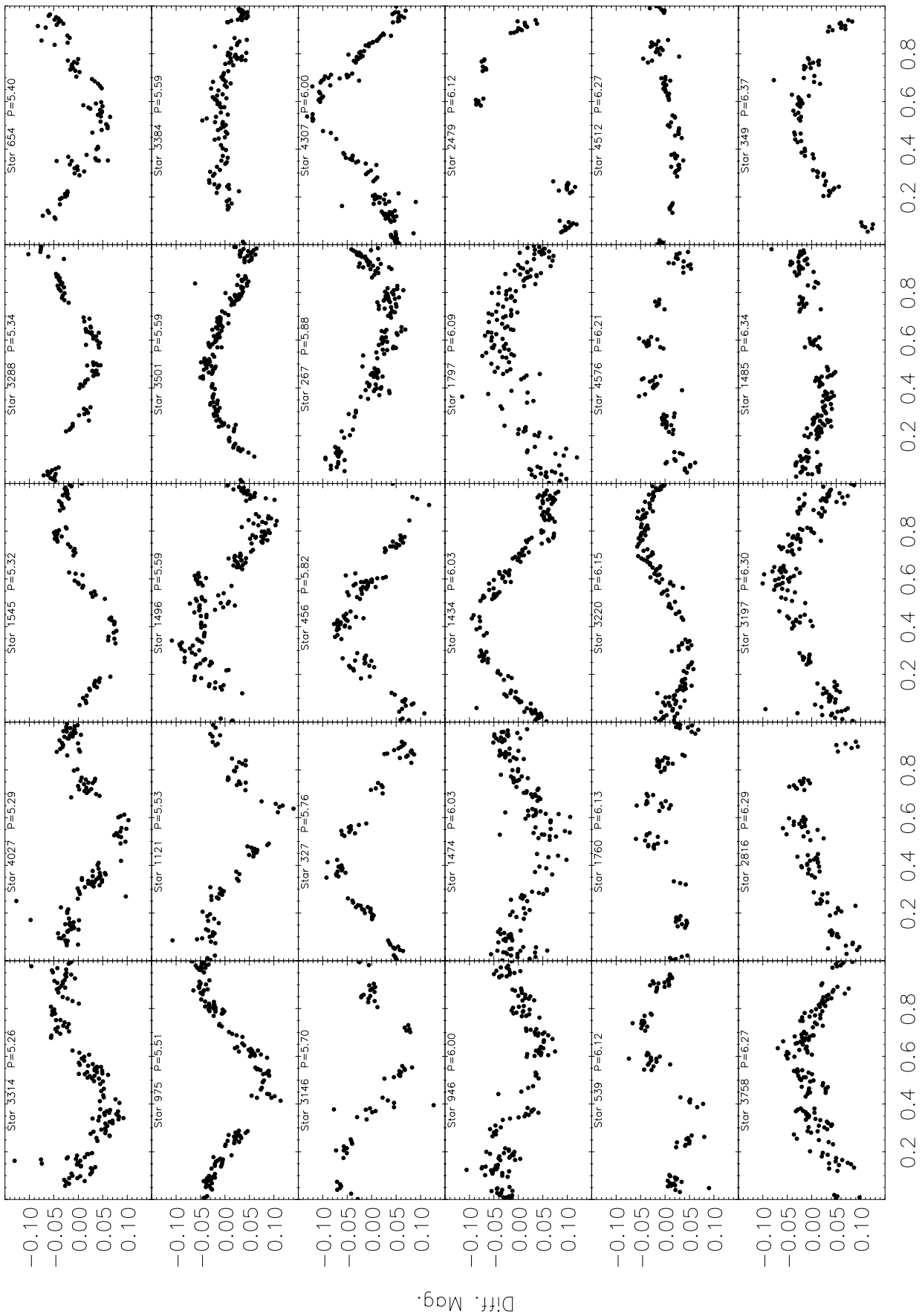


Phase

Fig. 4c

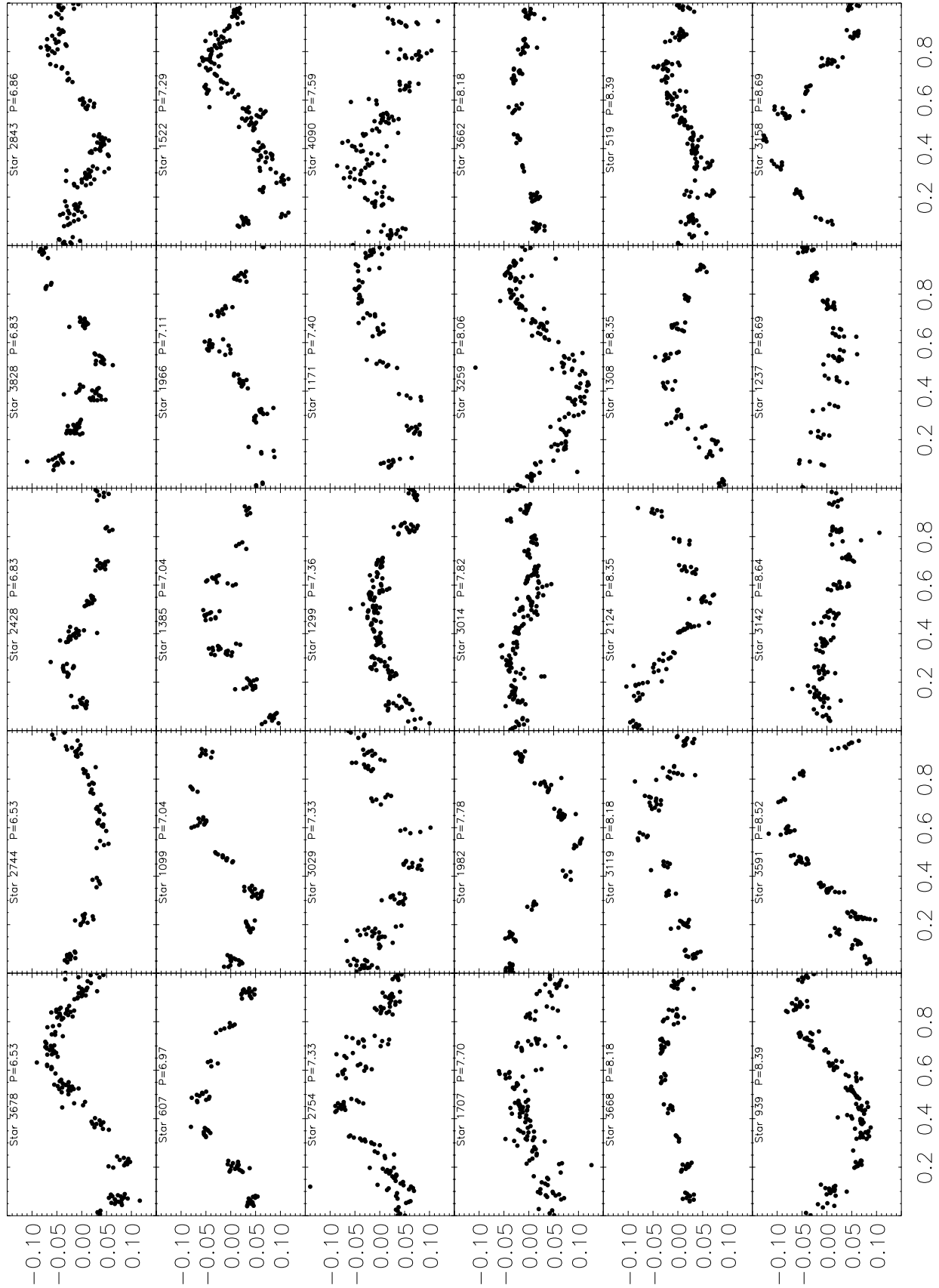


Phase
FIG. 4d

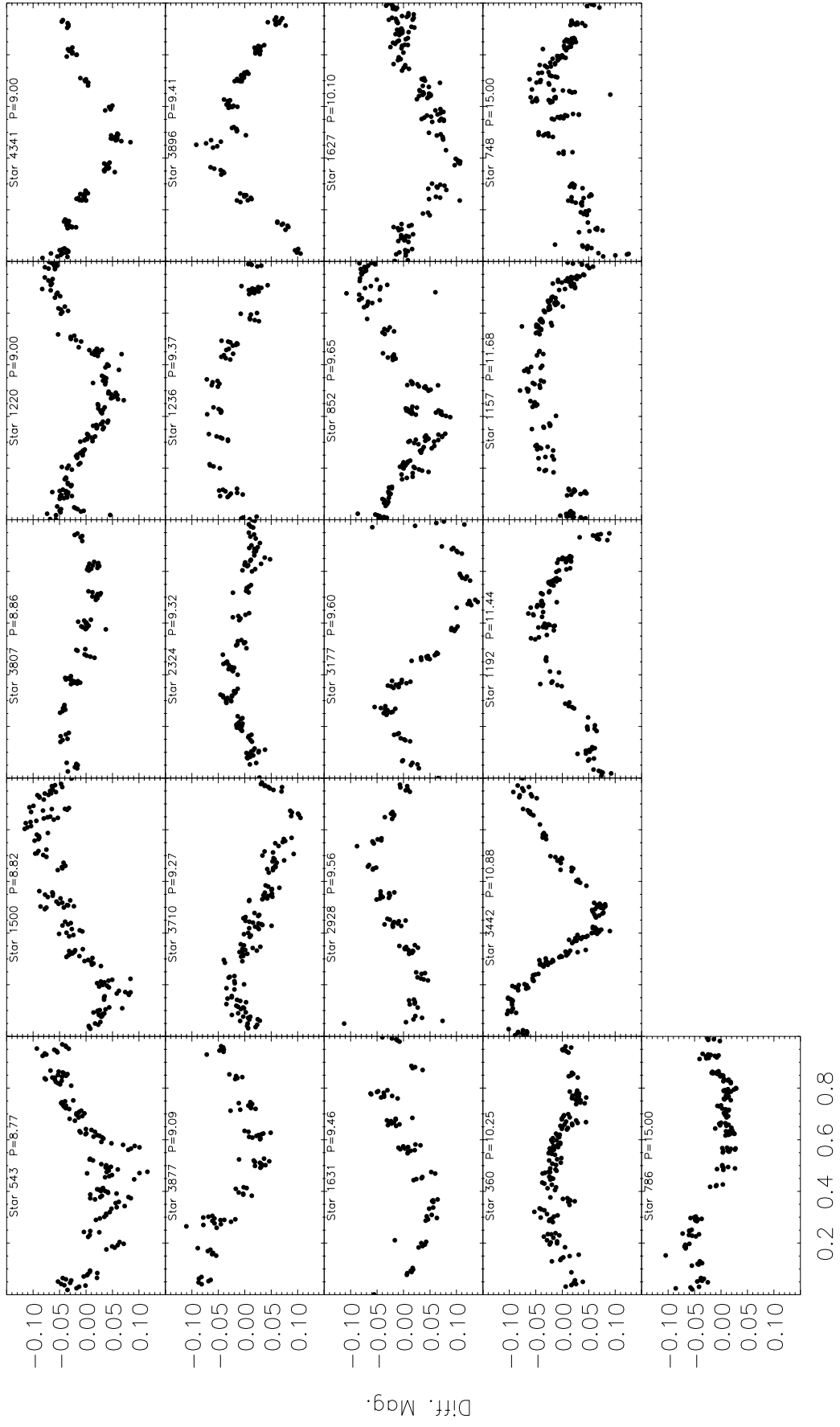


Phase

Fig. 4e



Phase
FIG. 4f



Phase
FIG. 4g

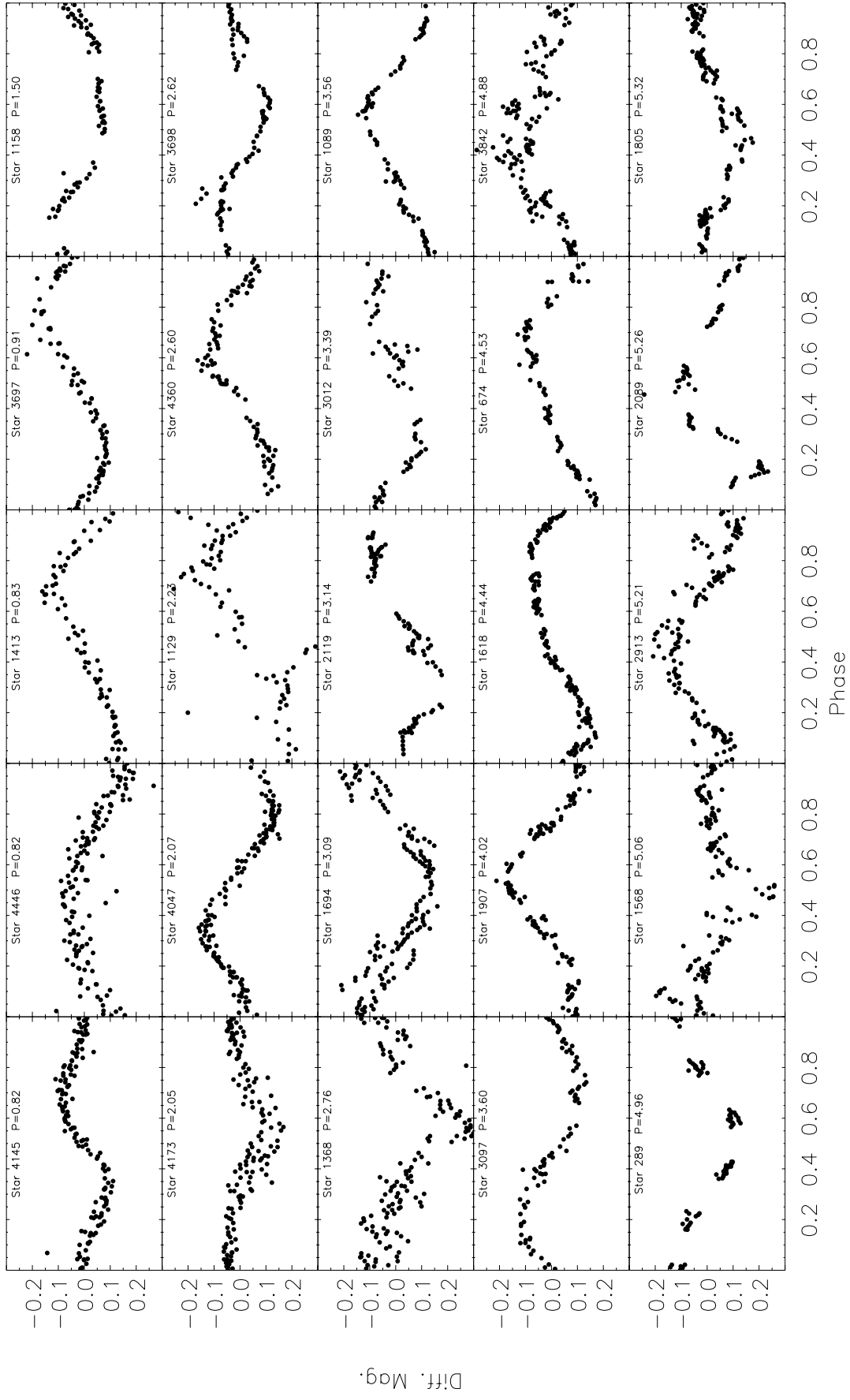
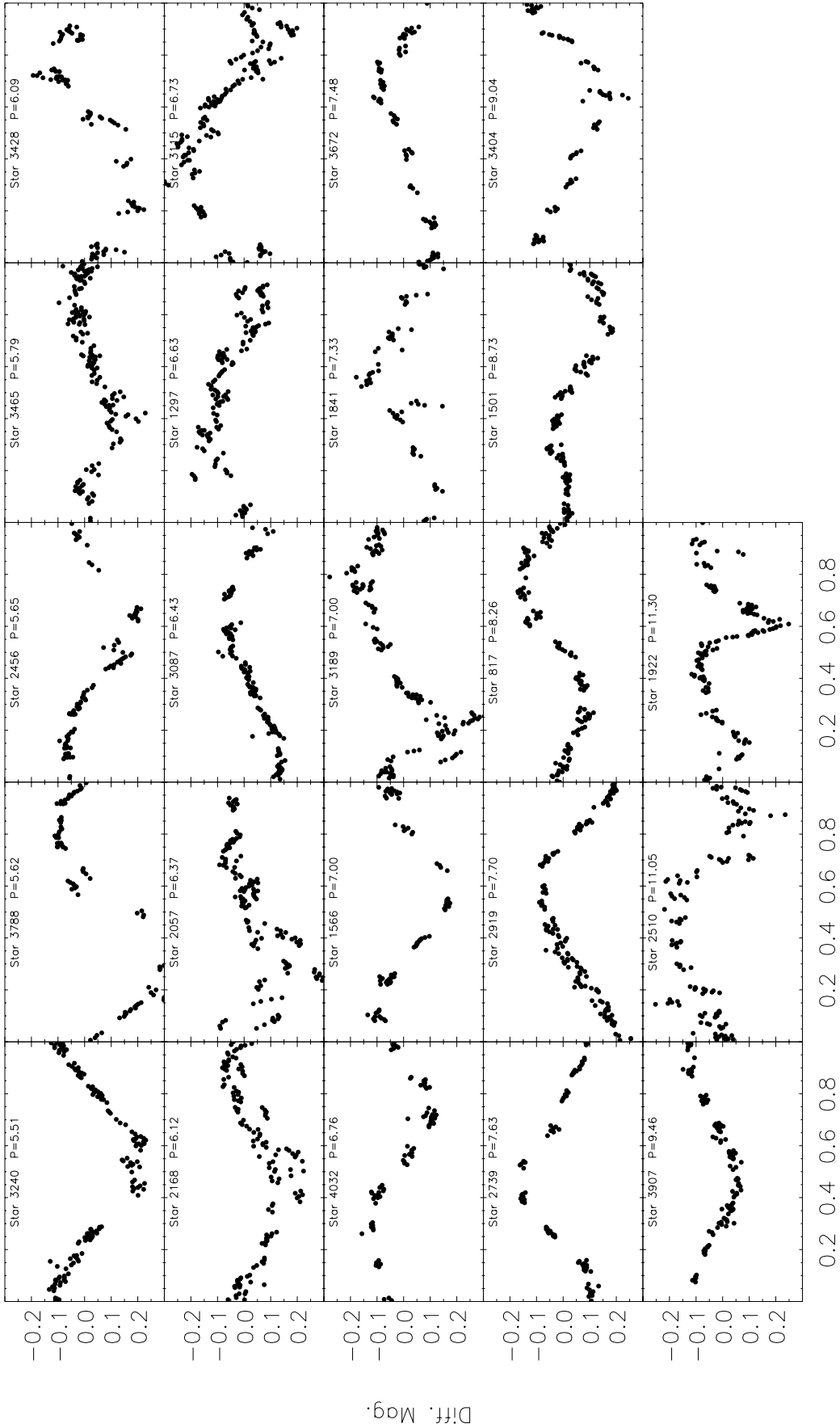


FIG. 4h



Phase

FIG. 4f

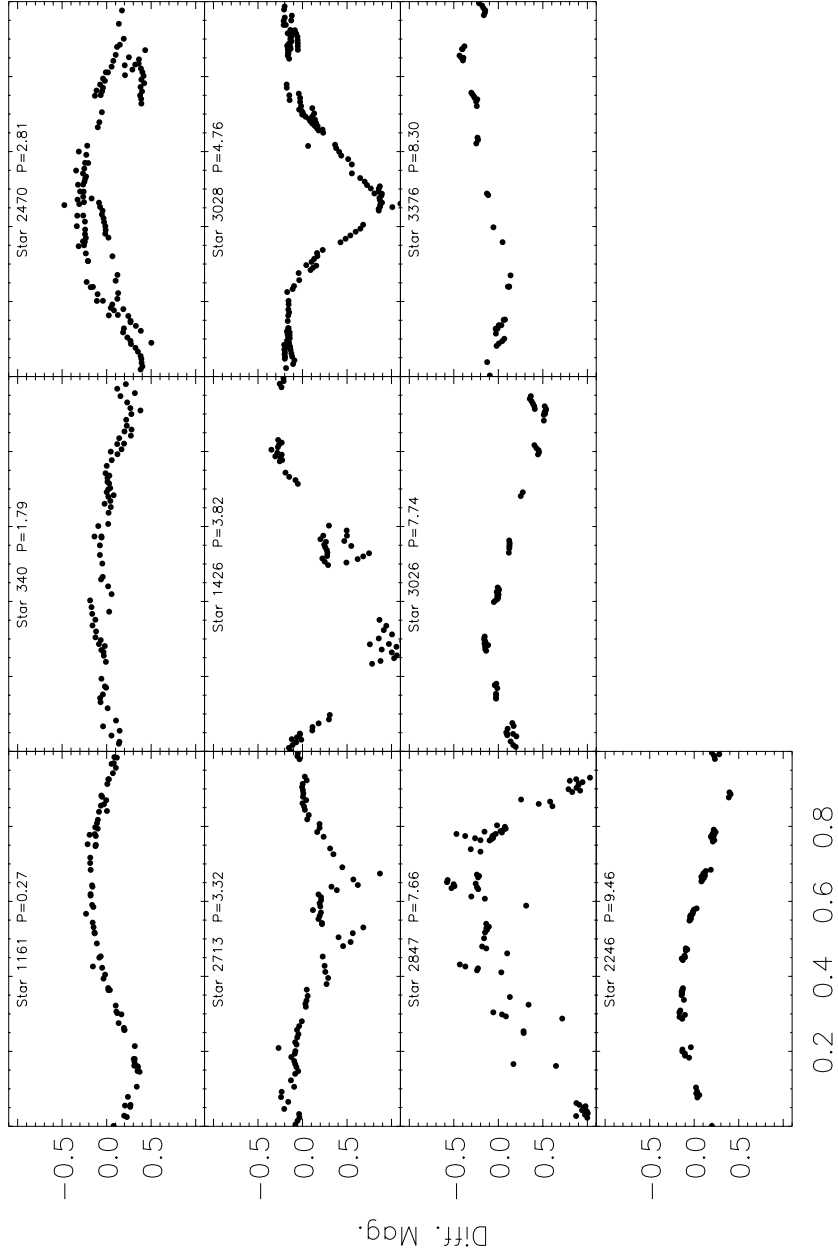


FIG. 4j

TABLE 1
DATA FOR ROTATOR SAMPLE

Star	JW ^a	R.A. ^b	Decl. ^b	<i>I</i> (mag)	<i>P</i> (days)	σ_P^c (days)	P_{CH}^d (days)	$W_j(\text{Hz})^e$ (Å)	$W_j(\text{Li})^f$ (Å)	FWHM(Li) ^f (Å)	R.V. (km s ⁻¹)	Memb. ^a (%)	M^s (M_\odot)	R^e (R_\odot)	v/b_{br}	$\Delta(I-K)^h$
57	05 33 43.16	-06 05 23.4	14.6	4.02	0.13										
169	05 33 51.80	-05 54 25.2	14.0	5.21	0.22										
190	05 33 53.18	-04 56 04.9	14.2	0.74	0.00		0.0	0.39	2.2	26.6					
210	05 33 54.49	-06 02 08.2	13.3	3.00	0.07										
267	05 33 57.64	-05 40 04.9	13.7	5.88	0.08		0.0	0.54	0.8	29.8					
273	05 33 57.87	-05 36 25.9	14.6	1.14	0.01		0.0	0.58	0.7	28.9					
289	05 33 59.38	-04 43 04.4	13.7	4.96	0.20					19.7					
316	05 34 01.01	-06 02 26.3	13.3	3.05	0.07										
327	05 34 01.63	-05 46 51.1	13.7	5.76	0.27					22.3					
340	05 34 02.41	-06 04 30.6	15.9	1.79	0.03										
349	05 34 02.83	-05 49 44.0	13.9	6.37	0.32										
360	05 34 03.61	-05 22 18.6	14.0	10.25	0.84										
456	05 34 08.95	-05 24 04.9	14.0	5.82	0.27		0.0	0.50	0.7	29.8					
507	05 34 12.28	-05 41 33.5	15.7	1.22	0.01										
519	05 34 12.94	-05 42 12.0	13.8	8.39	0.56					24.6					
539	05 34 13.99	-05 47 21.7	14.6	6.12	0.30										
543	05 34 14.15	-05 42 19.7	13.8	8.77	0.62										
607	05 34 17.48	-06 03 37.8	13.8	6.97	0.39										
614	05 34 17.95	-05 33 32.4	12.9	3.19	0.08		0.0	0.61	0.8	21.7		0.28	2.21	0.23	0.29
654	05 34 20.26	-04 58 56.2	14.4	5.40	0.23		0.0	0.56	0.9	24.0					
674	05 34 21.37	-04 55 47.6	14.6	4.53	0.16										
727	05 34 25.11	-04 45 11.0	13.9	4.88	0.19		0.0	0.45	0.7	27.4					
748	05 34 25.99	-05 07 33.2	14.5	15.00 ^j	1.80										
786	05 34 27.75	-05 42 08.9	14.2	15.00 ^j	1.80										
809	05 34 28.75	-05 47 13.6	12.5	1.92	0.03		1.9	0.56	1.4	22.5					
812	05 34 28.99	-05 14 14.2	13.0	3.37	0.09		0.0	0.53	1.2	31.6	0	0.27	3.09	0.36	0.55
817	05 34 29.19	-05 14 39.4	12.7	8.26	0.55		3.1 ⁱ	0.49	0.8	29.1	0	0.80	3.10	0.09	0.57
832	05 34 29.78	-05 04 05.4	14.2	3.69	0.11		0.0	0.61	0.8	27.8					
839	05 34 30.12	-04 58 30.1	13.9	0.75	0.00		0.0	0.40	2.3	18.7					
852	05 34 31.06	-05 21 55.6	14.0	9.65	0.75		0.0	0.53	0.8	25.3	99	0.30	2.08	0.07	0.11
878	05 34 32.83	-05 00 40.1	13.5	0.50	0.00		0.0	0.47	1.9	25.8					
880	05 34 32.92	-05 57 46.6	14.0	1.16	0.01										
939	05 34 36.03	-05 42 14.0	13.2	8.39	0.56					...					
946	05 34 36.47	-05 36 16.1	12.9	6.00	0.29		0.0	0.59	1.4	23.4	33
965	05 34 37.62	-05 43 03.3	13.3	1.86	0.03		0.0	0.59	0.9	26.1					
975	05 34 38.02	-05 27 40.0	14.2	5.51	0.24		0.0	0.27	0.7	18.7	99	0.23	1.46	0.08	0.14
1019	05 34 40.05	-04 58 39.6	12.7	2.35	0.04		0.0	0.44	1.1	33.7					
1089	05 34 42.61	-04 42 14.9	13.1	3.56	0.10										
1093	05 34 42.88	-05 20 06.7	12.7	4.10	0.13		0.0	0.51	0.8	27.2	99	0.49	2.62	0.17	0.20
1099	05 34 43.32	-05 30 06.3	13.9	7.04	0.40	7.44					99	0.39	1.79	0.06	0.50
1121	05 34 44.35	-05 56 14.6	14.5	5.53	0.25										
1126	05 34 44.47	-04 42 14.6	12.3	1.62	0.02										
1129	05 34 44.66	-05 33 41.3	14.2	2.23	0.04										
1157	05 34 45.81	-05 41 08.6	14.2	11.68	1.09										
1158	05 34 45.82	-05 24 55.4	13.7	1.50	0.02		0.0	0.54	1.7	31.4	99	0.38	1.84	0.31	0.42
1161	05 34 45.93	-04 49 22.0	15.4	0.27	0.00		0.0	0.00	0.0	...					

TABLE 1—Continued

Star	JW ^a	R.A. ^b	Decl. ^b	<i>I</i> (mag)	<i>P</i> (days)	σ_P ^c (days)	P_{CH}^d (days)	$W_\lambda(\text{H}\alpha)^e$ (Å)	$W_\lambda(\text{Li})^f$ (Å)	FWHM(Li) ^f (Å)	R.V. (km s ⁻¹)	Membr. ^a (%)	M^g (M_\odot)	R^g (R_\odot)	v/v_{br}	$\Delta(I-K)^h$
1171.....	83	05 34 46.48	-05 23 25.2	14.7	7.40	0.44						99	0.26	1.98	0.09	0.37
1192.....		05 34 47.42	-05 46 30.1	13.2	11.44	1.05										
1219.....	95	05 34 48.23	-05 37 21.9	12.8	1.31	0.01		2.4	0.55	1.9	18.8	95	0.40	1.96	0.39	0.22
1220.....		05 34 48.33	-05 05 01.4	13.7	9.00	0.65		0.0	0.53	0.8	20.1					
1224.....		05 34 48.40	-05 41 57.2	12.7	3.00	0.07		0.0	0.47	0.9	28.5					
1235.....	99	05 34 48.74	-05 23 17.5	13.0	1.69	0.02		43.4 ⁱ	0.40	2.6	20.2	99	0.24	2.97	0.72	0.50
1236.....	101	05 34 48.80	-05 31 45.1	15.1	9.37	0.70						99
1237.....		05 34 48.83	-04 57 14.1	15.2	8.69	0.60										
1279.....	120	05 34 50.77	-05 29 24.5	14.3	0.75	0.00		0.0	0.59	2.1	15.1	99	0.16	1.83	0.96	-0.06
1292.....		05 34 51.33	-05 00 11.2	14.7	3.16	0.08		0.0	0.50	0.8	30.2					
1297.....	123	05 34 51.47	-05 25 12.6	13.0	6.63	0.35		14.6 ⁱ	0.43	0.7	24.1	99	1.38	1.90	0.04	1.28
1299.....		05 34 51.67	-05 39 23.1	13.7	7.36	0.43		0.0	0.39	0.7	22.2					
1308.....	128	05 34 52.09	-05 22 31.8	12.6	8.35	0.56		0.0	0.52	0.7	24.7	97	0.15	3.96	0.28	0.32
1325.....	138	05 34 52.83	-05 28 58.5	14.7	4.44	0.16			0.00	0.0	...	99	0.20	1.30	0.09	0.49
1354.....	144	05 34 53.85	-05 27 48.6	15.8	0.80	0.01						99	0.23	1.67	0.66	-0.52
1357.....	148	05 34 54.10	-05 28 53.8	15.2	1.37	0.02						99	0.30	2.56	0.63	0.08
1368.....	149	05 34 54.55	-05 28 17.7	15.3	2.76	0.06						99	0.23	1.35	0.14	0.24
1385.....		05 34 55.34	-05 01 39.4	13.7	7.04	0.40		0.0	0.55	0.7	26.2					
1396.....	158	05 34 55.88	-05 29 25.8	13.3	1.92	0.03		0.0	0.55	1.0	27.6	99	0.28	2.03	0.33	0.71
1407.....		05 34 56.20	-06 04 17.3	13.8	4.39	0.15										
1413.....		05 34 56.46	-05 52 06.8	14.3	0.83	0.01		3.5	0.56	2.2	23.7					
1426.....	169	05 34 56.86	-05 22 06.1	16.2	3.82	0.12						99
1428.....	171	05 34 56.92	-05 22 59.6	14.9	1.16	0.01						99	0.17	1.31	0.37	0.13
1434.....		05 34 57.16	-05 42 01.9	14.1	6.03	0.29										
1440.....	174	05 34 57.36	-05 30 41.4	14.1	1.36	0.01	1.36		0.63	1.7	32.5	99	0.27	1.47	0.29	0.12
1452.....		05 34 57.83	-05 29 45.4	14.3	4.64	0.17										
1453.....	181	05 34 57.83	-05 29 45.4	15.1	1.36	0.01						99	0.23	1.66	0.38	0.52
1465.....	178	05 34 58.11	-05 09 27.5	14.0	1.28	0.01		5.8 ⁱ	0.61	0.8	18.3	17	0.27	1.85	0.44	0.40
1474.....	186	05 34 58.44	-05 32 49.2	16.0	6.03	0.29						99	0.23	2.30	0.14	-0.27
1485.....	188	05 34 58.81	-05 28 02.8	14.2	6.34	0.32		0.0	0.00	0.0	...	99	0.23	1.44	0.07	-0.03
1496.....		05 34 59.24	-05 05 30.1	14.1	5.59	0.25		24.3 ⁱ	0.47	0.7	28.0					
1500.....	191	05 34 59.47	-05 23 59.8	14.2	8.82	0.62	8.54		0.33	0.7	24.6	99	0.24	1.90	0.07	0.18
1501.....	192	05 34 59.53	-05 25 39.5	13.6	8.73	0.61		0.0	0.44	0.7	24.2	99	0.29	1.74	0.06	0.71
1511.....	196	05 35 00.16	-05 18 50.8	14.3	1.54	0.02		0.0	0.36	1.5	23.5	95	0.38	1.89	0.32	0.28
1522.....	203	05 35 00.74	-05 38 07.1	13.7	7.29	0.43		8.4 ⁱ	0.28	0.8	26.2	98	0.35	2.09	0.08	0.63
1541.....		05 35 01.27	-05 55 54.7	12.9	2.02	0.03										
1545.....	211	05 35 01.39	-05 28 20.2	14.0	5.32	0.23		0.0	0.46	0.7	21.7	99	0.25	1.79	0.11	0.24
1566.....	3013	05 35 02.01	-05 15 37.3	14.0	7.00	0.39		0.0	0.47	0.8	28.1		0.23	1.57	0.07	0.18
1568.....	222	05 35 02.08	-05 29 09.3	14.1	5.06	0.20	5.17	0.0	0.44	0.9	23.6	98	0.25	2.14	0.14	0.71
1618.....	239	05 35 03.82	-05 29 02.8	12.8	4.44	0.16		0.0	0.42	1.0	-6.1	99	0.24	2.80	0.25	0.38
1627.....	243	05 35 03.97	-05 26 36.7	13.6	10.10	0.82						99	0.26	1.93	0.06	0.64
1631.....	245	05 35 04.10	-05 26 27.4	14.0	9.46	0.72						99	0.25	2.08	0.07	0.61
1692.....	280	05 35 05.64	-05 26 25.7	13.4	1.99	0.03		0.0	0.55	1.5	31.7	99	0.21	2.35	0.46	0.37
1694.....	284	05 35 05.67	-05 33 55.1	14.4	3.09	0.08		48.5 ⁱ	0.42	0.8	23.0	99	0.22	1.89	0.21	1.18
1707.....		05 35 06.07	-05 45 30.9	13.2	7.70	0.47										
1753.....	308	05 35 07.52	-05 36 18.9	12.5	4.20	0.14						0	0.16	3.25	0.41	...
1760.....	311	05 35 07.75	-05 29 17.0	14.9	6.13	0.30	6.13					99	0.20	1.57	0.08	0.22
1795.....		05 35 09.06	-05 06 47.1	12.5	4.55	0.17		0.0	0.60	0.9	27.8					

TABLE 1—Continued

Star	JW ^a	R.A. ^b	Decl. ^b	<i>I</i> (mag)	<i>P</i> (days)	σ_P^c (days)	P_{CH}^d (days)	$W_\lambda(\text{H}\alpha)^e$ (Å)	$W_\lambda(\text{Li})^f$ (Å)	FWHM(Li) ^f (Å)	R.V. (km s ⁻¹)	Memb. ^a (%)	M^g (M_\odot)	R^g (R_\odot)	v/v_{br}	$\Delta(I-K)^h$
1797.....	3134	05 35 09.11	-05 30 57.9	16.3	6.09	0.30						
1805.....	334	05 35 09.50	-05 28 22.4	13.6	5.32	0.23		6.5 ⁱ	0.41	0.9	26.3	99	0.30	2.03	0.12	1.20
1841.....	347	05 35 10.51	-05 21 55.7	12.6	7.33	0.43	7.33	0.0	0.35	0.7	28.5	99	0.39	2.35	0.09	0.81
1872.....		05 35 11.17	-05 41 35.5	16.2	1.10	0.01										
1907.....		05 35 11.81	-05 45 37.7	13.3	4.02	0.13										
1922.....	379	05 35 12.08	-05 30 20.2	15.2	11.30	1.02	5.65	0.0	0.42	1.0	34.8	99	0.13	1.87	0.07	0.07
1944.....		05 35 12.44	-04 51 55.5	12.9	2.40	0.05										
1966.....	383	05 35 12.64	-05 16 13.5	14.5	7.11	0.40		0.0	0.48	0.9	29.3	99	0.22	1.86	0.09	0.33
1982.....	388	05 35 12.75	-05 15 24.0	13.5	7.78	0.48	9.08	0.0	0.52	0.8	23.1	99	0.37	2.72	0.11	0.06
2036.....	406	05 35 13.38	-05 17 10.3	13.9	2.26	0.04	2.25	0.0	0.43	1.5	27.3	99	0.21	3.89	0.86	0.31
2037.....	416	05 35 13.40	-05 30 48.2	14.1	2.14	0.04		0.0	0.46	0.8	22.2	99	0.21	1.73	0.27	-0.02
2057.....	422	05 35 13.57	-05 28 46.4	14.4	6.37	0.32		22.8 ⁱ	0.36	0.9	18.6	99
2089.....		05 35 13.94	-05 52 08.9	12.8	5.26	0.22		7.3 ⁱ	0.40	0.7	24.9					
2119.....		05 35 14.31	-04 55 22.2	14.4	3.14	0.08		9.8 ⁱ	0.58	0.9	28.7					
2121.....	447	05 35 14.35	-05 32 45.9	14.8	2.60	0.05						99
2124.....	439	05 35 14.38	-05 17 25.5	14.9	8.35	0.56	8.30	0.0	0.56	0.9	26.9	99	0.28	2.23	0.09	0.62
2168.....	467 ^k	05 35 14.83	-05 36 38.5	14.5	6.12	0.30		0.0				99	0.21	1.63	0.12	0.35
2169.....		05 35 14.84	-05 56 36.0	14.6	3.98	0.13							0.33	1.63	0.04	1.18
2246.....	485	05 35 15.63	-05 26 28.4	14.4	9.46	0.72						99	0.15	1.42	0.60	-0.08
2256.....		05 35 15.72	-05 03 26.1	16.2	4.46	0.16										
2301.....	517	05 35 16.18	-05 31 00.8	15.0	0.85	0.01						99
2318.....		05 35 16.33	-05 42 39.3	12.4	4.04	0.13		0.0	0.45	0.8	26.0					
2324.....		05 35 16.41	-05 40 18.1	14.0	9.32	0.69										
2390.....		05 35 17.06	-05 41 54.0	14.8	2.05	0.03										
2425.....	545	05 35 17.41	-05 09 49.1	15.2	1.71	0.02						99	0.13	1.44	0.33	-0.09
2428.....	550	05 35 17.45	-05 17 40.1	14.5	6.83	0.37		0.0	0.32	1.4	...	99	1.29	4.92	0.16	1.10
2456.....		05 35 17.79	-04 44 52.4	12.8	5.65	0.26										
2470.....	579	05 35 17.87	-05 35 15.7	14.7	2.81	0.06										
2479.....	563	05 35 17.91	-05 15 38.6	14.9	6.12	0.30	5.80					99	0.23	1.55	0.17	0.76
2510.....	3140	05 35 18.23	-05 31 42.0	16.0	11.05	0.98						99	0.36	2.38	0.12	-0.35
2583.....	614	05 35 18.90	-05 37 36.7	12.8	1.07	0.01		3.3	0.54	1.7	27.2	0	0.27	2.39	0.78	0.14
2654.....	628	05 35 19.72	-05 30 37.6	14.3	2.26	0.04		0.0	0.60	1.3	10.5	99
2667.....	639	05 35 19.87	-05 33 53.5	13.6	5.16	0.21						99
2698.....	649	05 35 20.20	-05 32 16.9	15.7	2.13	0.04						98	0.06	2.61	0.94	0.27
2703.....		05 35 20.27	-05 02 26.7	14.0	4.96	0.20		0.0	0.60	0.6	29.6					
2713.....	651	05 35 20.49	-05 20 43.4	15.2	3.32	0.09						99
2739.....	664	05 35 20.92	-05 16 37.5	14.2	7.63	0.47	7.19	0.0	0.47	0.9	32.2	99	0.49	2.59	0.09	-0.18
2744.....	672	05 35 20.96	-05 28 09.2	13.9	6.53	0.34		0.0	0.33	0.8	28.9	98	0.43	1.79	0.07	0.69
2754.....		05 35 21.15	-05 42 12.4	13.7	7.33	0.43		9.6 ⁱ	0.50	0.8	19.4					
2784.....	677	05 35 21.51	-05 09 49.7	14.7	3.96	0.13		24.3 ⁱ	0.28	0.8	22.1	99	0.22	1.26	0.09	0.60
2816.....	691	05 35 21.84	-05 15 01.0	15.5	6.29	0.32	6.34					98	0.16	2.58	0.19	0.22
2843.....	719	05 35 22.20	-05 35 26.7	14.4	6.86	0.38						99	0.14	1.92	0.12	0.10
2847.....	710	05 35 22.24	-05 24 14.3	13.0	7.66	0.47	7.63					99	0.27	2.45	0.11	0.68
2876.....		05 35 22.71	-05 44 42.7	13.5	0.57	0.00		0.0	0.72	3.8	28.5					
2913.....	735	05 35 23.24	-05 28 10.2	14.8	5.21	0.22						99	0.21	1.65	0.10	0.75
2918.....	733	05 35 23.32	-05 18 50.6	13.1	3.32	0.09		0.0	0.52	0.9	28.9	99	0.28	2.55	0.27	0.58
2919.....	731	05 35 23.38	-05 10 51.7	12.3	7.70	0.47	7.64					88	0.35	2.51	0.10	0.28
2928.....		05 35 23.56	-05 52 29.1	13.9	9.56	0.73										

TABLE 1—Continued

Star	JW ^a	R.A. ^b	Decl. ^b	<i>I</i> (mag)	<i>P</i> (days)	σ_P ^c (days)	P_{CH}^d (days)	$W_\lambda(\text{H}\alpha)^e$ (Å)	$W_\lambda(\text{Li})^f$ (Å)	FWHM(Li) ^f (Å)	R.V. (km s ⁻¹)	Memb. ^a (%)	M^g (M_\odot)	R^g (R_\odot)	v/v_{br}	$\Delta(I-K)^h$
2973.....	758	05 35 24.38	-05 26 31.6	14.1	2.49	0.05	2.51	39.5 ⁱ	0.29	1.7	21.5	99	0.15	2.75	0.55	0.48
3007.....	778	05 35 25.16	-05 33 21.1	15.0	1.71	0.02						99	0.16	2.43	0.64	-0.63
3012.....		05 35 25.29	-05 53 21.4	13.7	3.39	0.09										
3014.....	771	05 35 25.34	-05 10 48.1	12.5	7.82	0.49		0.0	0.44	0.7	22.3	96	1.13	1.74	0.03	-0.05
3016.....	776	05 35 25.35	-05 21 51.6	13.7	4.39	0.15		0.0	0.31	0.9	31.8	99
3026.....	787	05 35 25.60	-05 30 21.1	12.6	7.74	0.48					23.8	99	0.30	2.26	0.09	...
3028.....	788	05 35 25.61	-05 30 38.2	14.4	4.76	0.18		26.0 ⁱ	0.50	0.8	19.0	99	0.17	2.34	0.21	0.28
3029.....		05 35 25.62	-04 49 31.2	14.8	7.33	0.43										
3032.....	789	05 35 25.64	-05 29 35.5	16.0	3.21	0.08		0.0	0.54	2.2	27.3	99	0.20	1.97	0.23	-1.07
3063.....		05 35 26.52	-04 56 06.6	13.2	0.91	0.01										
3082.....	813	05 35 27.36	-05 26 28.3	12.3	2.84	0.06	2.85		0.32	0.8	29.5	99	0.31	2.51	0.29	0.56
3087.....	815	05 35 27.42	-05 27 26.1	13.7	6.43	0.33	6.40		0.56	0.9	24.2	99	0.22	2.04	0.11	0.52
3088.....	818	05 35 27.43	-05 35 19.4	12.0	4.62	0.17		0.0	0.31	0.9	26.9	98	0.31	2.84	0.22	0.26
3097.....	816	05 35 27.66	-05 18 04.6	15.3	3.60	0.10			0.28	1.8	35.5	99	0.28	2.18	0.20	1.53
3113.....		05 35 28.08	-05 00 49.5	14.0	0.84	0.01		3.6	0.45	0.0			0.27	1.91	0.09	0.60
3115.....	822	05 35 28.10	-05 11 37.5	15.4	6.73	0.36		0.0	0.00	0.0	...	99	0.15	2.25	0.90	-0.11
3119.....		05 35 28.23	-05 59 13.1	13.9	8.18	0.54										
3122.....	828	05 35 28.28	-05 18 23.0	13.9	1.14	0.01		0.0	0.43	1.2	14.6	99	0.15	2.25	0.90	-0.11
3134.....		05 35 28.58	-04 47 26.6	14.3	5.21	0.22										
3142.....	835	05 35 28.82	-05 35 06.7	14.0	8.64	0.60		0.0	0.57	0.9	23.7	99	0.23	1.62	0.06	0.24
3146.....		05 35 28.92	-05 49 48.5	12.2	5.70	0.26										
3152.....		05 35 29.21	-05 45 38.1	14.4	1.69	0.02	10.77		0.41	1.2	27.4					
3158.....	837	05 35 29.39	-05 16 33.3	13.2	8.69	0.60		0.0	0.30	2.7	28.7	99	0.34	2.21	0.08	0.62
3161.....	843	05 35 29.59	-05 31 12.4	13.7	0.84	0.01			0.30	0.9	19.9	98	0.27	1.89	0.70	0.02
3177.....		05 35 30.15	-05 51 16.8	13.2	9.60	0.74		0.0	0.30	0.9	24.7	99	0.20	1.98	0.14	0.35
3178.....	848	05 35 30.20	-05 25 51.8	13.7	5.03	0.20		29.4 ⁱ	0.29	0.8	24.7	99	0.30	1.54	0.06	0.79
3189.....	855	05 35 30.41	-05 28 30.7	14.2	7.00	0.39	7.02		0.37	0.8	19.9	99	0.20	2.13	0.13	0.15
3197.....	860	05 35 30.58	-05 27 16.9	14.0	6.30	0.32	6.35		0.50	0.9	22.7	99	0.23	1.35	0.10	0.59
3205.....		05 35 30.83	-05 43 05.3	13.3	3.86	0.12		0.0	0.24	0.5	16.4	99	0.14	2.56	0.23	-0.06
3217.....	864	05 35 31.13	-05 12 28.0	14.3	3.74	0.11		0.0	0.46	2.3	28.9	99
3218.....		05 35 31.16	-05 58 33.2	14.0	3.71	0.11										
3220.....		05 35 31.18	-05 40 10.7	13.4	6.15	0.30										
3230.....		05 35 31.46	-05 40 27.7	15.4	4.04	0.13										
3240.....	878	05 35 31.61	-05 30 04.2	14.5	5.51	0.24	1.65		0.62	0.7	24.1	99	0.20	1.42	0.08	-0.05
3259.....		05 35 32.19	-05 44 06.0	14.6	8.06	0.52					24.5	99	1.12	1.80	0.16	-0.20
3263.....	883	05 35 32.27	-05 18 07.8	13.2	0.85	0.01		0.0	0.44	0.9	23.8	96	0.39	2.42	0.13	0.09
3288.....		05 35 32.94	-04 43 59.0	12.7	5.34	0.23					26.9	99
3314.....	900	05 35 33.76	-05 38 20.5	14.6	5.26	0.22		0.0	0.62	0.7	24.1	99	0.20	1.42	0.08	-0.05
3341.....	907	05 35 34.83	-05 29 14.4	12.7	1.65	0.02					24.5	99	1.12	1.80	0.16	-0.20
3376.....		05 35 36.32	-05 01 15.5	11.6	8.30	0.55		11.7 ⁱ	0.44	0.9	23.8	96	0.39	2.42	0.13	0.09
3384.....	926	05 35 36.62	-05 37 41.3	12.7	5.59	0.25					26.9	96	0.39	2.42	0.13	0.09
3385.....		05 35 36.62	-05 58 55.9	14.1	3.58	0.10										
3397.....	925	05 35 37.09	-05 10 29.5	13.8	4.71	0.18						93
3404.....		05 35 37.38	-05 51 28.0	15.6	9.04	0.06										
3406.....	930	05 35 37.50	-05 27 16.6	14.0	2.79	0.05	2.87		0.29	0.9	26.6	99	0.54	2.03	0.16	-0.71
3428.....		05 35 38.45	-04 59 41.0	14.2	6.09	0.30		29.1 ⁱ	0.50	0.8	29.4	99
3430.....	935	05 35 38.56	-05 09 56.6	15.3	3.00	0.07						99
3438.....	943	05 35 38.81	-05 36 33.0	15.5	2.55	0.05						32	0.14	1.55	0.24	0.08

TABLE 1—Continued

Star	JW ^a	R.A. ^b	Decl. ^b	<i>I</i> (mag)	<i>P</i> (days)	σ_P ^c (days)	P_{CH}^d (days)	$W_\lambda(\text{H}\alpha)^e$ (Å)	$W_\lambda(\text{Li})^f$ (Å)	FWHM(Li) ^f (Å)	R.V. (km s ⁻¹)	Membr. ^a (%)	M^g (M_\odot)	R^g (R_\odot)	v/v_{br}	$\Delta(I-K)^h$
3442.....		05 35 38.94	-05 40 59.6	13.5	10.88	0.95		0.0	0.50	0.7	25.5				1.90	-0.13
3447.....	940	05 35 39.00	-05 08 56.4	12.0	1.16	0.01		1.9	0.61	2.5	35.6	95	0.16	3.87		
3461.....		05 35 39.76	-04 44 04.9	13.0	1.69	0.02					...					
3465.....		05 35 39.88	-05 06 36.8	15.6	5.79	0.27		0.0	0.00	0.0	...					
3501.....		05 35 40.97	-05 06 25.4	14.1	5.59	0.25		0.0	0.49	0.6	25.4					
3560.....	968	05 35 43.17	-05 09 17.1	12.0	1.03	0.01		2.3	0.61	2.2	31.7	1	0.62	3.04	0.76	-0.20
3591.....		05 35 44.55	-04 50 09.7	13.6	8.52	0.58										
3613.....	984	05 35 45.49	-05 28 23.0	13.7	1.13	0.01	8.46	0.0	0.50	1.3	26.5	95	0.22	1.87	0.56	0.45
3638.....		05 35 46.33	-05 41 00.4	13.6	1.10	0.01		2.9	0.57	1.9	18.6					
3662.....	995	05 35 47.31	-05 13 18.4	12.9	8.18	0.54		0.0	0.53	0.8	25.0	98	0.26	2.24	0.09	0.22
3666.....	998	05 35 47.39	-05 22 49.5	13.2	4.91	0.19		0.0	0.58	0.8	26.2	99	0.23	2.19	0.16	0.11
3668.....	996	05 35 47.46	-05 12 17.9	13.7	8.18	0.54		0.0	0.00	0.0	20.1	0	0.66	1.20	0.02	-0.18
3672.....	1000	05 35 47.57	-05 19 14.3	15.3	7.48	0.45		0.0	0.00	0.0		77	0.30	1.27	0.04	1.43
3678.....	1004	05 35 48.08	-05 31 55.7	13.7	6.53	0.34		0.0	0.46	0.7	25.0	99	0.36	1.61	0.06	0.31
3697.....		05 35 48.77	-05 00 28.3	14.7	0.91	0.01		0.0	0.00	0.0	24.6					
3698.....		05 35 48.90	-05 01 39.2	14.0	2.62	0.06		3.0	0.53	0.8	27.6					
3710.....	1008	05 35 49.41	-05 35 26.1	12.7	9.27	0.69		0.0	0.46	0.7	27.6	92	0.30	2.24	0.08	0.03
3742.....		05 35 51.02	-05 07 09.0	12.4	4.98	0.20		2.6	0.56	0.8	26.3					
3756.....	1020	05 35 51.94	-05 28 47.2	12.6	4.91	0.19		0.0	0.47	0.8	25.9	99	0.60	1.76	0.07	-0.01
3758.....		05 35 52.12	-05 39 24.4	14.7	6.27	0.31										
3788.....		05 35 53.98	-04 47 19.5	13.9	5.62	0.25		0.0	0.00	0.0	...					
3799.....		05 35 54.61	-05 06 27.9	15.5	0.73	0.00		0.0	0.00	0.0	...	0
3807.....	1031	05 35 54.90	-05 13 15.6	13.9	8.86	0.63		0.0	0.00	0.0	...					
3828.....		05 35 55.99	-04 56 55.0	12.8	6.83	0.37		0.0	0.49	0.6	28.2					
3831.....		05 35 56.09	-05 52 28.3	14.1	0.51	0.00		0.0	0.15	2.2	61.0					
3842.....		05 35 56.81	-05 45 19.1	14.6	4.88	0.19		0.0	0.51	0.9	23.3					
3853.....		05 35 57.43	-05 39 51.0	14.5	1.77	0.03		0.0	0.00	0.0						
3877.....		05 35 58.89	-05 59 08.1	14.2	9.09	0.66		0.0	0.00	0.0						
3885.....	1044	05 35 59.40	-05 37 09.4	14.6	2.99	0.07		0.0	0.00	0.0	18.9	87	0.16	1.84	0.24	0.23
3891.....		05 35 59.86	-05 04 30.9	16.2	1.01	0.01										
3896.....		05 36 00.13	-04 43 46.1	14.5	9.41	0.71										
3907.....		05 36 00.70	-05 41 06.1	13.0	9.46	0.72										
3918.....	1048	05 36 01.30	-05 19 10.5	15.0	1.18	0.01										
3933.....		05 36 02.55	-05 07 36.6	12.5	2.52	0.05		0.0	0.54	0.9	25.3	99	0.12	1.70	0.63	-0.20
3965.....		05 36 04.42	-05 09 28.8	12.5	1.11	0.01		0.0	0.55	1.4	28.9					
3993.....		05 36 06.35	-04 41 54.0	13.2	0.55	0.00		3.7	0.29	0.8	22.4					
4005.....		05 36 07.20	-05 40 21.8	13.0	4.48	0.16		3.6	0.55	0.8	23.8					
4021.....	5087	05 36 08.61	-05 21 02.0	13.8	0.81	0.01		0.0	0.45	2.2	21.4		0.18	2.10	1.03	-0.02
4027.....		05 36 08.89	-05 44 47.8	14.2	5.29	0.22		0.0	0.51	0.8	25.1					
4032.....		05 36 09.10	-05 51 02.7	13.8	6.76	0.37					25.8					
4046.....		05 36 09.89	-05 05 35.5	16.2	0.54	0.00										
4047.....	5123	05 36 09.97	-05 27 31.7	15.5	2.07	0.03		0.0	0.00	0.0	...		0.21	2.27	0.42	-0.97
4079.....		05 36 11.31	-05 38 51.2	14.9	0.34	0.00										
4090.....	5162	05 36 12.06	-05 33 29.5	15.9	7.59	0.46							0.16	2.69	0.17	-0.25
4112.....		05 36 12.98	-04 55 13.6	14.7	4.10	0.13		0.0	0.40	2.3	46.3					
4145.....		05 36 14.57	-05 37 34.6	13.3	0.82	0.01										
4163.....		05 36 15.69	-04 55 20.0	15.4	1.24	0.01										
4173.....		05 36 16.26	-05 40 01.8	15.4	2.05	0.03										

TABLE 1—Continued

Star	JW ^a	R.A. ^b	Decl. ^b	<i>I</i> (mag)	<i>P</i> (days)	σ_P^c (days)	P_{CH}^d (days)	$W_\lambda(\text{Hz})^e$ (Å)	$W_\lambda(\text{Li})^f$ (Å)	FWHM(Li) ^f (Å)	R.V. (km s ⁻¹)	Memb. ^g (%)	M^g (M_\odot)	R^g (R_\odot)	v/v_{br}	$\Delta(I-K)^h$
4226.....		05 36 19.18	-05 00 28.3	15.7	1.57	0.02		0.0	0.00	0.0	...					
4307.....		05 36 24.15	-05 44 48.4	12.5	6.00	0.29					18.2					
4338.....	5065	05 36 25.48	-05 18 41.9	15.3	1.31	0.01										
4341.....		05 36 25.71	-04 50 19.8	13.4	9.00	0.65										...
4358.....		05 36 26.77	-05 56 29.8	16.2	2.21	0.04										
4360.....		05 36 26.82	-04 55 06.0	16.0	2.60	0.05										
4366.....		05 36 27.24	-05 46 42.2	12.6	5.08	0.21										
4418.....	5079	05 36 29.66	-05 20 06.8	13.7	5.06	0.20		9.6 ⁱ	0.52	0.9	27.1		0.34	1.80	0.10	0.44
4426.....	5078	05 36 30.07	-05 20 06.0	13.5	2.46	0.05		3.1	0.53	1.2	29.6	
4446.....	5117	05 36 31.44	-05 25 59.6	16.3	0.82	0.01		0.0	0.00	0.0	...		0.11	0.79	0.30	...
4450.....		05 36 31.58	-05 26 35.4	14.2	4.60	0.17		0.0	0.59	0.9	23.8					
4471.....		05 36 32.79	-06 00 49.9	15.7	0.65	0.00										
4505.....		05 36 34.28	-05 40 54.4	15.4	1.26	0.01										
4512.....		05 36 34.55	-05 32 13.8	12.7	6.27	0.31		0.0	0.51	0.8	27.8					
4556.....		05 36 36.96	-05 04 40.9	12.8	3.67	0.11		8.8 ⁱ	0.53	1.2	54.0					
4576.....		05 36 38.03	-05 37 09.9	15.2	6.21	0.31										

NOTE.—Units of right ascension are hours, minutes, and seconds, and units of declination are degrees, arcminutes, and arcseconds (2000.0).

^a Source: Jones & Walker 1988. ID numbers 3000- and 5000- correspond to ID numbers from Hillenbrand 1997.

^b Coordinates referenced to USNO-A1.0 astrometric database.

^c Uncertainty computed as in text. A value of zero indicates an uncertainty less than 0.005 days.

^d Source: CH.

^e A value of zero indicates no detected Hz emission outside the nebular line. Values indicate *emission* strength.

^f A value of zero indicates no detected Li absorption. Values indicate *absorption* strength.

^g Source: Hillenbrand 1997.

^h Source: Hillenbrand et al. 1998.

ⁱ Strong Hz emitter.

^j Detected at limit of period search.

^k Hillenbrand (1997) identifies this star as JW466.

on all frames using the DAOFIND algorithm, with the sharpness, roundness, and threshold detection parameters set liberally to ensure detection of all stellar sources. We extract instrumental magnitudes for all detected objects on each frame and assemble a raw light curve (a time series of instrumental magnitudes) for each star.

A particular star may fail to appear on a given frame for various reasons. For example, stars near the edges of our frames may be missed on some exposures because of telescope pointing errors, while stars near the CCD saturation limit may be missed because of variations in seeing, sky brightness, and sky transparency. Our light curves are therefore inhomogeneous to varying degrees, with some detected objects appearing on every frame, others appearing only once. Typically, however, a star either appears on nearly every frame, with spurious sources (e.g., cosmic rays, nebular “knots”) appearing only once or twice. To eliminate spurious sources, we have manually inspected our CCD frames at the positions of all detected sources, and have rejected objects visually indistinguishable to us from nebular structure. In addition, to ensure our ability to perform time-series analysis on stars in our database, we have eliminated stars that appear on fewer than 15 frames (typically stars near the edges of our CCD frames and/or stars near our magnitude limits). Finally, we removed stars with photometry strongly contaminated by close neighbors. The resulting database contains 4693 sources with approximately $12 < I < 18$. Nearly all JW stars in this magnitude range are included.⁷ A typical star has about 75 measurements, spanning 10 nights, with a sampling rate of 1 hr^{-1} . Stars with Wise data (1076 stars, $\sim 25\%$ of our database) benefit from an increase in number of measurements (~ 150), time span (17 days), and phase coverage (Wise data largely fill in diurnal gaps in KPNO/USNO data). The sample light curve in Figure 3 shows our typical sampling pattern.

We apply the Honeycutt (1992) algorithm for differential CCD photometry on an inhomogeneous ensemble to our raw light curves to remove noncosmic frame-to-frame photometric variations. We favor this technique for differential photometry because it does not require a particular set of comparison stars to be chosen a priori, nor does it require a star to appear in every frame. Outside the heavy nebulosity in roughly the central $3'$ of the survey region, our photometry is flat-field limited ($\sigma_{\text{mag}} \sim 1\%–2\%$) for $I < 16.5$. Stars in the center of the region typically have $\sigma_{\text{mag}} \sim 5\%$.

2.2.3. Final Database Construction

We constructed our final photometric database by merging the light curves from our KPNO, USNO, and Wise data. We searched our USNO and Wise data for positional matches to stars in our KPNO data. Because of the poorer seeing in our USNO and Wise data, relatively few matches were made in the central $2'–3'$ of the nebula. Beyond about $3'$ of the center of the nebula, however, nearly

all sources were positively matched. Consequently, most stars within $2'–3'$ of the center of the nebula have light curves spanning only 5 days, whereas stars beyond about $3'$ have light curves spanning 10–17 days.

We have adjusted our instrumental magnitude scale to an absolute one by comparing our mean instrumental magnitudes for the JW stars in our database to the magnitudes determined by JW. The distribution of residuals (difference between mean I magnitude determined by us and I magnitude reported by JW) shows an rms spread of about 0.2 mag. This spread is probably a reflection of the stellar photometric variability that typifies stars in this region (0.1–0.2 mag). We thus caution that our reported mean I magnitudes are only approximate, not only because we have not strictly calibrated our photometry, but because of the ubiquity of photometric variability among the stars in our database.

In summary, our synoptic photometric database contains light curves for 4693 objects with $12 < I < 18$ in a $40' \times 80'$ region centered on the Orion Nebula. Of these, 2637 stars have $12 < I < 16.5$, for which our photometric precision is flat-field limited to $\lesssim 0.02$ mag. Photometric precision is also a function of location in the field, with stars within the central $2'–3'$ having degraded photometric precision of approximately 0.05 mag caused by heavy nebulosity. In addition, most stars in this central part of the nebula have light curves spanning only five nights because of difficulties with source matching. In this study, we restrict our analysis to the subset of 2279 stars with $12 < I < 16.5$ and with light curves spanning at least 10 days. This sample includes 698 stars with data spanning 17 days.

2.3. Photometric Period Detection

Periodic photometric variability, presumably due to the presence of stellar spots, is a commonly used diagnostic of stellar rotation period in photometric variability studies of TTS (e.g., CH; Herbst et al. 1994). Unfortunately, periodic photometric variability can be difficult to observe among TTS. Spots are notoriously transient, often appearing one observing season but not another (e.g., CH). In addition, TTS often exhibit irregular (i.e., nonperiodic) variability that may mask any underlying periodicity. When available, however, photometric periods are superior to $v \sin i$ measures of stellar rotation in that the observed period yields the stellar rotation period directly, free from inclination projection effects.

In this section we describe the method by which we detect periodic variability in our synoptic photometric database. We also discuss our assessment of the quality of these periods and our period detection efficiency. We report periods for 254 stars in our sample.

2.3.1. Technique

The Scargle (1982) periodogram analysis is commonly employed to detect periodic variability, because of its ability to handle unevenly sampled data and because its statistical characteristics are well understood. We apply the periodogram to search a grid of 1000 frequencies corresponding to periods $0.1 < P < 15$ days. We adopt these search limits because our pseudo-Nyquist minimum period is twice the average sampling period, or 2 hr in our case, and because a star with a 15 day period will complete slightly more than one cycle if it has data spanning all 17 nights. The nonregularity of our sampling pattern carries with it the benefit

⁷ About 10% of the JW stars in this magnitude range do not appear in our database because: (1) Many stars near the bright end of this range were saturated on many of our CCD frames and were consequently culled for possessing too few good observations. (2) Some JW stars are situated on our CCD frames such that saturation bleeds from neighboring bright stars prevented their measurement via aperture photometry. And, most importantly, (3) ubiquitous photometric variability among these stars makes the I magnitudes uncertain by 0.1–0.2 mag.

that the strong aliasing arising from an evenly spaced sampling pattern is mitigated in our data.

Typically, a false alarm probability (FAP)—the probability that a signal detected at a certain power level could have been produced by statistical fluctuation—is quoted as the statistical measure of confidence in a detected period. The FAP statistic provides a measure of the confidence with which a detected period violates the null hypothesis. Horne & Baliunas (1986) provide an analytical expression for estimating a FAP for relatively evenly spaced data, and Press et al. (1992) give a more generalized scheme for estimating a FAP via Monte Carlo simulation.

As discussed by Herbst & Wittenmyer (1996), however, these methods are not entirely suitable when applied to synoptic studies of TTS, because they only test against random fluctuations of a purely statistical nature (i.e., measurement error) and do not additionally account for correlated fluctuations intrinsic to the source. TTS, particularly CTTS, frequently exhibit large-amplitude intrinsic photometric variability on timescales that are long compared to the highly frequent sampling rate of a monitoring campaign such as ours. Our repeated measurement of such objects during a single night are not, therefore, independent and uncorrelated. Consequently, typical schemes for estimating a FAP, which account only for a single-dispersion source of uncorrelated noise in the data stream, will overestimate the significance of any measured periodic variability, because a single-dispersion model will ascribe very high statistical significance to multiple data points in a given night clustered near a common value. A technique that accounts for stochasticity intrinsic to the source, in addition to that arising from measurement, is required.

Hence, we employ a two-dispersion Monte Carlo method for estimating the FAP of our detected periods, as per Herbst & Wittenmyer (1996). For each candidate star, we generate a set of 100 synthetic light curves, each consisting of normally distributed noise with two dispersions: one representing the variability of the candidate star during a night and one representing the night-to-night variability of the candidate star. We estimate the former by taking the mean of each night's standard deviation, and we estimate the latter by taking the standard deviation of nightly means. In this way, the test light curves have the freedom to vary on timescales that are long compared to our sampling interval, allowing them to mimic the random slow variability of stellar origin that could produce spurious periodic behavior over our limited observing window. We compute a periodogram for each test light curve and take the maximum observed power level in these 100 periodograms as the level of 1% FAP. Note that this Monte Carlo technique actually assumes nothing about the origin of the variability observed in a given star's light curve; this is not a simulation per se. Rather, it represents an expansion of the null hypothesis to include correlated variability on timescales long compared to the sampling interval. Furthermore, since for each star we generate test light curves with the same dispersions present in the actual data (rather than, say, injecting only 0.02 mag noise, because this is the typical precision of our photometry), we make no assumptions about the level of noise present in the data. We emphasize that this approach is more conservative than that described in Press et al. (1992), in which a single noise component, the overall variance of the data, is used in the Monte Carlo analysis.

We adopt this measure of FAP as our basic criterion for accepting or rejecting detected photometric variability; we accept only periods whose periodogram signals are stronger than the 1% FAP level. We report our detection of periodic photometric variability for 254 stars in our database in Table 1. In Table 2 we list an additional 16 stars that appear periodic in our database, with $1\% < \text{FAP} < 5\%$, as a way to suggest that they be monitored further, as well as to provide additional comparisons with the periods reported by CH. These 16 stars are not all the stars for which we detected periods with $1\% < \text{FAP} < 5\%$, but those which in our opinion are particularly suggestive of periodicity. Phased light curves for the 254 stars with detected periods are shown sorted by period in Figure 4.

Despite the statistically rigorous tests to which we subject our detected periods and our subjective confidence in their quality, an independent assessment of period believability is desirable. Unfortunately, we do not have multiple seasons of observation at our disposal by which to corroborate periods detected in one season as opposed to another. Instead, we compare the periods detected by us to those determined for the same stars by other researchers. In addition, we check for agreement between our photometric periods and spectroscopic $v \sin i$, as measured from our high-resolution spectra of a subset of these stars (§ 2.4).

Our photometric database shares 53 stars in common with the database of periodic variables discovered by Herbst and collaborators (most recently published in CH). Among these, 25 satisfy our criteria for periodic variability (see Table 1). The agreement of our periods for these 25 stars with those reported in CH is excellent; our periods generally agree to within a few percent. The disagreement is largest (by as much as about 10%) for our periods longer than about 8 days, where the CH periods are more accurate given their longer time baseline and, in some cases, repeated detection over multiple observing seasons. This good agreement extends to another five stars from the CH database which appear in our database with $1\% < \text{FAP} < 5\%$ (see Table 2). Of the remaining 23 stars shared in common with CH, only seven (JW 145, 275, 345, 381, 481, 792, and 850) show some (weak) evidence in our light curves for variability consistent with periodic behavior as reported by CH; the rest show either no variability or strictly random variability in our light curves. Such transience is characteristic of periodic variability among TTS (e.g., CH), and presumed to be due either to spots that have dissipated or to increased erratic variability.

In only two cases do we report a period inconsistent with that reported by CH: stars 1922 (JW 379) and 3613 (JW 984). Our period for the former is exactly twice the period reported by CH, and may represent another instance of “period doubling” as discussed in CH, where, in this case, the light curve observed by us shows direct evidence for spots on opposite hemispheres (also see stars 812, 1501, 3217, and 3341). The second star (3613) is detected by us at a significantly shorter period than that found by CH, near their short-period detection limit, and is almost certainly the result of our more frequent time sampling. We suggest that our periods for these two stars are the correct ones.

The quality of our detected periods is further supported by an observed correlation between photometric period and rotational line broadening within a subset of 121 stars (nearly half of those with detected periods; see § 2.4). Using the width of a photospheric line (Li $\lambda 6708$) as a measure of

TABLE 2
DATA FOR ROTATORS WITH $1\% < \text{FAP} < 5\%$

Star	JW ^a	R.A. ^b	Decl. ^b	<i>I</i> (mag)	<i>P</i> (days)	<i>P</i> _{CH} ^c (days)
758		05 34 26.43	−05 01 00.6	13.4	6.73	
905		05 34 34.17	−06 02 09.3	14.3	5.19	
1228		05 34 48.54	−04 47 49.9	14.7	5.01	
1638	248	05 35 04.28	−05 23 13.5	12.9	6.21	6.86
1784	326	05 35 08.58	−05 29 01.1	15.2	6.63	6.40
1997	393	05 35 12.93	−05 19 04.2	15.0	4.83	
2093	429	05 35 13.97	−05 19 52.2	12.6	5.24	
2481	566	05 35 17.93	−05 16 13.4	14.8	7.04	
3033	786	05 35 25.65	−05 26 42.0	14.0	8.47	8.80
3077	812	05 35 27.13	−05 30 24.8	14.0	4.39	
3084	811	05 35 27.40	−05 17 09.7	13.4	10.62	11.05
3228	872	05 35 31.33	−05 28 16.6	15.2	4.26	
3231		05 35 31.47	−05 05 47.4	15.6	12.91	
3359	914	05 35 35.53	−05 15 43.1	13.2	7.98	7.71
4370	5146	05 36 27.44	−05 30 55.3	13.2	5.88	
4409		05 36 29.19	−04 53 51.0	14.2	6.27	

NOTE.—Units of right ascension are hours, minutes, and seconds, and units of declination are degrees, arcminutes, and arcseconds (2000.0).

^a Source: Jones & Walker 1988. ID numbers 3000- and 5000- correspond to ID numbers from Hillenbrand 1997.

^b Coordinates referenced to USNO-A1.0 astrometric database.

^c Source: CH.

(projected) stellar rotation, we find that the expected linear trend of increased line broadening with increasing angular velocity is indeed observed. Figure 5 shows the FWHM of the Li $\lambda 6708$ line as a function of angular velocity ($1/P$), where the linear increase in Li FWHM with increasing angular velocity is evident. This good agreement between our photometrically derived rotation periods and observed line broadening confirms (1) the general reliability of our period determinations and (2) the basic interpretation of

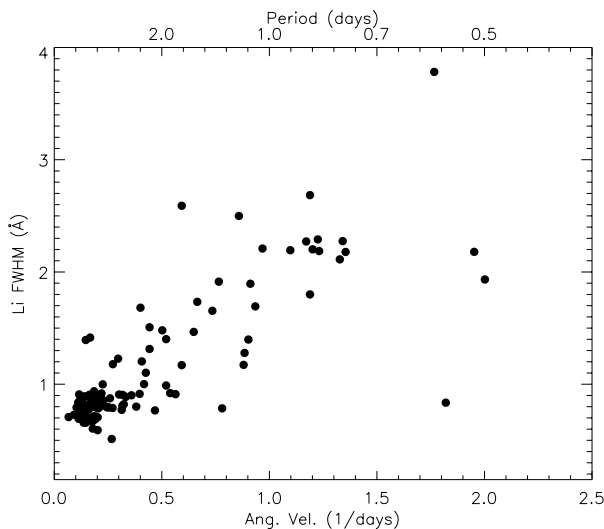


FIG. 5.—Correlation between photometric period and broadening of the Li line $\lambda 6708$ confirms the interpretation of periodic photometric variability as a measure of stellar rotation period. Shown is the FWHM of the Li line vs. $1/P$ (angular velocity, units of days^{-1}). The expected linear increase in line width with increasing angular velocity is apparent, and slow rotators have unbroadened lines. Instrumental resolution is about 0.6–0.7 Å.

periodic photometric variability as a measure of stellar rotation period.

2.3.2. Completeness

In contrast to other TTS photometric monitoring programs in the literature, where typically the survey region is monitored 1–2 times per night over many weeks to months (or years, e.g., CH), our ability to detect periods is very sensitive at extremely short periods (i.e., $P \lesssim 3$ days). Indeed, the unevenness with which our data are sampled gives us the capability of detecting periods that are significantly sub-Nyquist. We are thus confident that we are not significantly biased against detection of short-period photometric variability down to the limiting period that we searched (0.1 days). Practically speaking, we are limited to detection of peak-to-peak variability of about 0.05 mag, given our typical photometric precision of 1%–2%.

We are least sensitive to periods approaching the extent of our typical observing window. To quantify the effect of our observing window on our ability to detect long periods, we have conducted an experiment with which we directly measure our period detection efficiency as a function of period. Among the 254 stars for which we have determined periods, 142 stars (56%) possess Wise data, which provide a 17 day time baseline and more complete phase coverage. We use these stars to assess the effect of our more typical observing window of 10 days (with diurnal gaps) on our ability to detect periods. For each star, we search for a period on just the 10 night KPNO/USNO component of its light curve (i.e., we exclude the Wise data from the period search), applying the Scargle periodogram and Monte Carlo FAP calculation exactly as before. The fraction of these stars meeting our period detection criteria gives us a measure of our period detection efficiency.

Of the 142 periodic stars upon which we performed this experiment, 113 (80%) produced periods at the 1% FAP level. The period distribution of these stars, as a fraction of the total number of stars in each period bin, is shown in

Figure 6. This serves as a direct measure of our period detection efficiency. We see that our efficiency is approximately 90% for $P \lesssim 5$ days, presumably because in these cases we observe at least two full cycles over 10 nights. (The additional 10% detected by including the Wise data results from improved phase coverage.) Our efficiency decreases monotonically to longer periods, falling to about 60% at $P = 8$ days. We fail to detect any periods with $P > 10$ days, indicating that our FAP statistic effectively limits us to detecting periods no longer than our observing window. In addition, nine stars that fail our period detection criteria are nonetheless detected with the correct period with $1\% < \text{FAP} < 5\%$. In only two cases do we detect a bogus period with $\text{FAP} < 1\%$, roughly consistent with expectation, if 1% of our detected periods (142 in this numerical experiment) are “false alarms.”

Comparing periods detected with only 10 nights of data to those detected with 17 nights of data provides a measure of the precision of our periods. For periods shorter than about 2 days, we reproduce the same period to approximately 1%, with about 5% reproducibility for $P \lesssim 5$ days. For periods longer than about 5 days, our detected periods reproduce with approximately 10% precision. This result is in qualitative agreement with what we observe upon comparing our periods with those reported by CH (see above).

Despite our low efficiency for detecting long periods, our period distribution is probably not severely lacking in very slow rotators. Herbst and collaborators (Attridge & Herbst 1992; Eaton et al. 1995; CH), whose period distribution is presumably complete for very long periods, have shown that periods $P > 10$ days are rare. In addition, using spectra we have obtained for 142 stars with detected rotation periods and for 176 stars drawn randomly from our survey region without detected rotation periods (§ 2.4), we have checked for the possibility that our rotator sample is missing a large number of slow rotators. Although our spectra are of limited resolution, we do not find evidence for a disproportionate number of slow rotators in the control sample. Nonetheless, in our analysis of the rotation period

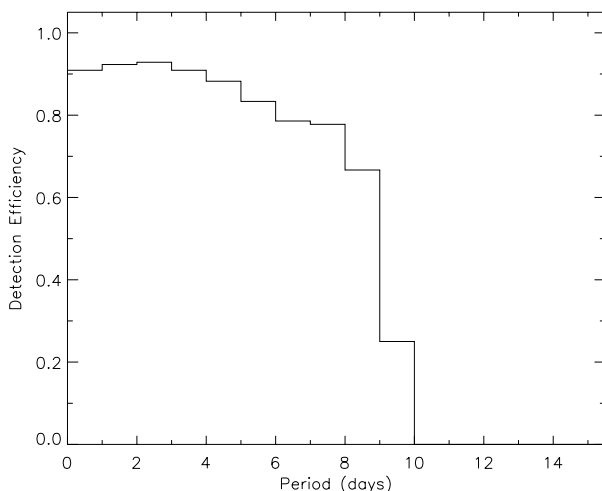


FIG. 6.—Period detection efficiency among stars with light curves spanning 10 days. Using the subset of 142 stars with light curves spanning 17 days as a control, we test our ability to detect periods among stars with our more typical 10 day observing window (see text). We successfully detect periods shorter than 8 days with relatively high efficiency, but rapidly become incomplete for periods longer than this.

distribution in our survey region and its relation to stellar properties of interest, we will focus on periods $P < 8$ days, for which we are not strongly biased.

2.4. Spectroscopy

We obtained spectra of objects in our photometric database so that we could (1) identify active accretion via measurement of stellar $H\alpha$ emission strength and (2) establish association membership via measurement of radial velocity and via detection of the Li $\lambda 6708$ line. All of our spectra were obtained at echelle resolution ($\Delta\lambda \approx 0.2 \text{ \AA pixel}^{-1}$, corresponding to a FWHM $\approx 0.5\text{--}0.8 \text{ \AA}$ given a spectrograph focus of 2.5–4 pixels depending on fiber number) with the WIYN Hydra multiobject spectrograph. We used two different spectrograph configurations, (1) the 6450–6850 \AA region (hereafter “red” configuration) and (2) the 6250–6550 \AA region (hereafter “blue” configuration).

With the red configuration we obtained spectra in 1997 March, 1997 December, and 1998 February for 132 of the stars for which we have determined rotation periods and for 176 additional stars for which no periods have been detected. This spectral region includes the $H\alpha$ Balmer line at 6563 \AA and the Li $\lambda 6708$ resonance line. Without exception, all of these spectra show (unresolved) $H\alpha$ in emission because of the strength of the nebular $H\alpha$ within which the stars in our sample are immersed. Spectra with the blue spectrograph configuration were obtained in 1996 December and 1997 December for 10 of the stars for which we have detected periods and for another 46 stars for which no periods have been detected. This spectral region is particularly useful for providing radial velocity measurements, because this bluer spectral region contains a wealth of lines for cross-correlation, but it contains neither of the two primary diagnostic lines ($H\alpha$ and Li $\lambda 6708$) we use in our analysis.

All spectra were reduced using the IRAF DOHYDRA task. We flat-fielded the target spectra using dome flats and wavelength-calibrated them using ThAr lamp spectra, each obtained with the same fiber configuration as was used for the target observations. Several fibers (~ 10) in each pointing were placed on blank “sky” positions. Because these fibers were typically placed within the nebula as well, they actually represent the sum of the true sky (solar + telluric) spectrum and the nebular spectrum at that location. For each pointing, the various sky fibers are median-combined to produce a single sky spectrum for that pointing.

In this section we describe our methods for measuring stellar $H\alpha$ emission strength, radial velocities, and Li $\lambda 6708$ absorption. These spectroscopic diagnostics of accretion, association membership, and stellar youth will figure importantly in our analysis of the connection among stellar rotation, accretion, and circumstellar disks.

2.4.1. $H\alpha$ Emission: Accretion Diagnostic

Strong stellar $H\alpha$ emission has been a defining property of CTTS since their discovery (e.g., Herbst 1962). In the modern picture, this emission is associated with the accretion of circumstellar disk material onto the stellar surface (e.g., Muzerolle et al. 1998a, 1998b). In this section we describe our technique for measuring the strength of $H\alpha$ emission in our target spectra, and we establish criteria by which we identify stars undergoing active accretion.

For the purpose of measuring stellar $H\alpha$ equivalent widths (EWs), we do not sky-subtract our target spectra

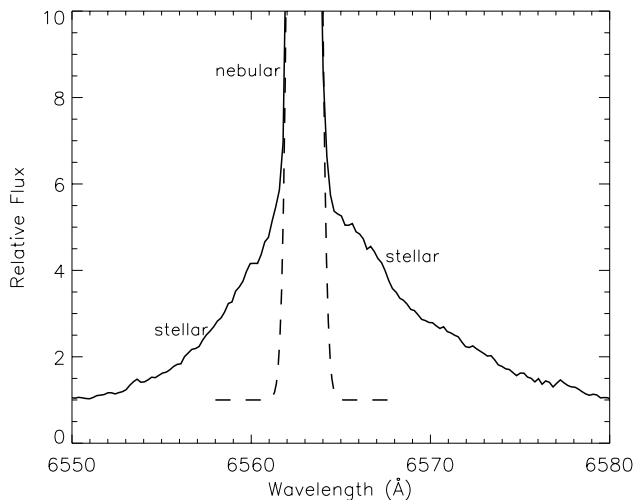


FIG. 7.—Strong stellar H α emission indicative of active accretion in the spectrum of star 1235 ($P = 1.69$ days). The continuum has been normalized to unity. A Gaussian fit to the nebular emission line (dashed line) assists in determining the region beyond which we measure H α EW (see text). This star has $W_{\lambda}(\text{H}\alpha) = 43.4$ Å outside the nebular line (see Table 1).

because spatial variations in the nebula make for extremely poor subtraction of nebular lines. We instead subtract a smooth fit to the sky spectrum continuum, leaving the structure of any emission lines untouched. As a result, the nebular H α emission remains (prominently!) in our target spectra, and we are unable to measure any stellar contribution under the nebular line. We thus take only emission outside the nebular line to be of stellar origin. To demarcate clearly the extent of the nebular emission, we fit a Gaussian to the nebular line with its base forced to the stellar continuum. We emphasize that we do not attempt to subtract this fit, but instead use it only to identify the region where nebular emission is safely negligible. We measure the EW of any emission beyond the wings of this fit by direct summation (as opposed to any kind of fit). This EW measure thus represents a lower limit to the true stellar H α emission EW.⁸ H α EW lower limits for stars with detected periods are reported in Table 1. We use these EWs in our analysis as proxies for active accretion. A sample spectrum is shown in Figure 7.

The dominant source of uncertainty in our EW estimates is the subtraction of sky continuum from our target spectra. Because of the highly variable nature of the nebular background spatially, our sky fibers show varying levels of sky continuum. In some cases, our sky fibers show residual nebular continuum (residual in the sense of having been sky-subtracted using the same median sky continuum applied to our target spectra) at levels of approximately 15% of our faintest targets. This 15% uncertainty in the sky continuum level translates directly into a 15% uncertainty in our EW measurements for our faintest stars. Thus we take this 15% uncertainty as an upper limit on the uncertainty in our measured EWs, reminding the reader that the EWs we report are lower limits.

⁸ This statement would be false for early-type stars (i.e., G and earlier), in which the stellar H α line is frequently observed strongly in absorption. The stars in our sample are of considerably later type (\sim K5 and later); see Fig. 2.

Very broad stellar H α emission can also indicate active accretion in young stars. Thus we also measure the breadth of any stellar emission present in our target spectra. In many cases, we see stellar H α full widths several times that expected from the widths of photospheric absorption lines in the same spectrum. Though WTTS can exhibit broad low-level H α emission, with widths 2–3 times $v \sin i$ (Walter 1998, private communication), we see several instances of H α lines that are considerably broader still.

We can use these H α diagnostics to identify those stars likely to be undergoing active accretion. First, stars exhibiting emission with EWs greater than that observed among WTTS likely have their H α emission powered by the accretion of circumstellar disk material. Second, stars exhibiting particularly broad emission are also good candidates for active accretion activity. Thus we adopt the following as criteria for the identification of active accretion:

1. Stellar H α EW lower limits of at least 20 Å. The strongest H α typically observed among late-type WTTS is about 10 Å (Walter 1998, private communication).
2. Stellar H α full width of at least 6 times the FWHM of a photospheric absorption line. We use the Li λ 6708 for this comparison because it appears in nearly every one of our target spectra. We adopt this factor of 6 to allow for a factor about 2 to roughly convert FWHM to full width and an additional factor of 3 to account for the width of chromospheric H α emission in some WTTS.

Twenty stars in our sample of rotators satisfy one or both of the above criteria for H α emission indicative of active accretion (Table 1). Of course, these 20 stars do not represent *all* CTTS in our sample. In addition to the limitations imposed on us by the strong, ubiquitous nebular H α emission, many of the stars in our sample with near-IR signatures of circumstellar disks do not evince “strong” H α emission as defined in the criteria above (see also § 3.3).

2.4.2. Radial Velocities and Lithium: Membership Diagnostics

Critical to this study is the confirmation that the stars in our sample of rotators are bona fide PMS stars and that they are physically associated with Orion OB1c/d. In this section we describe our methods for confirming the youth and membership of our sample of stars with detected rotation periods.

Membership probabilities for stars in the ONC have been determined by JW in their proper-motion study of approximately the central 15′ radius of the region. Where such measurements are not available for stars in our survey region, we use radial velocities as a diagnostic of cluster membership. True stellar members of Orion OB1c/d possess a common heliocentric radial velocity of about 25 km s⁻¹ with a dispersion of about 2 km s⁻¹ (e.g., JW; R. Mathieu, unpublished data). In addition, strong lithium absorption is a good indicator of stellar youth. Among low-mass stellar members of the Pleiades, $W_{\lambda}(\text{Li})$ is never greater than 0.25 Å; stronger lithium absorption implies PMS status. We assume that stars in our survey region showing such strong lithium absorption are likely to be association members. Thus, we also use the strength of lithium absorption in our target spectra as an indicator of membership.

Using an M2 dwarf spectral standard (HD 95735) as a template (appropriate for the typical spectral types represented in our sample), we measure radial velocities via cross-correlation, masking out prominent nebular features

in the target spectra. Because we only obtained a spectrum of our template star in the red spectrograph configuration, we instead use a solar spectrum obtained in the blue spectrograph configuration for stars with blue spectra.

Of the 142 stars with measured rotation periods which also possess spectra for measuring radial velocities, 130 (92%) are of sufficient signal-to-noise to permit reliable velocity measurements. These are reported in Table 1. In Figure 8 we show the distribution of radial velocities for these 130 stars, as well as a best-fit Gaussian. With the exception of five stars, these radial velocities are consistent with a single distribution of velocities centered at $v_r = 25.6$ km s⁻¹, with a measured dispersion of $\sigma_v = 3.7$ km s⁻¹.

In Table 1 we also present EWs for the stars showing lithium absorption. We detect lithium securely in 90% (118/132) of our sample of rotators that we have observed spectroscopically. In only three cases where we detect lithium do we measure an EW less than 0.25 Å. Thus, the EWs we observe are consistent with an interpretation of these stars as young.

Combining our radial-velocity measurements (130 stars), our lithium measurements (132 stars), and the proper-motion membership probabilities of JW (114 stars), we can confirm which stars among our sample of rotators are members of Orion OB1c/d. Among 69 stars with both JW proper-motion membership probabilities and our own radial-velocity measurements, seven show velocities consistent with membership but low proper-motion membership probability (probability < 85%; stars 812, 817, 946, 1465, 2583, 3560, 3668). However, only one of these seven stars (3668) fails to show strong lithium in its spectrum. In only two instances (2847, 3217) do we detect lithium weaker than 0.25 Å EW in a JW proper-motion member. The former star is also the only instance in which we detect lithium weaker than 0.25 Å EW in a radial-velocity member (the latter star has a radial velocity inconsistent with the association but is a proper-motion member). Among the five stars lying outside our main radial-velocity distribution (Fig. 8), two have JW proper-motion membership probabilities; both are members (probability > 85%). Four of the five show

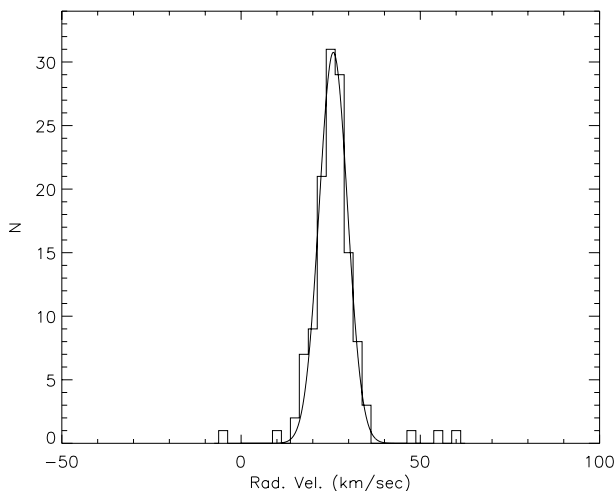


FIG. 8.—Radial velocities indicating membership among our sample of rotators. The Gaussian fit has a mean of 25.6 km s⁻¹ and an rms of 3.7 km s⁻¹, consistent with membership in Orion OB1c/d. Five stars lie outside the distribution, only one of which is likely to be a nonmember; these five stars may be spectroscopic binaries.

$W_\lambda(\text{Li}) > 0.25$ Å. These outliers may therefore be spectroscopic binaries. The union of these data provides determinations of youth and membership for a total of 175 stars in our sample of rotators. Of these, 170 stars satisfy at least one criterion for youth and membership (166 without contradictory information). We note that stars satisfying membership criteria on the basis of lithium and radial velocity are spread over the entire area of our survey region, extending well beyond the JW proper-motion survey region. Based on this spectroscopic and proper-motion sample, representing 70% of the 254 stars with measured rotation periods, we conclude that with few exceptions the stars in our sample of rotators are bona fide PMS members of Orion OB1c/d.

2.5. Summary

From a synoptic photometric database of 2279 stars with approximately $12 < I < 16.5$ in a $40' \times 80'$ region centered on the Trapezium (see Fig. 1), we have determined rotation periods for 254 stars (see Fig. 4). Our light curves are sampled approximately 1 hr⁻¹ and span 10–17 days. Using the subset of our sample with light curves spanning a full 17 nights as a control, we find that our period detection efficiency is $\geq 90\%$ for $P \lesssim 5$ days, falling to about 65% for $P \sim 8$ days (Fig. 6). Fortunately, the long-term monitoring of part of this region by Herbst and collaborators (e.g., CH) indicates that periods much longer than this are rare. We have observed more than half of the 254 stars in our sample spectroscopically to derive accretion and membership diagnostics. Combining our radial-velocity and lithium diagnostics of association membership with proper-motion membership data from the literature, we find that nearly all stars for which we have membership information (170/175) are likely members. We thus infer that stars in our sample are with few exceptions members of Orion OB1c/d. In addition, we use H α emission to identify a set of actively accreting stars.

The stars in our sample are homogeneous in terms of youth ($4 \lesssim \log \tau \lesssim 6.5$), mass ($0.15 \lesssim M/M_\odot \lesssim 0.4$), and internal structure. Our one bias is our lack of adequate light curves for stars in the most central portion ($2'-3'$) of the nebula. Since the stars in our sample are fully convective, and are expected to remain so throughout their PMS evolution, we can explore the evolution of angular momentum without such complicating factors as complex changes in moment of inertia.

3. RESULTS

Having discussed in detail our observations, our methods for determining stellar rotation periods, stellar youth, and active accretion, and additional data from the relevant literature, we now summarize the salient results of our photometric and spectroscopic observations. In particular, for our sample of stars with photometrically derived rotation periods, we consider (1) the distribution of stellar rotation periods, (2) spectroscopic evidence for active accretion, and (3) near-IR detections of circumstellar disks taken from the literature. We use these diagnostics in concert to form a composite picture of the role of circumstellar disks in the rotational evolution of young stars.

3.1. Rotation Period Distribution

We have determined rotation periods for 254 stars, roughly 10% of our total sample of 2279 stars, on the basis

of periodic photometric variability. As we have seen, the periodic variables in our sample are bona fide PMS members of the Orion OB1c/d association, are roughly homogeneous in mass ($0.15 \lesssim M/M_{\odot} \lesssim 0.4$), with derived ages ranging from about 10^4 yr to $\gtrsim 3 \times 10^6$ yr, and with a typical age of approximately 10^6 yr. We begin this section with a description of the morphology of the rotation period distribution, taking special note of a physically significant short-period cutoff. We then report on statistical analyses we have conducted to test for the presence of the period “gap” observed by other investigators.

3.1.1. Distribution Morphology: Evidence for a Physical Short-Period Cutoff

The rotation period distribution we have determined for stars in Orion OB1c/d is shown in Figure 9 (*panel a*). The distribution shown has been truncated at $P = 8$ days as we are strongly biased against longer periods (Fig. 6). The distribution appears roughly uniform in period over the range to which we are sensitive. Correcting the distribution for incompleteness (Fig. 9, *panel a*, *dashed line*) does not significantly alter its morphology. We address the structure of the distribution more quantitatively in § 3.1.2.

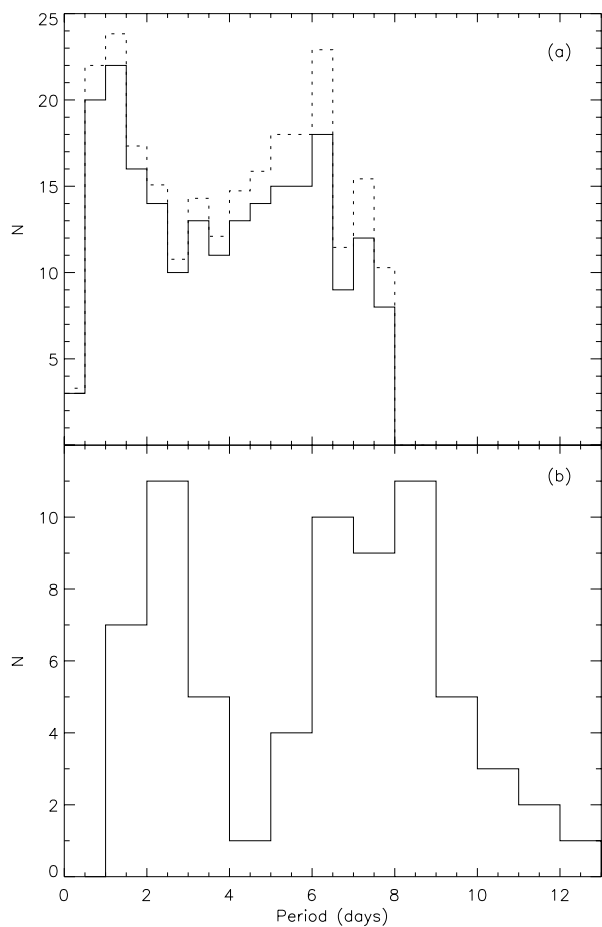


FIG. 9.—(a) Orion OB1c/d rotation period distribution as determined by us with half-day bins (*solid histogram*). The distribution has been truncated at $P = 8$ days as we are strongly biased against periods longer than this (see Fig. 6). Also shown is the distribution corrected for incompleteness (*dotted histogram*). The distribution is statistically indistinguishable from a uniform distribution. (b): For comparison, the ONC distribution of CH is also shown, with one-day bins. Note that the range of the abscissa excludes five stars at longer periods.

Our distribution shows evidence for a physically significant short-period cutoff. Below 1 day the distribution drops sharply, with only 3 stars having periods shorter than 0.5 days. The shortest detected period is 0.27 days. The sharp cutoff of periods below about 0.5 days seen in our period distribution is not an artifact of the period-detection method we employ, nor does it arise from a limitation in our sampling. Considering our typical time sampling of about 1 hr^{-1} , our pseudo-Nyquist period limit is 2 hr, 3 times below the shortest period we detect. In Figure 10 we show that this short-period cutoff can be physically associated with breakup velocity, v_{br} , for the stars in our sample, which we compute using masses and radii available from Hillenbrand (1997) for 108 of our rotators together with our own rotation periods for these stars. These data are also given in Table 1. We see that stars with very short periods are predominantly rotating at or near breakup velocity. The short-period cutoff evident in the period distribution, therefore, is probably a direct consequence of a physical limit in the rotational properties of these stars. To our knowledge, this is the first determination of the short-period limit of the rotation period distribution for PMS stars, the result of our high-frequency sampling.

As an aside, we note that the 254 periodic variables we detected constitute roughly 10% of our total sample (2279 stars). Obviously, all stars in our sample do rotate, and any star with stable stellar spots will exhibit some kind of periodic variations. The detectability of these periodic variations depends primarily on their amplitude and on any competing erratic variations, presumably due to the accretion process. We assume that some fraction of periodic variables could not be detected as such because of larger erratic variations. The approximately 10% detected periodic variables represent those stars that had large enough periodic variation during our observations to be detected in our data. Interestingly, the 50 periodic variables identified by CH also represent about 10% of their total sample (525 stars), as do the 11 periodic variables identified by Eaton et al. (1995) from their sample of 126 stars. This suggests that the fraction of detectable periodic variables may not vary significantly.

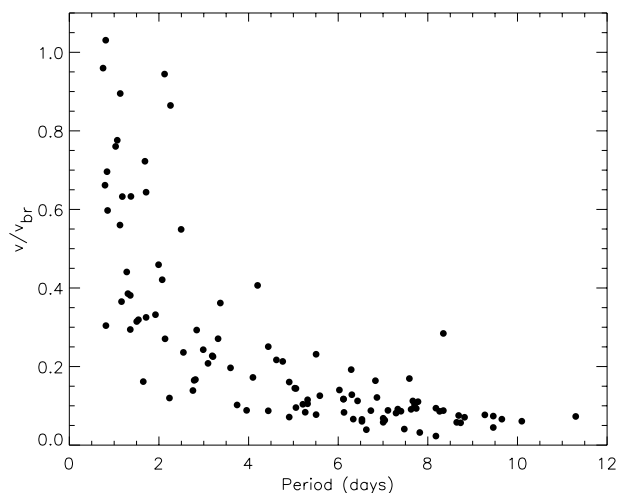


FIG. 10.—Stars rotating at or near breakup velocity in our sample, explaining the observed short-period cutoff evident in the distribution of rotation periods (see Fig. 9).

3.1.2. Statistical Analysis of Structure in the Distribution

Previous investigations of the rotation period distribution in this region (e.g., CH) have emphasized an apparent bimodality marked by a “gap” in the distribution at $P = 4\text{--}5$ days (see Fig. 9, *panel b*)⁹. In this section, we describe statistical analyses we have performed to investigate the presence of such bimodality in the distribution newly determined by us. We report a negative result.

Longward of the short-period cutoff discussed in the previous section, we do not find strong evidence for statistically significant structure in the rotation period distribution, and in particular do not find evidence for a “gap” at $P = 4\text{--}5$ days. Considering periods in the range $0.5 < P < 8$ days (the range above the cutoff over which we do not suffer significant incompleteness), a one-sample K-S test indicates a difference from uniformity at less than 1σ confidence.

Indeed, the CH distribution itself may not differ significantly from a uniform distribution. A one-sample K-S test of the CH distribution against a uniform distribution for $1 < P < 10$ days reveals that the two are only distinguishable at just above the 1σ confidence level. (We choose the period range $1 < P < 10$ days for this comparison because CH were not sensitive to subday periods and because beyond $P = 10$ days their distribution is very sparse.)

We note, however, that the K-S test is not particularly sensitive to deep, narrow notches in distributions because of its reliance on the *cumulative* distribution of the data (Press et al. 1992). Though it is not clear that the “gap” in the distribution observed by CH is sufficiently deep and narrow to be problematic for the K-S test, it is possible that the K-S test may not be well suited for testing the hypothesis of bimodality in this instance. We have attempted to identify more powerful statistical tests for multimodality. A number of tests that are perhaps better suited to identifying departures from unimodality have been suggested to us by E. Feigelson (1999, private communication) and S. Vardeman¹⁰ (1999, private communication), including a Cramer-von Mises test (e.g., Conover 1971) and a quantile-quantile plot analysis (e.g., Nair & Freney 1994). These tests are “K-S-like” in that they compare the observed cumulative distribution to a null hypothesis model (uniform distribution in this case). The Cramer-von Mises test, however, considers the sum-of-square residuals rather than the supremum difference between the model and the data. Similarly, the quantile-quantile plot analysis simultaneously compares all points in the observed distribution with the null hypothesis, rather than comparing the distribution with the model only at the point of maximum departure. Like the K-S test, these tests report that the CH distribution is consistent with the null hypothesis: The Cramer-von Mises test gives a probability of 0.22 that the CH distribution is consistent with a uniform distribution for $1 < P < 10$ days, while a quantile-quantile plot analysis gives a probability of 0.18.

To gain some further insight into the statistical frequency of bimodality, we have also performed a simple Monte Carlo simulation proposed by the referee, in which we gen-

erated 1000 sets of uniformly distributed random numbers, and visually inspected each histogram. For each simulated distribution, we generated 63 numbers between 1 and 10, the same as in the distribution observed by CH. We classified each distribution based on our visual impression of its morphology, reserving “bimodal” for cases showing a deep “dip,” i.e., at least two consecutive bins showing a small number of counts relative to “humps” on either side. We observe bimodality so defined in some 10% of the simulated distributions. Though this approach is subjective, it provides plausibility for the conclusions drawn from the K-S test. We nonetheless encourage continued exploration of the statistical nature of the distributions observed by CH and by us. In what follows, we proceed to apply the K-S test for various statistical analyses, keeping the above discussion in mind.

CH report different period distributions when they consider stars in different spatial subregions of their survey area; the distribution for stars outside regions of high nebulosity contains a larger proportion of rapid rotators. Might a difference between our distribution and that determined by CH become apparent if we conduct separate comparisons of stars near the center of the nebula and stars in more peripheral regions? To test this, we perform a comparison of the CH distribution with our distribution in several spatial subregions (Fig. 11). For these comparisons we take stars with $1 < P < 8$ days (the range over which both samples are not strongly biased), which includes 47 stars from CH and 190 from our sample. First, we compare only stars in the 10 subfields of the JW region surveyed by CH (indicated in Fig. 1; 45 stars). In these regions, a two-sample K-S test yields a probability of 0.92 that the two distributions are indistinguishable. The close resemblance of our distribution to that of CH arises because the two samples of rotators in these 10 subregions share 25 stars in common. We note that the 20 new stars from our sample are uniformly distributed. A one-sample K-S test shows that our distribution in these subregions is indistinguishable from a uniform distribution (K-S probability of 0.60). We also consider the JW region as a whole, this being a region of similar radial extent but one completely surveyed by us. When we compare stars within the entire JW region (94 stars) with the CH distribution, a K-S test gives a probability of 0.55 that the two samples do not differ. Again, a one-sample K-S test shows that our distribution is indistinguishable from a uniform one (K-S probability of 0.30). Finally, comparing our distribution over our entire survey region with the CH distribution yields a K-S probability of 0.10 that the two distributions are similar, representing a difference at less than 2σ confidence. In short, the distribution determined by us and the CH distribution are consistent with each other to within 2σ over our entire survey region. And, as we have shown above, both distributions are statistically indistinguishable from a uniform distribution.

Do stars in our distribution show any spatial trends when compared with each other? To test this, we also perform a spatial comparison between stars in our distribution within $10'$ of the center of the cluster (which we take to be the position of $\Theta^1\text{C Ori}$; 74 stars) to stars beyond $10'$ (180 stars). Once again, a two-sample K-S test shows a difference at less than 1σ confidence.

Because of our bias against detecting periods in the central $2'\text{--}3'$ of the nebula, we cannot perform a spatial analysis of periods for stars very near the Trapezium with

⁹ Note that the CH distribution shown here differs slightly from that shown in CH (their Fig. 7), because for three stars in their sample (JW 167, 174, 907) we have plotted the alternate (lower FAP) period they report. Our independent period determinations for two of these stars (JW 174, 907) corroborate these alternate periods.

¹⁰ Department of Statistics, Iowa State University.

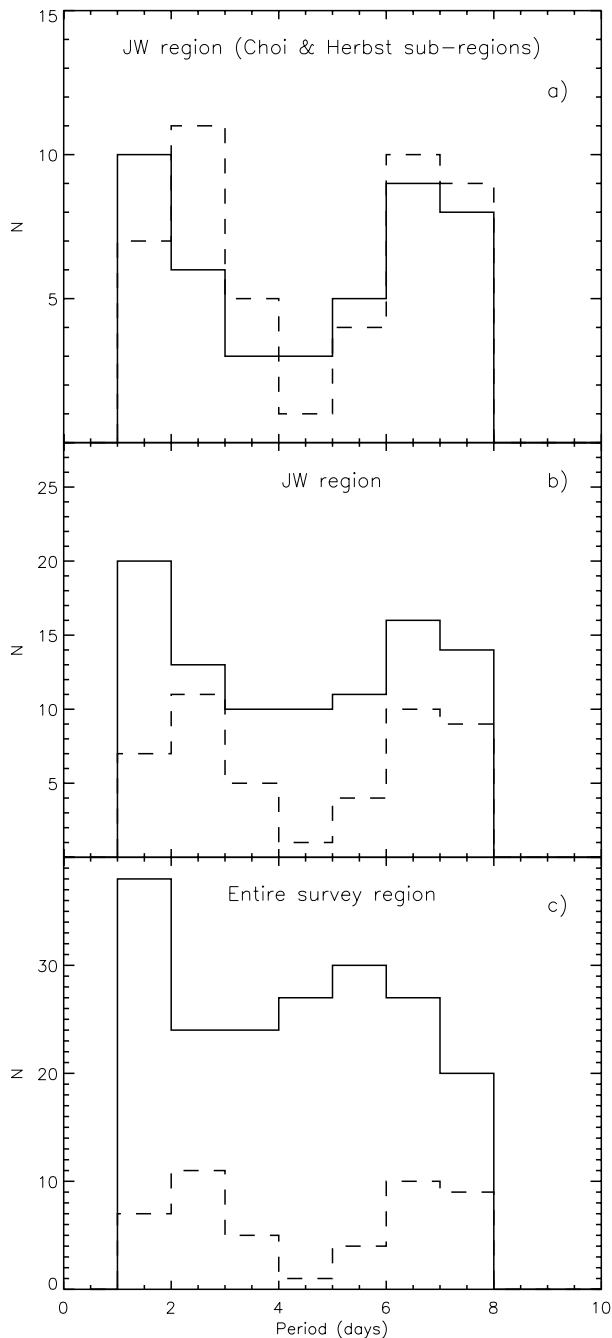


FIG. 11.—Comparisons of our period distribution to that of CH in various spatial regions. For these comparisons, only stars with $1 < P < 8$ days are considered, where both the CH study (dashed histogram) and our study (solid histogram) are not strongly biased. (a): The two distributions for stars in the 10 small subregions of the JW region surveyed by CH (see Fig. 1) strongly resemble one another, because of the presence of 25 stars in common to both studies. (b): Stars drawn from the entire JW proper motion survey region. (c) Stars in the entire region surveyed by us. In all cases, our distribution is consistent with a uniform distribution for $P < 8$ days, and is not statistically distinguishable from the distribution determined by CH.

our own data. However, the central $4' \times 4'$ field surveyed by CH (see Fig. 1) covers this region where we are biased. A one-sample K-S test of the period distribution for the 20 stars with periods reported by CH near the Trapezium reveals that it is consistent with a uniform distribution for

$1 < P < 10$ days (probability of 0.18). In addition, a two-sample K-S test does not indicate a significant difference between the 20 stars in the central CH field to the CH stars outside this central field. These results suggest that our exclusion of stars very near the Trapezium may not significantly affect the morphology of period distribution we have determined.

Is it possible that the lack of an observed bimodality in our distribution is the result of poor resolution in our period detection technique? In other words, might low-frequency resolution resulting from our limited observing window “smear out” an underlying bimodal distribution sufficiently to produce the observed uniform distribution? As discussed by Kovács (1981), the resolution of the periodogram is given by

$$\delta\nu = \frac{3\sigma}{4T\sqrt{NA}},$$

where σ is the uncertainty in the data, T is the total time spanned by the data, N is the number of independent data points, and A is the amplitude of the detected signal. Taking values of σ , T , and A typical of periodic variables in our sample (0.02 mag, 10 days, 0.06 mag, respectively) and taking a very conservative value of 10 for N (assuming that only one measurement per night is truly independent), the frequency resolution of our periodogram is $\delta\nu = 0.008 \text{ day}^{-1}$, corresponding to a resolution in period of 0.16 days for periods in the period gap ($P = 4\text{--}5$ days). We have convolved a hypothetical bimodal distribution consisting of two Gaussian components centered at $P = 2.5$ days and $P = 8.3$ days (simulating the period distribution observed by CH) with a Gaussian kernel with $\sigma_\nu = 0.008 \text{ day}^{-1}$. The resulting smeared period distribution closely reproduces the original bimodal distribution. We conclude, therefore, that we are able to resolve structure in the rotation period distribution at $P = 4\text{--}5$ days.

In summary, the rotation period distribution determined by us for stars in Orion OB1c/d does not show strong evidence for bimodality and is in fact statistically consistent with a uniform distribution over the range of periods to which we are sensitive (though we expect based on the CH distribution that this uniformity does not extend beyond $P \sim 10$ days, where the number of stars drops rapidly). Our intent in comparing our findings with a uniform distribution here is not to propose a particular model for the expected distribution of rotation periods, but instead to test for any significant structure in our period distribution. This result is not changed when we consider spatial subsets of our sample, and we rule out the possibility that we have failed to resolve an underlying bimodal distribution because of a limitation in our period resolution. Our period distribution shows a strong cutoff at $P \lesssim 0.5$ days, corresponding to breakup velocity for the stars in our sample.

3.2. Accretion Among the Rotators

An important question addressed by our work is the connection, if any, between accretion and stellar rotation. In this section, we discuss the signatures of active accretion among our sample of rotators.

Figure 12 (panel a) shows the period distribution (truncated at $P = 8$ days) of those stars for which we have measured “strong” H α emission (as defined in § 2.4.1) and those stars for which Hillenbrand et al. (1998) measure the

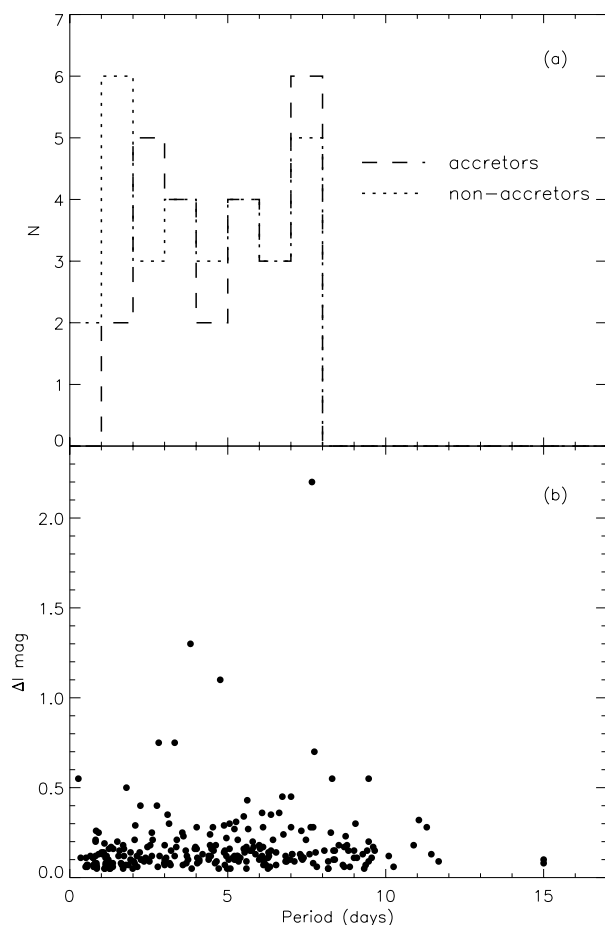


FIG. 12.—Period distributions of stars showing active accretion signatures. (a): Period distribution of stars exhibiting spectral signatures ($H\alpha$ and Ca II emission) of active accretion (*dashed histogram*) is indistinguishable from both the distribution of stars for which spectra are available but do not show evidence for strong accretion (*dotted histogram*) and from the entire distribution (see Fig. 9). The distributions shown have been truncated at $P = 8$ days. (b): Peak-to-peak amplitude of photometric variability against rotation period. Amplitude of variability is not correlated with rotation period.

Ca II triplet in emission.¹¹ Notably, these 26 stars do not appear to cluster at any particular period regime in the distribution. In particular, we find stars showing accretion signatures with rotation periods ranging from among the shortest in our sample ($P = 1.3$ days) to among the longest ($P = 7.7$ days). This subsample of accretors is statistically indistinguishable both from the entire distribution (a two-sample K-S test yields a probability of 0.19 that the distribution of actively accreting stars could be drawn from the overall distribution) and from the distribution of stars for which spectra are available but which do not show evidence for accretion (K-S probability of 0.63), also shown in Figure 12. Furthermore, we find that 10% (11/109) of rapid rotators ($P \leq 4$ days) show accretion signatures and that 13% (19/145) of slow rotators ($P > 4$ days) do, so that again we find no evidence that stars with strong $H\alpha$ or Ca II emission are distributed preferentially in any region of period space.

¹¹ As discussed in Hillenbrand et al. 1998, because of the low spectral resolution ($\sim 5\text{--}8 \text{ \AA}$) of their observations, the Ca II emission and absorption features are blended together, so that *net* emission probably indicates strong accretion.

The amplitude of variability among our periodic variables might also be taken as an indicator, albeit a crude one, of accretion activity, as those with peak-to-peak variations exceeding about 0.5 mag are likely to possess hot spots on their surfaces (Herbst et al. 1994). Though the largest amplitude variable in our sample is a relatively slow rotator, we do not find any significant correlation between rotation period and amplitude of variability (Fig. 12, *panel b*). The periodic variables in our sample are predominantly relatively low-level variables, exhibiting peak-to-peak variations of about 0.1–0.2 mag. Ten periodic variables exhibit variability larger than 0.5 mag, including 5 stars with $P < 4$ days (one of which is the fastest rotator in our sample). As with $H\alpha$ and Ca II , we do not find evidence for a connection between rotation period and active accretion as traced by amplitude of variability.

Of course, our detection of rotation periods is naturally biased against stars whose photometric variations are irregular. It could be true, for example, that large amplitude irregular variables (LAIVs) are primarily slow rotators. To check this, we have compared the $v \sin i$ distribution of a sample of LAIV in our photometric database (which we take to be stars with $\sigma_{\text{mag}} > 0.1$ mag) to the $v \sin i$ distribution of our sample of rotators. Of 176 nonperiodic stars in our database that we have observed spectroscopically (see § 2.4), 50 are LAIVs. Though our spectral resolution is somewhat limited (0.5–0.8 \AA), we find no significant difference between the two $v \sin i$ distributions.

3.3. Disks among the Rotators

To explore connections between stellar rotation and circumstellar disks, we use the near-IR photometry recently determined by Hillenbrand et al. (1998) for stars in the central 30' of our survey region (the same region studied in Hillenbrand 1997; see Fig. 1). The “excess” $I-K$ color, $\Delta(I-K)$ —defined as the difference between the observed dereddened $I-K$ color and that expected from the stellar spectral type—provides an indicator of warm circumstellar material within a few stellar radii of the stellar surface.

The Hillenbrand et al. study provides measures of $\Delta(I-K)$ for 105 stars in our sample of rotators. Following their discussion of the observational uncertainties in their measurements, we require $\Delta(I-K) > 0.3$ for a star to be labeled as possessing a disk. This criterion ensures not only that circumstellar material is present (within a few stellar radii of the stellar surface), but that this material is accreting with $\dot{M} \gtrsim 10^{-9} M_{\odot} \text{ yr}^{-1}$ (see Fig. 8 in Hillenbrand et al. 1998). Stars with $\Delta(I-K) < 0.3$ either do not have accreting disks or possess disks that are cleared within a few stellar radii of the stellar surface.

How are stars with disks distributed in rotation period? Of the 105 periodic variables for which $\Delta(I-K)$ is available from the literature, 40 stars with $P < 8$ days satisfy our $\Delta(I-K) > 0.3$ criterion. In Figure 13 we compare the period distribution of these 40 disked stars with the overall rotation period distribution and with the distribution of stars with near-IR photometry available but which do not satisfy our criterion for circumstellar disks. These distributions are uniformly distributed and are not significantly different from each other.

In Figure 14 (*panel a*) we show infrared excess as a function of rotation period. Also indicated are those stars which are actively accreting, as indicated by strong $H\alpha$ emission (§ 2.4.1) or emission in the Ca II triplet as reported by Hill-

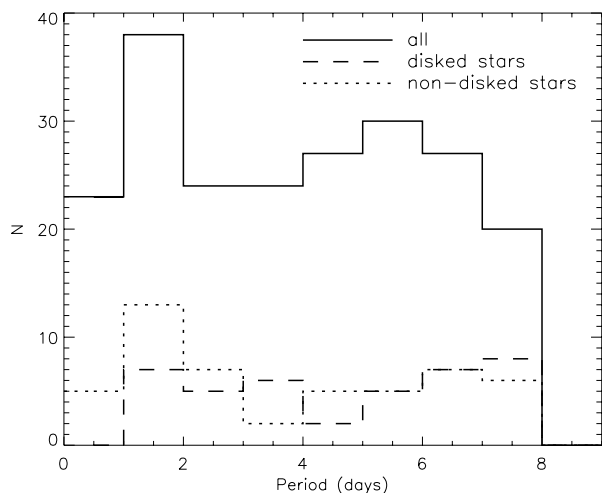


FIG. 13.—Period distribution of stars exhibiting near-IR excess emission compared with the entire distribution of rotation periods for our sample (*solid histogram*). Excess near-IR emission indicative of circumstellar disks is present among 40 stars (*dashed histogram*). Also shown is the period distribution for stars with infrared excess measurements that do not satisfy our criterion of $\Delta(I-K) > 0.3$ (*dotted histogram*). These distributions are not significantly different from one another, and they are consistent with a uniform distribution.

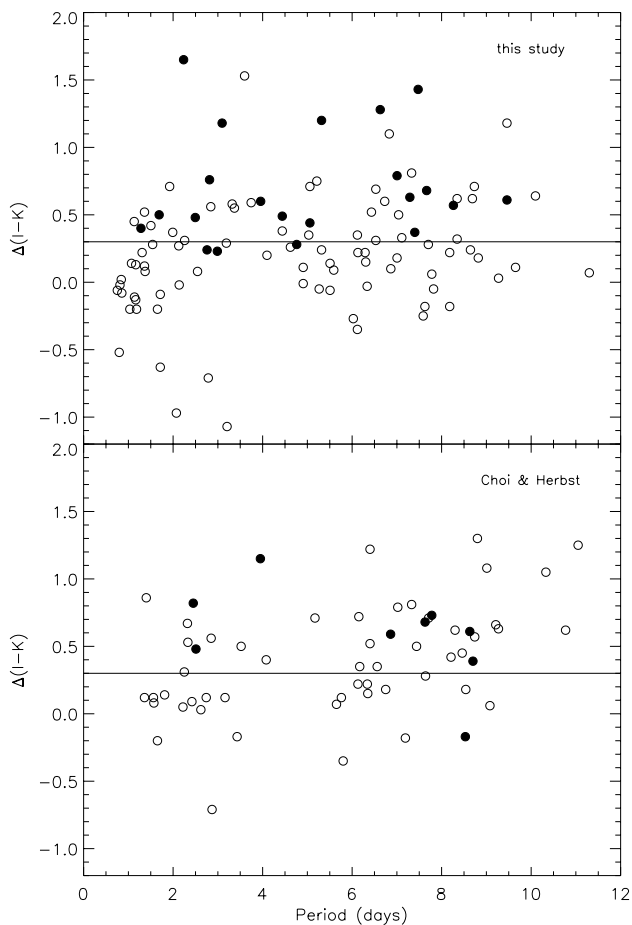


FIG. 14.—Connection between disks and stellar rotation period in the ONC for stars with rotation periods determined by us (*a*) and stars with rotation periods determined by CH (*b*). No correlation is apparent between near-IR excess emission and stellar rotation period. Note also that almost all of the filled symbols, representing stars exhibiting active accretion in H α and/or Ca II emission, lie above our near-IR criterion for actively accreting disks.

enbrand et al. (1998). Again, we take stars with $\Delta(I-K) > 0.3$ to be those with accreting circumstellar disks. Almost all stars evincing accretion in H α and Ca II emission lie above this value.¹² No correlation is apparent between rotation period and infrared excess within our entire sample, nor is there a correlation among stars that are actively accreting as indicated by strong H α or Ca II emission. We find this same result when we consider only those stars with periods reported by CH (IR data available for 69 stars from Hillenbrand et al. 1998), which includes stars in the central portion of the nebula where our sample is deficient (Fig. 14, *panel b*).

4. DISCUSSION

Having presented a newly determined rotation period distribution for stars in Orion OB1c/d, and evidence for active accretion and circumstellar disks among a subset of these, we now discuss the implications of these new results for several questions pertaining to angular momentum evolution in the PMS phase.

4.1. On the Bimodality of the Period Distribution

First proposed by Attridge & Herbst (1992) and advanced most recently by CH, the ONC rotation period distribution has previously been found to be distinctly bimodal, with a deep gap at $4 < P < 5$ days (see Fig. 9). CH argue that their bimodal distribution can be understood within magnetospheric accretion theory and hence provides support for it. Their basic argument, stated simply, is that slow rotators (median $P = 8.3$ days) are those which have been prevented from spinning up via magnetic coupling to their circumstellar disks, while rapid rotators ($P < 4$ days, median $P = 2.6$ days) are those which have disengaged their disk-lock (via, e.g., disk depletion); an evolutionary sequence is implied in the sense that slow rotators become rapid rotators. CH also point out that the slow-rotator “peak” in their distribution ($P \sim 8$ days) agrees well with theoretical predictions (Shu et al. 1994). Together with the finding by Edwards et al. (1993b), that only stars with $P > 4$ days exhibit near-IR signatures of circumstellar disks, the bimodal distribution of rotation periods has constituted important evidence in support of disk-regulated stellar rotation.

However, as we have discussed, our data do not lend support to the existence of a bimodal distribution of rotation periods. Our distribution does not yield statistically compelling evidence of structure for periods $0.5 < P < 8$ days. Indeed, the distribution determined by CH may itself not be securely statistically distinguishable from uniform (see § 3.1.2). Researchers studying other (although slightly older) young clusters and associations (e.g., Upper Sco by Adams et al. 1998 and NGC 2264 by Kearns et al. 1997 and Kearns & Herbst 1998) have recently produced similar results, finding no evidence for bimodality in their observed period distributions. The authors in these cases use the sug-

¹² It must be noted, however, that not all stars with $\Delta(I-K) > 0.3$ show H α emission. This may indicate that accretion activity as traced by H α emission is sporadic enough to escape our detection; or it may mean that the accretion rate in these stars is low enough to produce H α emission below our detection limit or that H α emission in these stars is narrow enough that we cannot detect it because of the presence of nebular emission. Hillenbrand et al. 1998 similarly report that not all stars exhibiting large $\Delta(I-K)$ show Ca II emission.

gested bimodality in the ONC to estimate timescales over which a presumed disk-lock mechanism operates.

CH used a spatial comparison as evidence for their thesis that the rapid rotators in their sample represent an evolved state of the slow rotators. They take stars in the Trapezium and NU Ori regions to be younger than stars in their surroundings, on the basis of the relatively high nebulosity in these regions, in lieu of age estimates from stellar models. They show that these presumed younger stars constitute a larger proportion of slow rotators than stars in the less nebulous regions that they surveyed.

Comparing stars in different regions of the Orion OB1c/d association is important because of the differences in stellar ages across the region. Blaauw (1964) and others (Warren & Hesser 1977; Brown et al. 1994 and references therein) have studied the relative ages of the four principal subgroups of the Orion I OB association, using a variety of techniques, including massive star “turn-up,” main-sequence fitting to the bluest ZAMS stars, PMS evolutionary models, “runaway” stars, gas dynamics, and cluster expansion arguments. Many of these studies have concluded that a temporal sequence exists from Ia–Id, with the Ia subgroup being the oldest. Nevertheless, age estimates from the different techniques (and between different authors) have produced considerable ambiguity particularly between the Ic and Id subgroups, whose age estimates range from 0.5–3 Myr and 0.01–10 Myr, respectively. A summary of these studies can be found in Warren & Hesser (1977), who report their own age estimates of about 0.5 Myr and 1–5 Myr for Id and Ic, respectively. Most recently, Brown et al. (1994) have reported ages similar to those of Warren & Hesser (1977) on the basis of *VBLUW* photometry (though they place the Ib subgroup intermediate in age to the Ic and Id subgroups).

The physical significance of these historical subdivisions and the differences between stars in and out of the identified clusterings have recently been investigated by several researchers. Hillenbrand & Hartmann (1998) have questioned the distinction between the Trapezium and ONC (Id and Id1 in the notation of Warren & Hesser 1977), arguing that the Trapezium and ONC are probably part of one and the same cluster. Gomez & Lada (1998) have investigated the spatial distribution of stars in Orion from head to sword as a way of quantifying the degree of stellar clustering, finding that, while several stellar clusterings do exist in the Ic/d region, less than half of the strongest H α -emission sources identified by the Kiso H α survey reside in the identified “clusters.” This is similar to Allen’s (1996) finding that only 25%–50% of stars less than 1 Myr old in L1641 are found in “aggregates” or “clusters,” with the majority (50%–75%) of the youngest stars possessing a more distributed spatial morphology. At the same time, Hillenbrand (1997) has found that the youngest stars in the ONC are preferentially located in the center-most part of the cluster, and Allen (1996) has found marginal evidence that stellar aggregates and/or clusters in L1641 tend to harbor a larger *relative* fraction of the youngest stars. Thus the linkage between spatial location and stellar age is complex and not clearly understood.

We have considered the dependence of our results on stellar age. Our statistical comparisons of radial spatial subsets of our sample do not reveal any statistically significant differences in the period distributions of stars based upon spatial location (§ 3.1.2). A more direct assessment of the bimodality of the period distribution in the context of

stellar age is achieved by using derived stellar ages to look for trends in the period distribution with age. Ages are available from Hillenbrand (1997) for 108 ONC stars in our distribution, with ages ranging from $3.65 < \log \tau < 6.57$. In Figure 15 we show the distribution of rotation periods for these stars in the three age ranges (1) $\log \tau \leq 5$, (2) $5 < \log \tau \leq 5.7$, and (3) $\log \tau > 5.7$, chosen simply to populate each distribution with a significant number of stars. No trend in stellar rotation period with stellar age is apparent in this time sequence. A similar (but model independent) result can be inferred from the positions of slow rotators ($P > 4$ days) and rapid rotators ($P \leq 4$ days) in the H-R diagram (Fig. 16). These two sets of stars do not populate different regions of the diagram, indicating that there are no trends of stellar rotation period with stellar parameters (over the range spanned by our sample). Nonetheless, continued period determinations for stars very near the Trapezium are needed to complement this study. The Wesleyan observations have proven vital in this regard, and we look forward to substantial increases in the sample size.

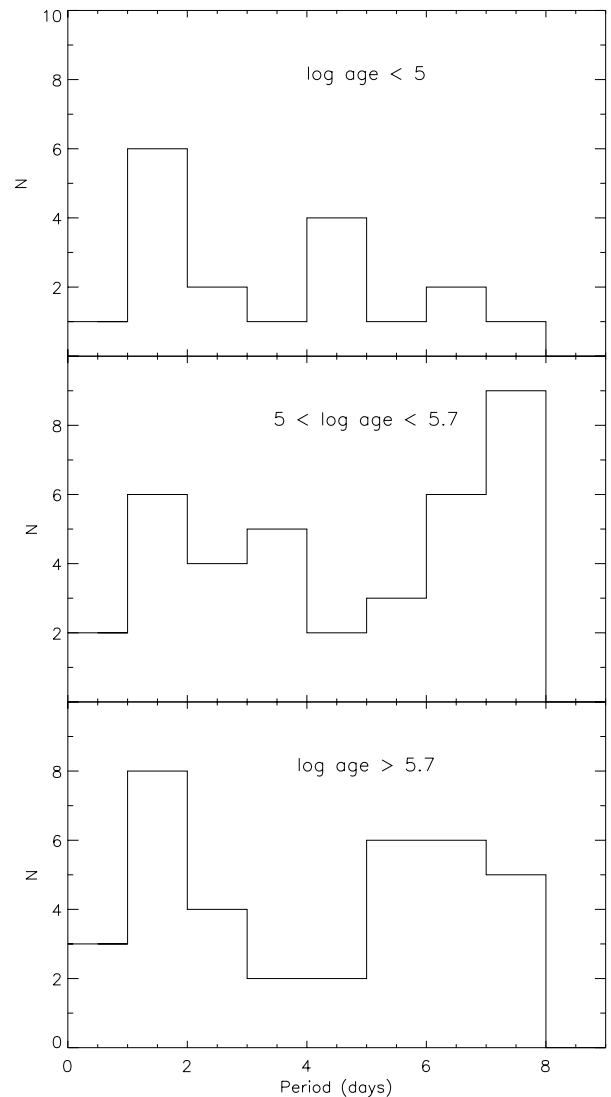


FIG. 15.—Age evolution of the ONC rotation period distribution. Taking stellar ages from Hillenbrand 1997, a time sequence of the rotation period distribution is shown from top to bottom: stars with ages $\log \tau < 5$, $5 < \log \tau < 5.7$, and $\log \tau > 5.7$. No trends with age are apparent.

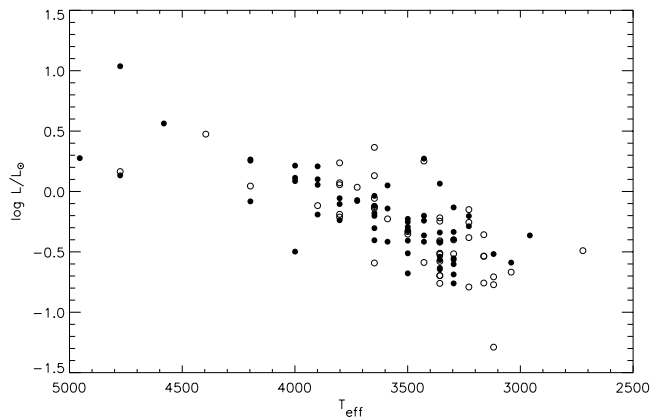


FIG. 16.—Comparison of slow and fast rotators in the H-R diagram. Stars with $P < 4$ days (*open symbols*) do not populate the H-R diagram differently than stars with $P > 4$ days (*filled symbols*).

The morphology of the rotation period distribution, whatever its form, does not in and of itself reveal the mechanism by which stellar rotation is regulated in the PMS phase. We turn now to a discussion of the evidence for the regulation of PMS stellar rotation by disks.

4.2. On the Regulation of Rotation by Disks

The long-standing astrophysical problem of angular momentum regulation in the PMS phase (embodied classically in the typically low $v \sin i$ observed in CTTS) has in recent years been explained within the framework of a magnetic star-disk coupling mechanism, formalized in part by Shu and collaborators (Shu et al. 1994; Ostriker & Shu 1995; Najita 1995). Following the work of Edwards et al. (1993b), which showed a correlation between stellar rotation period and the presence of excess K-band emission among 34 stars in Taurus-Auriga and the ONC, studies of rotation among young stars (e.g., Eaton et al. 1995; CH; Kearns et al. 1997; Kearns & Herbst 1998; Adams et al. 1998) have contextualized their observations within the disk-locking scenario. It is in this context that the notion of a bimodal rotation period distribution is particularly appealing. As discussed in the previous section, however, we do not find strong evidence in the morphology of our rotation period distribution to support the notion of distinct “locked” and “spun-up” populations.

How might disk-regulated rotation best manifest itself observationally? Previously, researchers studying the connection between disks and stellar rotation have looked primarily for a correlation between the directly observed diagnostics of disks and rotation: excess IR emission and rotation period. However, no unambiguous correlation between stellar rotation and near-IR diagnostics of disks has been forthcoming. Eaton et al. (1995) observed numerous slowly rotating stars in the ONC without near-IR excesses, as well as two rapidly rotating stars with excesses. The evidence presented by Edwards et al. (1993b), perhaps the most compelling of all, similarly contains a large fraction of slowly rotating stars ($\sim 40\%$) without near-IR disk signatures. Bouvier et al. (1993) observed that CTTS in their sample of 26 stars in Taurus-Auriga rotate more slowly than the WTTS in their sample *on the average*, but derive a mean rotation period of 4.1 days for the WTTS, in the period gap observed by Herbst and collaborators. Finally,

as we have seen (§ 3.3; Fig. 14), our data, coupled with near-IR measurements from the literature for stars in the ONC, do not show a correlation between stellar rotation period and near-IR excess emission. What conclusions can we draw, then, about the ability of the disk-locking hypothesis to explain the observations? Is a correlation between directly observed quantities actually the best way to observe disk-locking in action?

While a direct correlation between diagnostics of disks and of stellar rotation may be expected on theoretical grounds (e.g., Kenyon et al. 1996), perhaps a more physically meaningful way to explore a causal connection between disks and stellar rotation under the disk-locking hypothesis is to consider *the evidence for disk material at the corotation radius, R_c , from the star*. R_c is the distance from the star at which disk material will rotate with Keplerian angular velocity equal to the stellar angular velocity. If disks do act to govern stellar rotation, a straightforward prediction is that disk material will be present near R_c .

How do our results compare with this prediction? We show in Figure 17 the near-IR disk signature, $\Delta(I-K)$, from Hillenbrand et al. (1998) versus the corotation radius, R_c (in units of stellar radii) and v/v_{br} for the 105 stars in our sample with the requisite data [$v/v_{br} = (R_c/R_*)^{-3/2}$]. Stars above the solid horizontal line $\Delta(I-K) = 0.3$ mag show detected excess near-IR emission. As the $\Delta(I-K)$ diagnostic is not sensitive to disk material situated more than a few stellar radii from the star, excess emission will not be readily detected among stars with $R_c \gtrsim 3R_*$ if they possess disks truncated at R_c (Hillenbrand et al. 1998; note that this value of $3R_*$ is only approximate because it varies somewhat from star to star, depending upon various factors such as stellar radius, inclination, etc.). This threshold is shown by the dashed vertical line.

We consider stars in the four quadrants of Figure 17 separately: (1) stars with large R_c and no detected excess near-IR emission, (2) stars with large R_c that do show excess near-IR emission, (3) stars with small R_c that show excess near-IR emission, and (4) stars that do not show excess near-IR emission despite having R_c near the stellar surface. To facilitate a simple, initial exploration of this figure and its implications, we consider stars in these four quadrants assuming canonical values of the stellar magnetic field strength and mass accretion rate, $B_* \sim 1$ kG and $\dot{M} \sim 10^{-8} M_\odot \text{ yr}^{-1}$.

Quadrant 1. Stars in this quadrant are perhaps the easiest to understand in terms of the disk-locking hypothesis. These stars rotate at small fractions of v_{br} , so that R_c is many stellar radii from the stellar surface. Relating R_c to \dot{M} , B_* , and other stellar parameters as per Ostriker & Shu (1995) yields

$$\frac{R_c}{R_*} = \left(\frac{B_*^4 R_*^5}{GM_* \dot{M}^2} \right)^{1/7}.$$

Thus, typical accretion rates and stellar magnetic field strengths predict large R_c among these stars. If the disk truncation radius, $R_{trunc} \approx R_c$, then no excess near-IR emission is expected from these stars, consistent with the observations. Of course, that stars in this quadrant possess truncated disks must still be verified; observations at longer IR wavelengths should reveal the presence of disks.

Quadrant 2. Stars in this quadrant are not so readily understood within the disk-locking model. These stars

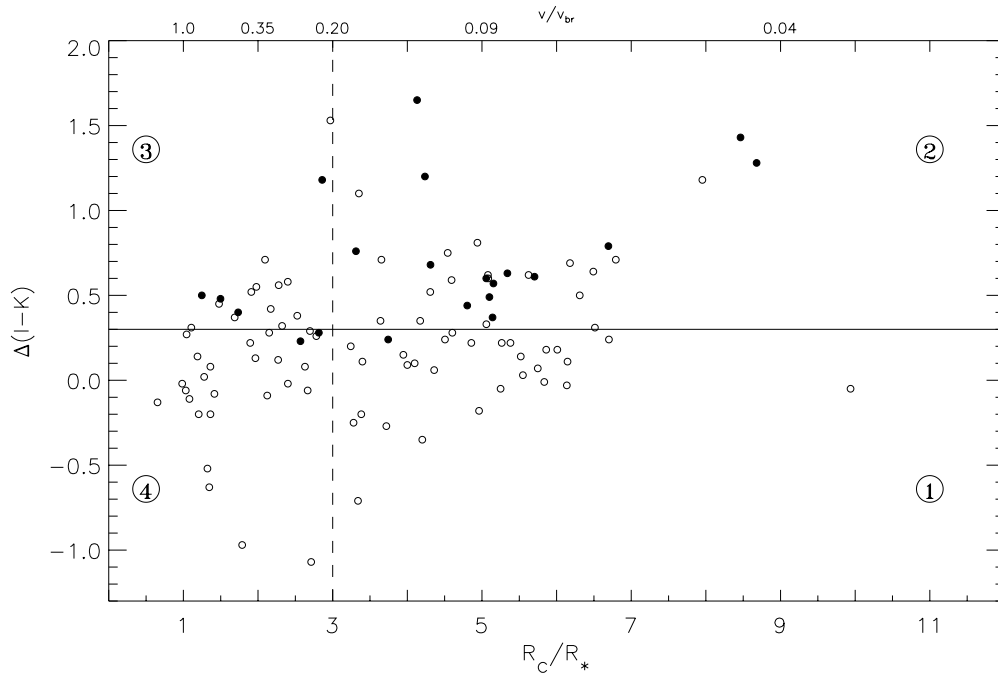


FIG. 17.—Testing for disk material at the corotation radius. The near-IR excess emission is plotted against the corotation radius (in units of stellar radii) for 105 stars in our sample with the requisite data. Filled symbols indicate those stars that show evidence for active accretion (strong H α or Ca II emission). Stars with $\Delta(I-K) > 0.3$ (horizontal line) likely possess circumstellar disks extending to within a few stellar radii of the stellar surface. Stars with disks that are truncated within greater than a few stellar radii (vertical line) will probably not exhibit near-IR excess emission. See § 4.2 for discussion of this figure.

rotate at only about 10% of breakup, yet show significant near-IR excess emission, indicating that they possess disks extending to within a few stellar radii of the stellar surface. While magnetospheric accretion models predict that disk material will drift 0.1–0.3 R_c within R_c before being lifted off the disk midplane (e.g., Ostriker & Shu 1995; Kenyon et al. 1996), typical accretion rates and magnetic field strengths do not straightforwardly account for the presence of disk material so close to the stellar surface in these stars.¹³

Quadrant 3. Stars in quadrant 3 rotate at appreciable fractions of breakup velocity. Such rapid rotation is consistent with the observed near-IR excess emission from these stars, indicating the presence of disk material at R_c to which these stars may be locked. However, like stars in quadrant 2, the presence of disk material so close to the stellar surface cannot be explained by typical accretion rates and magnetic field strengths.

Quadrant 4. Stars in this quadrant are presumably not disk-locked because there is no near-IR evidence for disk material, despite the close proximity of R_c to the stellar surface. Stars lacking near-IR excess emission have been interpreted in previous studies as descendants of once disk-locked systems. Even so, these stars are the most problematic for the disk-locking paradigm; they still require large angular momentum loss prior to the main sequence with no evident mechanism to explain it.

Some of the disagreement between the disk-locking hypothesis and the implications of Figure 17 can be mitigated by relaxing the assumptions of typical accretion rates and magnetic field strengths, particularly for stars in quad-

rants 2 and 3. For stars in quadrant 2, for example, a high accretion rate ($\dot{M} \sim 10^{-5} M_\odot \text{ yr}^{-1}$) can “crush” the stellar magnetosphere down to the stellar surface, explaining the observed near-IR excess emission and rotation near breakup velocity. Such high accretion rates are typically observed only in the most extreme cases (e.g., FU Ori events). Since episodes of such high accretion are transitory, any spin-up these stars might presently be experiencing as a result of disk-locking close to the stellar surface may be sufficiently brief that the observed slow rotation remains largely unaffected. Indeed, one might imagine a scenario in which these stars oscillate between quadrants 1 and 2, with the inner edge of the disk encroaching toward the stellar surface during brief episodes of enhanced accretion (quadrant 2 stars) and then quickly receding back out to many stellar radii during longer periods of quiescence (quadrant 1 stars).

A high accretion rate (i.e., $\dot{M} \sim 10^{-5} M_\odot \text{ yr}^{-1}$) can similarly explain the presence of disk material close to the stellar surface among stars in quadrant 3. However, the rotation of these stars at or near breakup velocity places R_c at or near the stellar surface, requiring that the disk *persist* at or near the stellar surface, in contradiction to the expectation that such high accretion rates occur only episodically. Instead, small magnetic field strengths (i.e., $B_* \sim 50$ G) among these stars could allow typical accretion rates to push R_c close to the stellar surface, producing disk-locked rotation at or near breakup velocity. Appealing to weak magnetic fields to bring the disk-locking hypothesis into agreement with quadrant 3 stars is problematic, however. Is disk-locking truly viable under such weak magnetic fields? Is the assumption of weak magnetic fields consistent with the presence of the spots we have observed on these stars?

Appealing to a high accretion rate among stars in quad-

¹³ Presuming that magnetospheric accretion streams do not produce the observed IR excesses.

rant 2 has its difficulties as well. Episodes of such high accretion are, presumably, short-lived phenomena. If quadrant 2 stars are required to spend most of their time in quadrant 1 so as to maintain their slow rotation, we should not see such a large fraction (roughly half) of quadrant 1/quadrant 2 stars in quadrant 2. A modification to the theory in which $R_{\text{trunc}} \ll R_c$ seems to be required to bring the predictions of the disk-locking hypothesis in line with the observations for these stars. Such a modification of the theory would need to be applied *only to quadrant 2 stars*, however, since their quadrant 1 counterparts show no evidence for $R_{\text{trunc}} \ll R_c$.

These difficulties notwithstanding, to our mind it is the quadrant 4 stars that pose the greatest challenge to the disk-locking paradigm. We can say definitively that these stars do not possess disks extending to R_c , because such disks would be readily detected in the $\Delta(I-K)$ diagnostic. Might these stars be coupled to disks with $R_{\text{trunc}} \gg R_c$, and thereby be undergoing an epoch of rapid spin-down at present? While measurements at longer infrared wavelengths are required to probe for disk material situated at greater distances from the stellar surface, these stars show no evidence for the signatures of active accretion (in H α or Ca II emission) that might be expected if the stars are connected to disks via magnetically channeled accretion streams. It is more likely that many, if not all, of these quadrant 4 stars have already dissipated their disks.

What, then, is to be the subsequent evolution of quadrant 4 stars? As we discuss in the following section, the stars in our sample show evidence for continued angular momentum depletion over the next few Myr. In addition, we show that the distribution of $v \sin i$ among stars in our sample is very similar to that observed among low-mass Pleiades stars, indicating that the relative distribution of angular momentum presently observed among stars in our sample is preserved over approximately the next 100 Myr. These findings imply that quadrant 4 stars, like the rest of the stars in our sample, must still deplete considerable angular momentum. More fundamentally, these stars still face contraction in size by factors of about 5–10 as they approach the main sequence, yet already rotate at or near breakup velocity! Apparently, for these stars at least, alternative mechanisms are required to explain the subsequent evolution of angular momentum.

The evidence considered in this section does not provide a compelling case for disk-regulation of stellar rotation in the PMS phase. Indeed, for at least some stars in our sample, the observations seem to reject the disk-locking hypothesis. Future measurements at longer IR wavelengths will provide an important constraint on the presence of disks truncated at many stellar radii (e.g., among stars in quadrants 1 and 4). In addition, photometric (e.g., Vrba et al. 1988; Bouvier et al. 1993) and polarimetric (e.g., Stassun & Wood 1999) diagnostics of spot properties among these stars would help further test the predictions of magnetospheric accretion theory.

4.3. On the Depletion of Angular Momentum

The apparent depletion of angular momentum in the PMS phase is a continuing challenge to star formation theory. Studies of rotation in young clusters such as the Pleiades (e.g., Queloz et al. 1998) indicate that low-mass ZAMS stars are predominantly slow rotators, with typical $v \sin i \lesssim 10 \text{ km s}^{-1}$, and a smaller number of more rapidly

rotating stars extending to about 100 km s^{-1} . This occurs despite contraction in size of more than an order of magnitude and the accretion of circumstellar material of high specific angular momentum during the PMS phase.

Attempts to model the rotational evolution of stars from TTS ($\lesssim 1 \text{ Myr}$) to the Pleiades ($\sim 100 \text{ Myr}$) have been carried out by several researchers (e.g., Bouvier et al. 1997; Krishnamurthi et al. 1997; Keppens et al. 1995; Collier Cameron et al. 1995). All of these efforts model changes in PMS stellar rotation as arising from a combination of (1) spin-up due to changes in stellar moment of inertia, (2) spin-down due to a Skumanich-like wind-braking law (i.e., $d\omega/dt \propto \omega^3$), and (3) enforced constant angular velocity due to star-disk coupling. Some models include the effects of differential rotation due to core-envelope decoupling, but these effects probably do not apply for very low mass (i.e., fully convective) stars (e.g., Krishnamurthi et al. 1997).

Disk-locking has proven to be an extremely valuable mechanism for these models, because enforced constant angular velocity provides an efficient angular momentum drain (i.e., $\Delta J \propto \Delta R^2$) in the PMS phase. Such an efficient mechanism for dissipating angular momentum is necessary because in most models the contraction (i.e., spin-up) timescale is 1–2 orders of magnitude shorter than the wind-braking timescale for ages up to about 20–30 Myr. Furthermore, braking by winds alone is difficult, because it is necessary to account simultaneously for the presence on the ZAMS of both slow rotators and ultrafast rotators (UFRs). Thus, wind-braking models are most effective at providing for rapid spin-down on and just prior to the ZAMS, and they typically allow for a saturation parameter in order to prevent excessive spin-down of the rapid rotators (e.g., Stauffer & Hartmann 1987; Barnes & Sofia 1996). In most models, then, the disk lifetime together with wind-braking saturation for UFRs provide the key tunable parameters for matching model predictions to the observed rotational evolution of low-mass PMS and ZAMS stars.

An important input ingredient in all prescriptions of PMS angular momentum evolution is the initial conditions. Based on studies of TTS rotation available heretofore (e.g., CH; Bouvier et al. 1993) and on theoretical grounds (e.g., Shu et al. 1994), researchers modeling the rotational evolution of PMS stars have typically assumed that young stars begin as relatively slow rotators, with a narrow distribution of rotation periods centered on $P \sim 8 \text{ days}$.

How do our new results impact the problem of PMS angular momentum evolution, especially if some kind of star-disk coupling mechanism is not in fact governing the rotational evolution of PMS stars? The results of this study in some respects exacerbate the PMS angular momentum problem. In particular, our discovery of a population of stars rotating at or near breakup velocity (Fig. 10) poses a serious challenge to our present picture of rotational evolution in young stars. What is to be the fate of these stars, considering that stars in our sample must still contract in size by factors of 5–10 (!) before reaching the main sequence? Even if we suppose for the sake of argument that disk-locking is an important angular momentum drain for some stars, as discussed in the previous section, many of these very rapid rotators do not evince disks in the diagnostics considered here.

The disk-locking hypothesis notwithstanding, the data suggest that the stars in our sample are presently undergoing a period of significant angular momentum loss. In

Figure 18 we show the distribution of v/v_{br} for stars in three age ranges. A clear evolution in the distribution is apparent. The youngest stars have a roughly uniform distribution of v/v_{br} , including several stars at or near breakup velocity. Progressively older stars show fewer instances of rotation at breakup, and the distribution becomes increasingly skewed toward the canonical $v/v_{br} \sim 10\%$. By an age of $\log \tau \sim 6$, very few stars rotate at any appreciable fraction of breakup velocity. This effect is also readily seen by considering the time dependence of angular momentum directly. In Figure 19 we show the quantity $(R_*/R_\odot)^2/P$, which is proportional to specific angular momentum, J/M , as a function of derived age for the 108 stars with the requisite data. Although the range of specific angular momenta remains large at all ages, a trend toward decreasing specific angular momentum is apparent. Thus we see that the time spanned between the ages of roughly 10^5 and $\geq 10^6$ yr is one marked by significant angular momentum depletion.

Furthermore, the data reveal that angular momentum depletion must continue over about the next 100 Myr as

these stars approach the ZAMS. As can be seen in Figure 20, the distribution of $v \sin i$ among stars in our sample bears remarkable resemblance to the $v \sin i$ distribution of Pleiades stars with $M < 0.6 M_\odot$ (see Bouvier et al. 1997 and references therein). The $v \sin i$ distribution for our sample was derived by combining our rotation periods with radii from Hillenbrand (1997) and simulating $\sin i$ [by generating uniform random numbers, p , and computing $(2p - p^2)^{1/2}$]. If we are to connect the ONC and the Pleiades in an evolutionary sequence, this implies (1) that the distribution of rotational velocities among low-mass ZAMS stars is determined by an age of approximately 1 Myr and (2) that these stars must continue to dissipate considerable amounts of angular momentum over about the next 100 Myr as they approach the ZAMS. For in order to be able to contract in size by about 5–10 times and still roughly preserve their original $v \sin i$ distribution, these stars must also deplete their angular momenta by a factor of about 5–10.

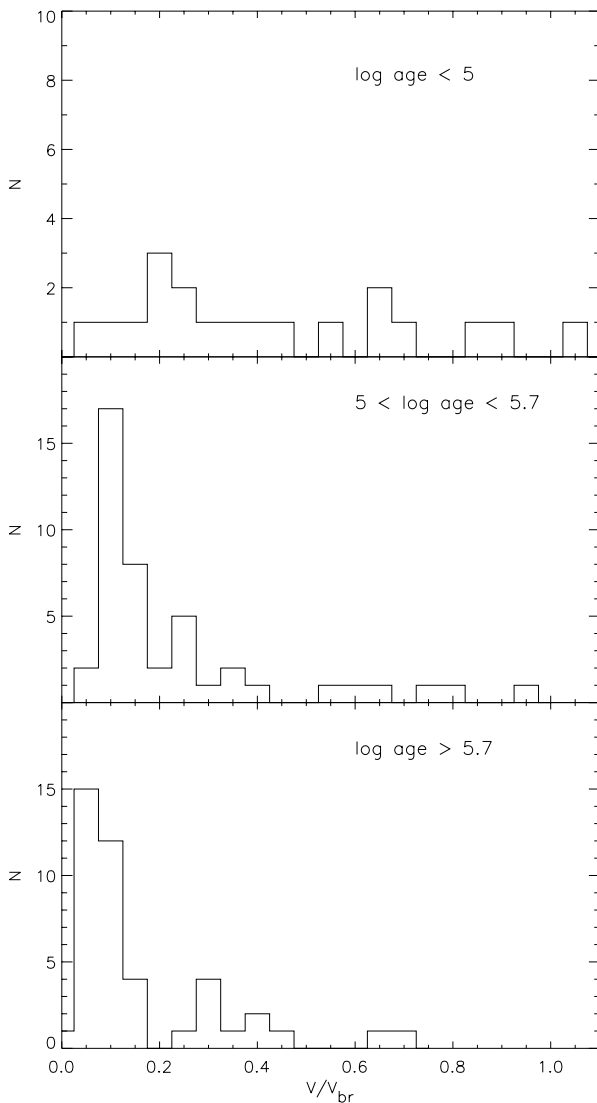


FIG. 18.—Depletion of stellar angular momentum with time, apparent in the evolution of the distribution of v/v_{br} . The distribution of v/v_{br} is shown for stars with ages in three age ranges from top to bottom, as in Fig. 15.

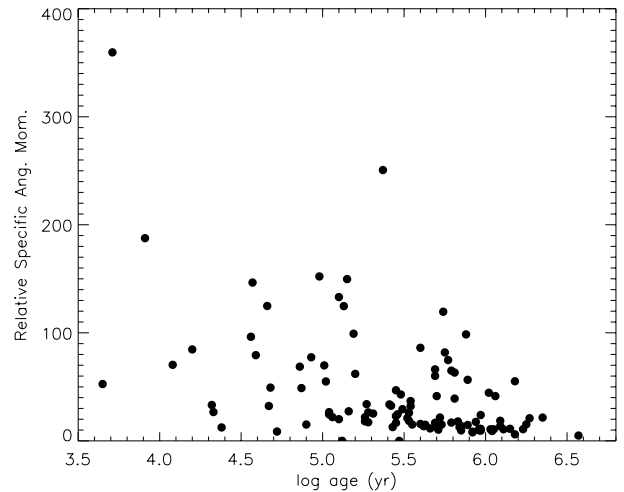


FIG. 19.—Depletion of stellar angular momentum with time, directly apparent in the evolution of stellar specific angular momentum (normalized to the Sun) with stellar age. The time spanned between ages of about 10^5 and 10^6 yr is marked by significant angular momentum depletion.

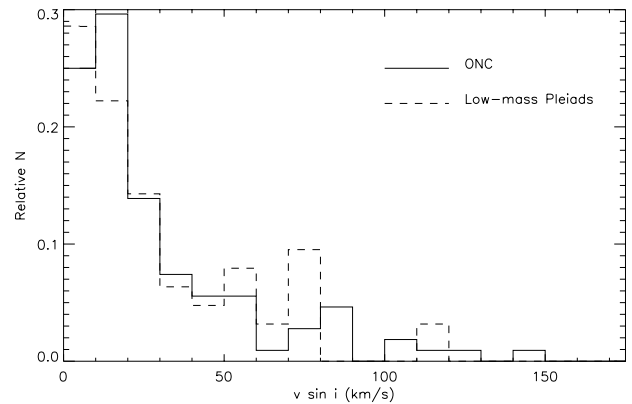


FIG. 20.—ONC and Pleiades $v \sin i$ distributions, showing remarkable similarity. The $v \sin i$ distribution (*dashed histogram*) for 63 Pleiades stars with $M < 0.6 M_\odot$ is from Bouvier et al. 1997 and references therein. The similarity between these distributions for stars differing in age by approximately 100 Myr indicates that considerable angular momentum must continue to be depleted long after typical disk lifetimes (see text).

The close resemblance of the ONC and Pleiades $v \sin i$ distributions further challenges the case for disk-regulated angular momentum. Even if disk lifetimes as long as $\gtrsim 10$ Myr were typical, low-mass stars such as those in our sample would still face spin-up by a factor of about 2–3 (as well as a small factor of about 1.5 for changes in internal structure; Rucinski 1988) as they complete their contraction to the main sequence. Other mechanisms for angular momentum loss, such as wind-braking, may therefore play an important role. Nevertheless, as discussed above, the timescales over which such winds operate may be too long to account for angular momentum evolution leading to the ZAMS (e.g., Bouvier et al. 1997).

While a detailed discussion of the implications of this result for theoretical models of angular momentum evolution is beyond the scope of this paper, we do note that the similarity of the ONC and Pleiades $v \sin i$ distributions implies that the relative distribution of stellar specific angular momentum observed on the ZAMS is already present among TTS; angular momentum evolution models should not invoke mechanisms that significantly alter the “initial” relative distribution of angular momentum observed among TTS. Future modeling efforts should also consider the changes in initial conditions suggested by this study: accretion and circumstellar disks occur among stars spanning the full range of rotation periods present in the ONC ($P \sim 0.5$ –10 days).

We should emphasize that the similarity between the ONC and Pleiades $v \sin i$ distributions apparently only holds for very low mass stars. Solar-mass Pleiades stars, for example, exhibit a $v \sin i$ distribution much more heavily concentrated toward lower $v \sin i$ values, with very few stars showing $v \sin i > 20 \text{ km s}^{-1}$ (see, e.g., Bouvier et al. 1997 and references therein). This probably occurs because solar-mass stars complete their main-sequence contraction by an age of about 30 Myr, so that (solar-analog) winds can effectively brake their rotation by the age of the Pleiades, possibly aided by rotational decoupling of the core and envelope (Rucinski 1988).

We must caution that the various trends with stellar age we have discussed in this section could be the result of underestimated uncertainties in Hillenbrand (1997). If, for example, ONC stars are precisely isochronal, the apparent trends of v/v_{br} and J/M with stellar age could arise from the fact that stars observed at higher luminosities are interpreted to be both larger and younger. Consequently, “younger” stars are interpreted both to be closer to breakup velocity and to possess higher specific angular momentum since $v/v_{\text{br}} \propto R^{3/2}$ and $J/M \propto R^2$ for a given rotation period.

The observed similarity between the $v \sin i$ distributions of the ONC and Pleiades, however, is independent of the derived ages in the ONC. More comprehensive rotational studies of PMS stars with ages intermediate to the ONC and the Pleiades would be of tremendous value in “filling in” the rotational evolution of stars toward the main sequence and determining whether the distribution of $v \sin i$ is indeed preserved between 1 and 100 Myr.

5. SUMMARY AND CONCLUSIONS

We have presented the results of a comprehensive search for periodic photometric variables in a large region centered on the Trapezium, which we conducted to study the evolution of angular momentum in the PMS phase and to test

the current paradigm of disk-locking as a viable mechanism for angular momentum depletion. Our region includes and extends beyond the Orion Nebula Cluster (ONC). Among 254 stars for which we have determined rotation periods, we use our spectroscopic observations and data from the literature to confirm that these stars are members of the Orion OBIC/d association. We further use our spectroscopic observations to identify a subset of stars undergoing active disk accretion. Finally, we use near-IR photometric data from the literature to identify those stars in the ONC possessing circumstellar disks. In a future paper we will present visible and near-IR photometry for our entire sample of stars with rotation periods.

The major findings of this study are the following:

1. The rotation period distribution of PMS stars in Orion OBIC/d is statistically indistinguishable from a uniform distribution; the present data do not support a well-separated bimodal distribution. While stellar age differences (~ 3 Myr) exist across our survey region, this result is independent of both spatial location and derived stellar ages.
2. The period distribution of stars exhibiting active accretion is indistinguishable from the distribution of stars that do not exhibit active accretion. Active accretion—as indicated by $H\alpha$ emission strength, Ca II emission, and amplitude of photometric variability—occurs over the entire range of periods studied.
3. No correlation is apparent between stellar rotation period and near-IR signatures of circumstellar disks among stars in the ONC.

These findings contrast with previous findings that have been presented in support of the disk-regulated stellar rotation hypothesis, including (1) a bimodal distribution of stellar rotation periods in the ONC, (2) the slower mean rotation by Taurus CTTS as compared to WTTS, and (3) a correlation between stellar rotation period and near-IR emission signatures of circumstellar disks.

In the light of these contrasting findings, we have also considered the evidence for circumstellar disk material being present and truncated near the corotation radius for stars in our sample. While this prediction of the disk-locking hypothesis is consistent with some stars in our sample, for many stars such consistency requires appeal to very high accretion rates or problematically weak stellar magnetic fields. Observations at longer IR wavelengths capable of probing disk material situated at many stellar radii are needed to further study this issue.

Furthermore, we have found:

1. The rotation period distribution shows a strong cutoff at $P \lesssim 0.5$ days, corresponding to breakup velocity for these stars. At an age of about 1 Myr, a population of stars rotating at breakup is already present.
2. Adopting the derived ages for these stars, specific angular momentum decreases with stellar age between about 0.1 and 3 Myr.
3. The ONC $v \sin i$ distribution bears a remarkable resemblance to the $v \sin i$ distribution of low-mass Pleiades stars. Stars in our sample must deplete their angular momentum content by a factor of about 5–10 over approximately the next 100 Myr, while maintaining the present relative distribution of specific angular momentum.

These results represent an important challenge for models of rotational evolution during the PMS phase. Based on our period distribution, we suggest that the distribution of initial rotation periods used in models should include $P \sim 0.5\text{--}10$ days at an age of 1 Myr. As such, *these models must confront the rotational evolution of stars rotating at or near breakup prior to contraction to the main sequence.* At a more detailed level, our observed similarity of the $\text{ONC } v \sin i$ distribution with that of low-mass Pleiades stars suggests that models of rotational evolution in the PMS phase should preserve the relative distribution of angular momenta present at 1 Myr.

Although magnetospheric accretion theory has proven promising in explaining the kinematics and morphology of mass flows in PMS systems, the disk-locking hypothesis does not appear to provide a complete solution for the dissipation of stellar angular momentum in the PMS phase. As described, we do not find correlations between observational diagnostics of accretion disks and stellar rotation period. While these results do not reject a disk-regulated paradigm for rotational evolution, neither do they provide

an observational foundation for its support. More fundamentally, we find many extremely rapidly rotating stars that do not show near-IR signatures of disks. Evidently, disk-locking cannot escort these stars to the main sequence.

This research was funded by an NSF Minority Graduate Fellowship (K. G. S.), a grant from the Wisconsin Space Grant Consortium (K. G. S.), a Grant-in-Aid of Research from the NAS, through Sigma Xi, The Scientific Research Society (K. G. S.), NSF grant AST 94-1715 (R. D. M.), and a grant from the Israel Science Foundation (T. M.). NOAO thesis observing support is gratefully acknowledged, as is the support and hospitality of the USNO staff. We thank Ian Frommer and Lee Nehoshtan who reduced the Wise data. It is also a pleasure to thank the many people who make WIYN the first-rate facility that it is. K. Rhode provided some of the “blue” spectra used in this study. We have benefited from discussions with W. Herbst, S. Strom, C. Dolan, E. Jensen, and D. Cohen, and from comments by the referee, J. Stauffer.

REFERENCES

- Adams, N. R., Walter, F. M., & Wolk, S. J. 1998, *AJ*, 116, 237
 Alexander, D. R., Augason, G. C., & Johnson, H. R. 1989, *ApJ*, 345, 1014
 Allen, L. E. 1996, Ph.D. thesis, Univ. of Massachusetts
 Allen, L. E., & Hillenbrand, L. A. 1999, in *ASP Conf. Ser., The Orion Complex Revisited*, ed., M. McCaughrean & A. Burkert (San Francisco: ASP), in press
 Attridge, J. M., & Herbst, W. 1992, *ApJ*, 398, L61
 Bally, J., Langer, W. D., Stark, A. A., & Wilson, R. W. 1987, *ApJ*, 312, L45
 Barnes, S., & Sofia, S. 1996, *ApJ*, 462, 746
 Basri, G., & Batalha, C. 1990, *ApJ*, 363, 654
 Basri, G., & Bertout, C. 1989, *ApJ*, 341, 340
 Beckwith, S. V. W., Sargent, A. I., Chini, R. S., & Güsten, R. 1990, *AJ*, 99, 924
 Blaauw, A. 1964, *ARA&A*, 2, 213
 ———, 1991, in *The Physics of Star Formation and Early Stellar Evolution*, ed., C. Lada & N. Kylafis (Dordrecht: Kluwer), 125
 Bouvier, J. 1990, *AJ*, 99, 946
 Bouvier, J., Bertout, C., Benz, W., & Mayor, M. 1986, *A&A*, 165, 110
 Bouvier, J., Cabrit, S., Fernandez, M., Martin, E., & Matthews, J. 1993, *A&A*, 101, 495
 Bouvier, J., Forestini, M., & Allain, S. 1997, *A&A*, 326, 1023
 Brown, A. G. A., de Geus, E. J., & de Zeeuw, P. T. 1994, *A&A*, 289, 101
 Canuto, V. M., & Mazzitelli, I. 1990, *ApJ*, 370, 295
 ———, 1992, *ApJ*, 389, 724
 Choi, P. I., & Herbst, W. 1996, *AJ*, 111, 283 (CH)
 Collier Cameron, A., Campbell, C. G., & Quaintrell, H. 1995, *A&A*, 298, 133
 Conover, W. J. 1971, *Practical Nonparametric Statistics* (New York: Wiley)
 D'Antona, F., & Mazzitelli, I. 1994, *ApJS*, 90, 467
 Eaton, N. L., Herbst, W., & Hillenbrand, L. A. 1995, *AJ*, 110, 1735
 Edwards, S., Hartigan, P., Ghandour, L., & Andrulis, C. 1994, *AJ*, 108, 1056
 Edwards, S. E., Ray, T., & Mundt, R. 1993a, in *Protostars and Planets III*, ed. E. H. Levy & J. Lunine (Tucson: Univ. of Arizona Press), 567
 Edwards, S. E., et al. 1993b, *AJ*, 106, 372
 Gomez, M., & Lada, C. J. 1998, *AJ*, 115, 1524
 Ghosh, P., & Lamb, F. K. 1979a, *ApJ*, 232, 259
 ———, 1979b, *ApJ*, 234, 296
 Hartigan, P., Edwards, S., & Ghandour, L. 1995, *ApJ*, 452, 736
 Hartmann, L., Hewett, R., & Calvet, N. 1994, *ApJ*, 426, 669
 Hartmann, L. W., Hewett, R., Stahler, S., & Mathieu, R. D. 1986, *ApJ*, 309, 275
 Hartmann, L. W., & MacGregor, K. B. 1982, *ApJ*, 259, 180
 Herbig, G. H. 1962, *Adv. Astron. Astrophys.*, 1, 47
 Herbst, W., Herbst, D. K., Grossman, E. J., & Weinstein, D. 1994, *AJ*, 108, 1906
 Herbst, W., & Wittenmyer, R. 1996, *BAAS*, 189, no. 49.08
 Hillenbrand, L. A. 1997, *AJ*, 113, 1733
 Hillenbrand, L. A., & Hartmann, L. W. 1998, *ApJ*, 492, 540
 Hillenbrand, L. A., Strom, S. E., Calvet, N., Merrill, K. M., Gatley, I., Makidon, R. B., Meyer, M. R., & Skrutskie, M. F. 1998, *AJ*, 116, 1816
 Honeycutt, R. K. 1992, *PASP*, 104, 435
 Horne, J. H., & Baliunas, S. L. 1986, *ApJ*, 302, 757
 Jones, B. F., & Walker, M. F. 1988, *AJ*, 95, 1755 (JW)
 Kearns, K. E., Eaton, N. L., Herbst, W., & Mazzurco, C. J. 1997, *AJ*, 114, 1098
 Kearns, K. E., & Herbst, W. 1998, *AJ*, 116, 261
 Kenyon, S. J., et al. 1994, *AJ*, 107, 2153
 Kenyon, S. J., Yi, L., & Hartmann, L. 1996, *ApJ*, 462, 439
 Keppens, R., MacGregor, K. B., & Charbonneau, P. 1995, *A&A*, 294, 469
 Königl, A. 1991, *ApJ*, 370, L39
 Kogure, T., Yoshida, S., Wiramihardja, S. D., Nakano, M., Iwata, T., & Ogura, K. 1989, *PASJ*, 41, 119
 Kovács, G. 1981, *Ap&SS*, 78, 175
 Krishnamurthi, A., Pinsonneault, M. H., Barnes, S., & Sofia, S. 1997, *ApJ*, 480, 303
 Lada, C. J., & Adams, F. C. 1992, *ApJ*, 393, 278L
 Maddalena, R. J., Morris, M., Moscowitz, J., & Thaddeus, P. 1986, *ApJ*, 303, 375
 Makidon, R. B., Strom, S. E., Tingley, B., Adams, M. T., Hillenbrand, L. A., Hartmann, L. W., Calvet, N., & Jones, B. F. 1997, *BAAS*, 191, 506
 Meyer, M. R., Calvet, N., & Hillenbrand, L. A. 1997, *AJ*, 114, 288
 Monet, D., et al. 1996, *USNO-SA1.0* (Washington: US Naval Obs.)
 Muzerolle, J., Calvet, N., & Hartmann, L. W. 1998a, *ApJ*, 492, 743
 Muzerolle, J., Hartmann, L. W., & Calvet, N. 1998b, *AJ*, 116, 455
 Nair, V., & Freeney, A. 1994, in *Statistical Methods for Physical Science*, eds., J. L. Stanford & S. B. Vardeman (San Diego: Acad. Press)
 Najita, J. 1995, *Rev. Mexicana Astron. Astrofis.*, 1, 293
 Nakano, M., Wiramihardja, S. D., & Kogure, T. 1995, *PASJ*, 47, 889
 Ostriker, E. C., & Shu, F. H. 1995, *ApJ*, 447, 813
 Press, W. H., Teukolsky, S. A., Vetterling, W. T., & Flannery, B. P. 1992, *Numerical Recipes in Fortran, Second Edition* (Cambridge: Cambridge Univ. Press), 621
 Queloz, D., Allain, S., Mermilliod, J.-C., Bouvier, J., & Mayor, M. 1998, *A&A*, 335, 183
 Rucinski, S. M. 1988, *AJ*, 95, 1895
 Scargle, J. D. 1982, *ApJ*, 263, 835
 Shu, F. H., Lizano, S., Ruden, S. P., & Najita, J. 1988, *ApJ*, 328, L19
 Shu, F. H., Najita, J., Ostriker, E. C., Wilkin, F., Ruden, S., & Lizano, S. 1994, *ApJ*, 429, 781
 Stassun, K. G., & Wood, K. 1999, *ApJ*, 510, 892
 Stauffer, J. R., & Hartmann, L. W. 1987, *ApJ*, 318, 337
 Strom, K. M., Strom, S. E., Edwards, S., Cabrit, S., & Strutskie, M. F. 1989, *AJ*, 97, 1451
 Vogel, S. N., & Kuhl, L. V. 1981, *ApJ*, 245, 960
 Vrba, F. J., Herbst, W., & Booth, J. F. 1988, *AJ*, 96, 1032
 Vrba, F. J., Rydgren, A. E., Chugainov, P. F., Shakovskaya, N. I., & Zak, D. S. 1986, *ApJ*, 306, 199
 Warren, W. H., & Hesser, J. E. 1977, *ApJS*, 36, 497
 Wichmann, R., Bouvier, J., Allain, S., & Krautter, J. 1998, *A&A*, 330, 521
 Wiramihardja, S. D., Kogure, T., Yoshida, S., Nakano, M., Ogura, K., & Iwata, T. 1991, *PASJ*, 43, 27
 Wiramihardja, S. D., Kogure, T., Yoshida, S., Ogura, K., & Nakano, M. 1989, *PASJ*, 41, 155
 ———, 1993, *PASJ*, 45, 643
 Wood, K., Kenyon, S. J., Whitney, B. A., & Bjorkman, J. E. 1996, *ApJ*, 458, L79
 Wood, K., Kenyon, S. J., Whitney, B., & Turnbull, M. 1998, *ApJ*, 497, 404
 Wood, K., & Whitney, B. A. 1998, *ApJ*, 506, L43